NTNU
Norwegian University of
Science and Technology

Press Form Hardening of Aluminium

The influence of hot forming, quench interruption and direct artificial aging on the mechanical properties of AA6082

Benedikte Jørgensen Myrold

Materials Science and Engineering (MTMT)
Submission date: March 2018
Supervisor: Bjørn Holmedal, IMA
Co-supervisor: Ola Jensrud, IMA

Norwegian University of Science and Technology
Department of Materials Science and Engineering

Preface

This report is submitted as the product of 'TMT4905 Materials Technology, Master's Thesis' in fulfilment of the degree of Master of Science in Materials science and engineering at the Norwegian University of Science and Technology. This master thesis is conducted in collaboration with the i-Pal project and the Ph.D. of Knut Erik Snilsberg. The work is a continuation of the thesis presented for the course 'TMT4500 Materials technology, specialization project'. The research has been conducted at the Department of Materials Science and Engineering under supervision of professor Bjørn Holmedal, professor Ola Jensrud and Ph.D. candidate Knut Erik Snilsberg.

Trondheim, March 2018

Benedikte Jørgensen Myrold

Acknowledgements

I would like to express my gratitude to my supervisors professor Bjørn Holmedal, professor Ola Jensrud and PhD candidate Knut Erik Snilsberg for valuable guidance, help, advice and discussions throughout the project.

I would like to thank chief engineer Pål Christian Skaret for the cooperation during the development and conduction of the experiments. Thanks to chief engineer Trygve Lindahl Schanche and staff engineer Torild Krogstad for various help and tutorials in operation of laboratory equipment. For helping me find an effective solution for temperature surveillance in the experiments, I would like to thank Harald Holm. Thanks to senior engineer Yingda Yu for assistance at the EM-laboratory.

I would also like to acknowledge AP&T and Lars-Olof Jönsson for building the pressing tool and at short notice fixing the tool when it broke. Thanks to the mechanical engineering workshop and staff engineer Øystein Gjervan Hagemo for the machining of samples and tensile specimens, and for helping me find good solutions to various challenges that arose concerning the pressing tool.

Finally, I would like to thank Maren Elise Juul and Jan Inge Meling for proofreading and giving feedback on the thesis.

Abstract

The automotive industry is in need of new lightweight solutions to meet stricter regulations regarding reduction in greenhouse gas emissions. Replacing steel components with age-hardenable high-strength aluminium alloys may significantly reduce the weight of a vehicle. Hot forming and in-die quenching of aluminium is a method under development with an overall aim to provide more effective and cheaper solutions for production of aluminium components for automotive applications. The method also introduces improved properties compared to cold forming in terms of geometrical tolerances, formability, ductility, springback and microstructural control.

Experiments were conducted on an extruded 6082.25 aluminium alloy profile to investigate the behaviour of the material during integrated hot forming and in-die quenching under various conditions. A flat steel pressing tool, with built-in channels for water cooling, was designed, built and attached to a hydraulic driven press. Samples were brought directly from solution heat treatment to the tool for simultaneous quenching and deformation. A feasible and reproducible test procedure was developed for the press tool experiments.

By shortening the closed-die time during integrated deformation and quenching from solution heat treatment before direct artificial aging, significant time might be spared in an industrial production process.

The effect of reduced closed-die time was investigated by interrupting the quenching from solution heat treatment at temperatures between 25-200°C before subsequent age hardening. The effect of direct artificial aging was investigated by bringing one set of samples directly to oil bath for artificial aging after quenching from solution heat treatment. A second set of samples was stored at room temperature for 30 minutes before artificial aging. It was found that quench interruption at temperatures below 150°C does not affect the alloy properties in a negative manner. Neither direct artificial aging imposes diminished properties of the alloy.

Sammendrag

I dagens bilindustri er det et økende behov for nye lettvektsløsninger for å møte stadig strengere reguleringer som følge av krav til reduksjon i utslipp av drivhusgasser. Ved å erstatte stålkomponenter med utherdbare, høystyrke aluminiumslegeringer, kan vekten av et kjøretøy reduseres betydelig. Integrert varmforming og bråkjøling i pressverktøy er en metode under utvikling med et overordnet mål om å effektivisere og redusere kostnadene i produksjon av bildeler. Metoden vil også medføre forbedrede egenskaper i form av geometrisk toleranse, formbarhet, duktilitet, springback og kontroll av mikrostruktur.

Forsøk ble utført på ekstruderte 6082.25 aluminiumprofiler for å undersøke materialets oppførsel under integrert varmforming og bråkjøling i verktøy ved ulike betingelser. Et flatt pressverktøy i stål med innebygde kanaler for vannkjøling ble designet, bygget og montert på en hydraulisk drevet presse. Prøver ble fraktet direkte fra innherding til verktøyet for samtidig bråkjøling og deformasjon. En gjennomførbar og reproduserbar metode ble utviklet for forsøk med verktøyet.

Ved å korte ned lukketiden på stemplene under bråkjøling og deformasjon, og droppe mellomlagring i romtemperatur etter bråkjøling og deformasjon, kan betydelige mengder tid spares i en industriell produksjonsprosess.

Effekten av redusert lukketid ble undersøkt ved å avbryte bråkjøling på temperaturer mellom 25-200°C før påfølgende utherding. Effekten av direkte utherding ble undersøkt ved å frakte et sett med prøver direkte til utherding etter bråkjøling fra innherding. Et annet prøvesett ble mellomlagret på romtemperatur i 30 minutter før utherding. Det ble funnet at avbrutt bråkjøling på temperaturer under 150°C ikke påvirker legeringens egenskaper på en negativ måte. Direkte utherding hadde heller ingen negativ påvirkning på hardhet eller styrke i materialet.

Table of Contents

1. Introduction

Environmental and climate changes have been global topics in recent years. An improvement is necessary with regards to energy efficiency and reduction of greenhouse gas emissions. Transportation is currently a major source of pollution and is the origin of about 20% [1] of the world's greenhouse gas emission. By replacing steel components in vehicles with aluminium, the weight can be significantly reduced. A passenger car containing 40% aluminium will during a lifetime save in average 680 litres fuel and thus spare the environment of 1950 kg CO_2 [2]. Choice of materials for vehicles is dominated by cost considerations where the material and production prices decide the outcome. Because of limitations in cost-effective production methods of complex aluminium components, aluminium has not yet been a profitable construction material in the automotive industry.

The aim of the i-Pal project is to develop an integrated hot forming and in-die quenching process, Press Form Hardening (PFH), of aluminium for automotive applications. The project is a collaboration between Raufoss Technology, Hydro, NTNU, AP&T and SINTEF, and is partly funded by Norwegian Research Council (NRC). The method is already applied to hardenable high strength steel. Fewer process steps are needed in the production process, as opposed to cold sheet forming. As a result, the energy consumption per part produced will decrease. Hot forming of aluminium increases the formability of high strength alloys, obtains a good ductility and reduces the springback issues associated to cold forming. This method will potentially lead to high productivity, less advanced tools and improved geometrical tolerances. In addition, the reduction of process steps makes Press Form Hardening a cheaper alternative to cold forming.

It has been suggested in several studies that the room temperature storage between solution heat treatment and artificial aging is detrimental for the final properties of the AA6082 alloy. This theory was tested for the 6082.25 aluminium alloy in the specialization project [3] and the results complied with this theory. The experiments conducted in this project is a continuation to determine if this is applicable when deformation is introduced. In addition, the results from the specialization project suggested that it is beneficial to interrupt the quenching from solution heat treatment at temperatures below 200°C before moving directly to artificial aging. This has been extended in the current study.

Quench interruption and direct artificial aging introduced to the hot deformation and in-die quenching process can reduce the production steps even further, leading to an improved efficiency where significant time, energy and costs can be spared.

2. Theory

The theory required for understanding and interpretation of the results are presented in this chapter. Parts of the theory are based on the theory section in the specialization project, Myrold, B. et al. [3]. The theory includes a short introduction to the alloy investigated in the current project, a description of typical heat treatment sequences and a brief presentation of the strengthening mechanisms in AA6082. Quench sensitivity and hot deformation of the alloy are of most relevance for the experiments as the thesis and experiments mainly are focused on the behaviour of the alloy during these stages of the process. Therefore, a more detailed explanation of the mechanisms occurring during hot deformation and quenching is presented.

2.1 Hardenable aluminium alloys

The material investigated in this project is flat extruded profiles of AA6082. AA6082 is an age hardenable wrought alloy containing Mg and Si. Due to high strength, good formability and ductility, this alloy is suitable and frequently used for automotive applications. Alloying elements, properties, heat treatment and production sequence are discussed in the following sections.

2.1.1 Aluminium-Magnesium-Silicon alloys

AA6082 is a part of the 6XXX series of aluminium alloys and is also referred to as Al-Mg-Si alloys. These alloys are commonly recognized as medium-to-high strength alloys with good formability and corrosion resistance. The material properties may be tailored by adding alloying elements in different amounts. Table 1 shows the chemical composition limits of AA6082.

Table 1: Chemical composition limits of AA6082 given in percentage by mass (wt%) [4].

Si	Fe	Cu	Mn	Mg	Cr	Zn	Ti
0.7-1.3	< 0.5	< 0.1	0.4-1.0	0.6-1.2	< 0.25	< 0.2	< 0.2

The alloy is strengthened through heat treatment where the main alloying elements, Mg and Si, precipitate from solid solution during age hardening to form strengthening precipitates. The equilibrium phase is Mg_2Si (β), while the strengthening is achieved by intermediate phases formed before equilibrium is reached [5].

The mechanical properties of Al-Mg-Si alloys often refer to hardness, yield stress ($Rp_{0.2}$), tensile strength (R_m), elongation (A_g), uniform strain and fracture area fraction [5].

2.1.2 Heat treatment

The final product of a part for car applications has been subjected to a series of heat treatments. A common heat treatment sequence includes casting, homogenization, extrusion or rolling, annealing, solution heat treatment, room temperature storage, pre-aging and artificial aging. All steps are carefully designed to optimize the effect of the following steps and the final properties. The cooling rate and cooling medium after exposure to higher temperatures are variables of importance in the process of achieving optimal final product properties and will be further addressed in Chapter 2.4. The heat treatment sequence relevant for the press form hardening process, from molten aluminium to the final product, is illustrated in Figure 1.

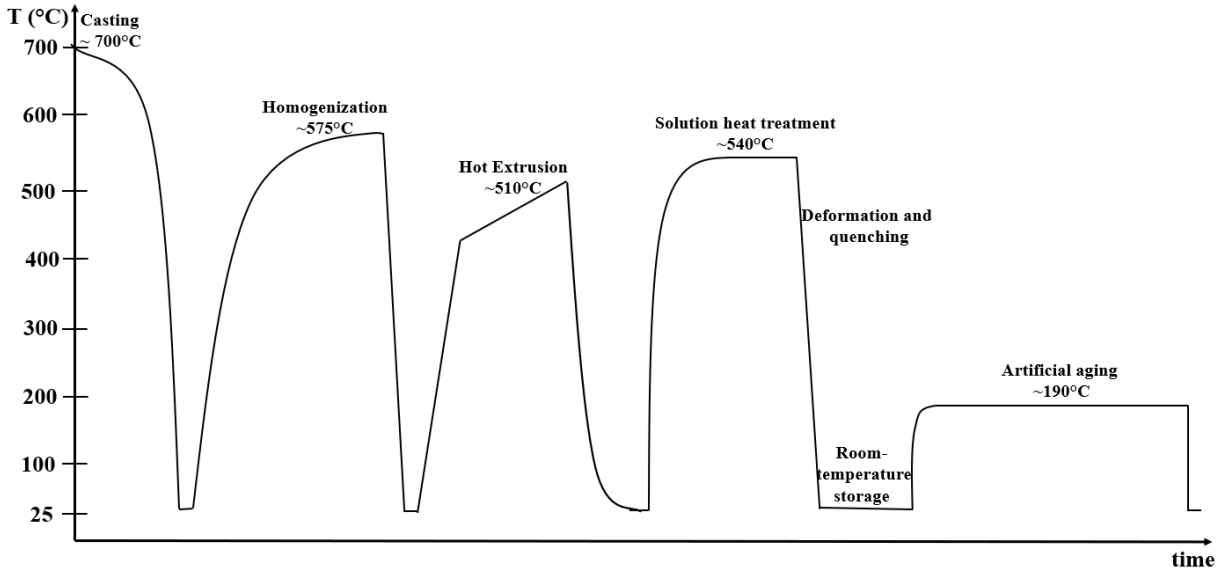

Figure 1: Typical heat treatment sequence of an age hardenable aluminium alloy.

Molten aluminium is cast into billets. The aluminium is heated to a temperature above the melting point, cast in suitable castings and solidified. Some phases and alloying elements other than aluminium solid solution may separate first from the melt and form primary intermetallic particles [6]. These particles are often coarse and have low solubility.

Homogenization is carried out below the eutectic point in the Al-Mg_2Si binary phase diagram for a certain period of time to dissolve solute concentrations in the as-cast matrix [7]. Due to increased temperature and thereof increased diffusion, low melting point eutectics dissolve and the concentration of alloying elements level out [7]. As many as possible of the crystals and intermetallics are taken back into solid solution to optimize the subsequent behaviour during rolling or extrusion [7]. A homogeneous solution is obtained and small particles called dispersoids are formed [8]. The dispersoids grow with increasing temperature and coarsen during holding time [8]. Homogenization is also a structure modification treatment as the structure rapidly evolves toward thermodynamic equilibrium [7, 9]. Internal casting stresses are also released [7].

Extrusion is a hot working process where solid metal is forced through an orifice in a steel die. The microstructure of the product may vary from end to end and through the cross section as the shear boundaries are larger close to the tool contact. The as-cast structures are somewhat

remained for the first metal passing through the die [7]. As the metal is continuously forced through, the cast structure is heavily deformed. Strain and high temperature affects the grains in such manner that they are hot worked and recovered or, in some cases, recrystallized [7]. An unrecrystallized extruded product generally obtains a fibrous grain structure.

Solution heat treatment is carried out with the intention of developing maximum amount of soluble elements, Mg and Si, into solid solution. The alloy is heated to a temperature slightly below the eutectic melting temperature. A sufficient holding time at the solution heat treatment temperature is necessary to achieve complete solid solution without suffering any recrystallization. In the alloy investigated in this thesis, recrystallization may be detrimental to the final properties. The result is a nearly homogeneous solid solution where all phases have dissolved [10]. The alloy is quenched to produce supersaturated solid solution. To avoid precipitation of the solute elements during cooling, a rapid quench is necessary [10, 11].

After solution heat treatment, the material is quenched to room temperature to obtain supersaturated solid solution (SSSS). In addition, at high temperatures the vacancy equilibrium concentration is high and by rapid quenching the vacancies are quenched in. The vacancies play an important role for subsequent clustering of nucleation sites for precipitation.

Age hardening, or precipitation hardening is conducted at room temperature and elevated temperature to initiate precipitation and growth of strengthening phases.

A typical production process includes a period of storage at room temperature after solution heat treatment. This storage period may also be referred to as natural aging and is conducted primarily for practical reasons. For most alloys the storage time results in increased alloy strength due to clustering of solute elements in the matrix [12-15]. However, with a Mg+Si content of more than 1wt%, the room temperature storage have a detrimental effect on the alloy strength due to formation of clusters, which do not act as nucleation sites for subsequent metastable β”-precipitates [16].

Finally, the alloy is artificially aged at a temperature between 170-190^{o}C. At elevated temperatures the precipitation process is accelerated as compared to room temperature, and precipitation of the β” phase is promoted [17]. The artificial aging temperature and time control size and number density of the strengthening precipitates [18]. The precipitates form and grow from nucleation sites such as vacancy clusters, grain boundaries, stacking faults and grown-in dislocations [14]. As the precipitates reach a critical volume factor, peak hardness (T6) is achieved. Further holding time at artificial aging temperature causes continued growth of the precipitates as long as there are solutes left in the matrix. Further artificial aging exceeding T6 causes coarsening of the precipitates, i.e. they become fewer and larger due to lack of solute [19]. The hardness decreases, and the alloy is overaged.

2.2 Strengthening mechanisms

There are several methods practiced to introduce strength to aluminium. Aluminium 6XXX alloys are age hardenable alloys that gain most of their strength through a suitable heat treatment process. Hardening mechanisms include precipitation, solid solution strengthening, grain refinement and work hardening. These strengthening mechanisms will be discussed in the following sections.

2.2.1 Strain hardening

Strain hardening is a result of plastic deformation and corresponds to the motion of large numbers of dislocations. The dislocation density increases drastically during plastic deformation due to multiplication of dislocations or formation of new dislocations [20]. As the distance between adjacent dislocations decreases, the dislocations will start to lock and form junctions, making movement more difficult. Consequently, the hardness, as well as yield and tensile strength, increase due to the dislocation network requiring more stress to overcome the obstacles. [20, 21] The Holloman equation approximates the stress and strain in the plastic region [20]:

$$\sigma = k\varepsilon^n \tag{1}$$

The coefficient, *k*, and the exponent, *n*, are strain hardening parameters for the specific alloy. The applied stress required to deform the alloy increases with increasing work. The relation between flow stress (shear stress required to cause plastic deformation, i.e. to move dislocations) and the dislocation density, ρ, is shown in Equation 2 [22]:

$$\tau = \tau_0 + \alpha G b \sqrt{\rho} \tag{2}$$

τ_0 is the original flow stress, *G* is the shear modulus, *b* is the burgers vector and α is a constant.

2.2.2 Grain size

The theory presented in this section is based on Dieter, G.E. [20]. Grain size strengthening is associated with dislocation barriers such as grain boundaries. A dislocation cannot continue its slip motion into another grain as it reaches a grain boundary. This is due to different orientations in slip planes and directions in two neighbouring grains. This causes a pile-up of dislocations at the grain boundary and hence the grain boundaries become obstacles for dislocation movements. As less distance can be travelled by a dislocation, less slip and thus less plastic deformation occur. The alloy properties, such as the yield strength, ultimate tensile strength and ductility, may be improved by reducing the grain size. A smaller grain size increases the hardness. However, it may also lower the hardening effect of precipitates. Therefore, finding an optimal grain size distribution is essential.

A general relationship between grain size and yield stress can be described by the Hall-Petch Equation 3 [20]:

$$\sigma = \sigma_0 + kD^{-\frac{1}{2}} \tag{3}$$

Where σ is the yield stress, σ_0 is the stress required to move a dislocation, *k* is the "locking parameter" which measures the relative hardening contribution of the grain boundaries and *D* is the grain diameter. The yield strength increases with decreasing grain diameter. The Hall-Petch equation expresses the grain size dependence of the flow stress at any plastic strain.

2.2.3 Solid solution strengthening

The theory presented in this section is based on Dieter, G.E. [20]. When introducing alloying elements into solid solution, these foreign atoms cause an increased alloy strength compared to the pure metal. Solute atoms with comparable size as the solvent, i.e. a relative size difference of less than 15%, will occupy lattice points of the solvent atoms. This is called substitutional solid solution strengthening. Smaller solute atoms occupy interstitial points in the lattice, which leads to interstitial solid solution strengthening. The atomic arrangement in the lattice is disturbed by the point defects, and an interference with the movement of dislocations, or slip, occur. The most relevant interaction mechanisms between solute atoms and dislocations in aluminium are elastic interactions and modulus interactions.

Elastic interaction is referred to the interaction between the elastic stress fields surrounding misfitting solute atoms and the core of edge dislocations. The relative size factors can be described by Equation 4 [20]:

$$\varepsilon_a = \frac{1}{a}\left(\frac{da}{dc}\right) \tag{4}$$

where *a* is the lattice parameter and *c* the atomic concentration of the solute. The strength increase caused by elastic interaction is directly proportional to the misfit of the solute.

A local alteration of the crystal modulus by the presence of a solute atom is referred to as modulus interaction. If the shear modulus of a solute is smaller than for the matrix, the strain field of the dislocation is reduced, and there will be an attraction between the solute and the matrix.

2.2.4 Precipitation

Precipitation hardening is the main strengthening mechanism in age hardenable aluminium alloys. After solution heat treatment and quenching of the alloy, second phase elements remain in solid solution. Subsequent aging at lower temperatures initiates precipitation of these second phase elements. The second phase elements must be soluble at elevated temperatures and exhibit lower solubility at lower temperatures to obtain precipitation hardening [20]. Before the equilibrium phases are formed, a sequence of metastable phases forms during artificial aging. The precipitation sequence in 6XXX alloys can be presented as follows [23]:

SSSS → Mg/Si clusters → GP zones → β" precipitates → β' precipitates → β phase

Where SSSS is supersaturated quenched-in solid solution after solution heat treatment. Mg/Si clusters occur at lower temperatures (0-100^{o}C). Guinier Preston (GP) zones are fine Mg and Si containing plates with a thickness of one atomic layer [6], and are monocline and partly coherent. With increasing artificial aging time, the GP zones may aggregate and form needles along the <100> direction. Metastable β" precipitates are monocline and consist of partly

coherent needles along the <100> direction [5]. The phase is described as Mg_5Si_6, but new research suggests that the phase may also contain some aluminium [24]. When the material has reached its maximum strength, T6, the structure consists mainly of β" precipitates [5]. Metastable β' precipitates form as partly coherent rods and have a hexagonal structure [5]. β phase is the equilibrium Mg_2Si phase with a cubic structure and forms as incoherent square plates [5, 12].

As clusters and zones are formed at lower temperatures, while Mg_2Si precipitates at higher temperatures, the precipitation sequence is not valid for every temperature. An increase of the Si to Mg ratio to approximately 6/5 enhance the stabilisation of β" phase [12]. Higher Mg content will cause the alloy to have a coarser precipitate distribution, which consists of a mixture of Si and phases that normally are formed during overaging [12].

2.2.4.1 Dislocation – precipitate interactions

At applied stress, the interaction between dislocations and precipitates prevent slip and therefore, provides increased strength in the material. Depending on how the dislocations interact with the particles, and the particle properties, these interactions can be divided into two basic mechanisms: particle cutting and particle looping [20]. If enough stress is applied and the repulsive forces between a shearable particle and the dislocation is not high enough, the dislocations will cut through the particle [20], as shown in Figure 2. The strength is increased as extra work is required for a dislocation to glide through a particle.

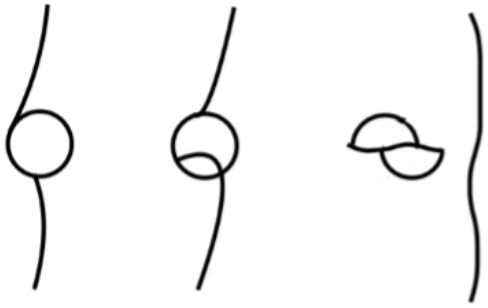

Figure 2: Dislocation cutting a particle.

The applied stress required to cut a particle can be expressed by Equation 5 [20]:

$$\tau = \frac{\alpha \gamma_1^{\frac{3}{2}} (fr)^{1/2}}{\mu b^2} \tag{5}$$

Where α is a numerical constant, γ_1 is the interfacial energy between the precipitate and the matrix, f is the volume fraction of precipitates, r is the mean radius of the precipitates, μ is the shear modulus and b is the Burgers vector.

The dislocations will bypass non-shearable particles by looping if there is not enough applied stress [20], as shown in Figure 3. This is also called Orowan looping. Each time a dislocation passes a particle a new loop is added, which strengthens the material.

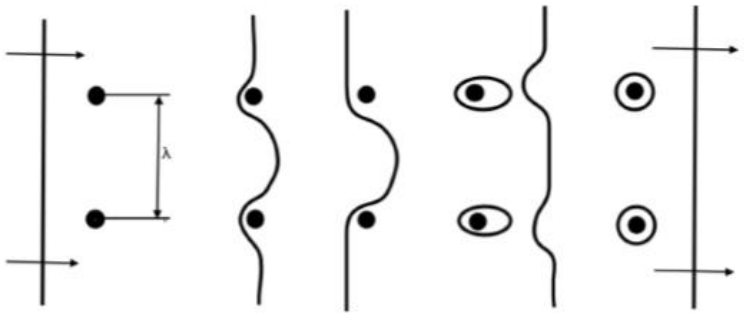

Figure 3: A dislocation bypassing a particle by looping.

The yield stress can be determined by the shear stress, τ_0, required to bow the dislocation line between two particles with a radius R and a distance λ ($\lambda > R$) [20]. The shear stress can be expressed by Equation 6 [20]:

$$\tau_0 = \frac{\alpha \mu b}{\lambda} \tag{6}$$

α is a numerical constant, μ is the shear modulus and *b* the Burgers vector.

As the dislocation reaches the two particles, the dislocation starts to bend around them until it reaches a critical curvature corresponding to $R = \lambda/2$ [20]. The dislocation can continue without further decreasing its radius of curvature. The segments of the dislocation meet as two opposite signs and annihilate each other over parts of their length leaving a loop around the particles [20]. The original dislocation is free to proceed moving.

Generally, at a critical dispersion, the strengthening is at maximum. Small particles or precipitates are often coherent and shearable by dislocations [20]. At a point during growth of the particles, the particles become incoherent and non-deformable and dislocations bypass by looping [20]. When dislocations pass through shearable particles by cutting, the properties of the particles are of greater importance than the particle size [20]. As the dislocations bypasses particles by looping, the alloy strength depends on the particle size and dispersion [20]. Figure 4 illustrates the dependence of the alloy strength on particle size. At a critical point, P, the alloy has reached its maximum strength, which decreases with further growth of the particles.

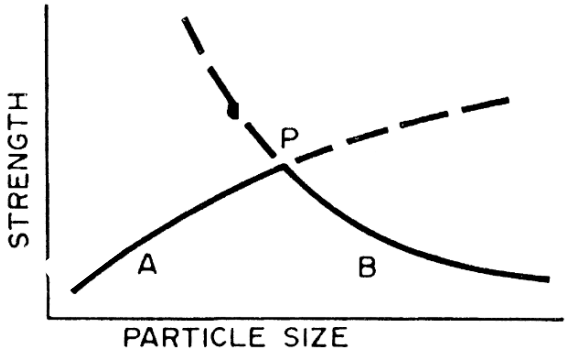

Figure 4: Relationship between strength and particle size for a typical hardenable aluminium alloy. A) Particles being cut by dislocations. B) Particles being looped by dislocations [25].

2.3 Intermetallic particles and dispersoids

Aluminium is often combined with transition metals that form intermetallic phases with little or no solubility in the matrix. During solidification of the molten aluminium, some phases may separate first from the melt and form different primary intermetallic phases [6, 26]. These particles are often coarse and, due to high melting point, have low solubility and remain stable in the aluminium during subsequent heat treatments [6].

Some of these alloying elements also form dispersoids, which are small particles, less than 1μm in size [11]. Growth of dispersoids occur with increasing temperature and coarsen with holding time during homogenization [8]. Dispersoids may have a significant effect on recovery, recrystallization and grain growth processes. Grain growth is prevented by pinning of grain boundaries [6]. Due to their large size compared to the precipitates, they are too few to give a significant strength contribution. The dispersoids tend to act as nucleation sites for strengthening precipitates [27].

The dispersoids formed during heating to homogenization temperature depends on the cooling rate from the extrusion temperature [28]. Manganese, chromium and iron form dispersoids during heating to homogenization temperature. If the cooling after extrusion has been too slow, the dispersoids formed act as nucleation sites for coarse, non-hardening Mg-Si precipitates [27]. Thus, the degree of supersaturation available for subsequent precipitation of strengthening precipitates is reduced. The type of nucleation sites formed by dispersoids is determined by their interface with the matrix, which depends on composition, crystal structure and size [28].

2.4 Quenching of AA6082

The heat treatment of AA6082 includes cooling or quenching from the solution heat treatment temperature. Slow cooling will cause alloying elements to form stable precipitates and diffuse from solid solution and concentrate at grain boundaries, voids, undissolved particles and other defects in the lattice. On the other hand, cooling too fast may lead to residual stresses, which again may cause cracking [16]. Different factors that may influence the material properties during cooling are addressed in the following sections.

2.4.1 Quench sensitivity

Quench sensitivity is associated with the reduction of age hardening potential due to too slow cooling rates. During quenching the heterogeneous precipitation depends on the degree of supersaturation and the diffusion rate as a function of temperature. The diffusion rate decreases with decreasing temperature and decreasing supersaturation [6]. Generally, as seen in Figure 5, where α represents Mg and Si in solid solution and β the Mg_2Si phase, the precipitation process is initiated sooner during cooling with increased alloy content (Mg + Si). Thus, the quench sensitivity is increased with increasing alloy content [29].

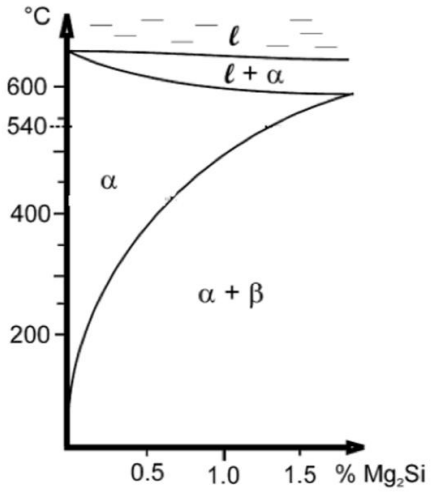

Figure 5: Quasi binary phase diagram of Al-Mg_2Si [29].

Figure 6 shows the quasi-binary phase diagram combined with time-temperature-transformation (TTT) curves of precipitates in AA6082. At higher temperatures precipitation of the equilibrium phase, β, occurs, while GP-zones and β" phase are formed at lower temperatures. The Mg_2Si precipitates formed at high temperatures are coarse and rod-shaped [17, 29], i.e. the β and β' phases are typically much larger than the size of the β" phase. At intermediate temperatures, the precipitation rate is highest due to a combination of high equilibrium concentration of Mg_2Si and a relatively high diffusion rate. This is valid for slow cooling rates.

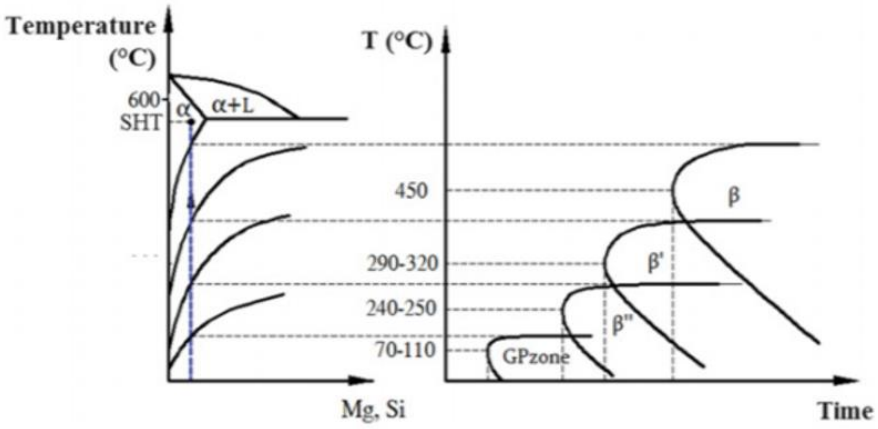

Figure 6: Schematic phase diagram and TTT curves of precipitates in AA6082 [17].

As the amount of precipitation is increased during quenching, the hardening potential is reduced as precipitated solute will be unavailable for further precipitation reactions. The precipitates formed during slow cooling in the high temperature region are coarse and does not provide any strength contribution [10]. Figure 7 shows the material after aging in the cases of slow cooling and quenching from solution heat treatment. For the case of slow cooling, the alloying elements are concentrated at the grain boundaries after cooling and have reduced solid solution available for the formation of strengthening precipitates during aging. This does not

provide any strength contribution [30, 31]. In the quenched material the alloying elements are maintained uniformly dispersed in solid solution and are available for subsequent growth of strengthening precipitates during aging [16].

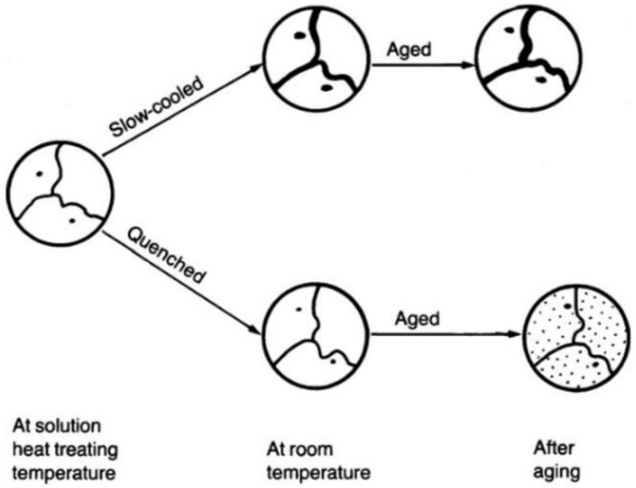

Figure 7: The precipitate distribution in an aluminium alloy after slow cooling and quenching from solution heat treatment and after aging [16].

In theory, the higher the quenching rate, the stronger and harder the alloy. However, in practice, by a controlled quenching rate, thermal stresses may be reduced and thereby gain a preferred combination of mechanical properties [32]. The quench sensitivity can be described by a time-temperature-property (TTP) curve, a C-shaped curve that describes the critical quenching rate at which the material loses its desired properties if exceeded during cooling. Examples of TTP-curves for AA6082 are obtained from Gao, M., et al. [32] and Shang B.C., et al. [33] shown in Figure 8.

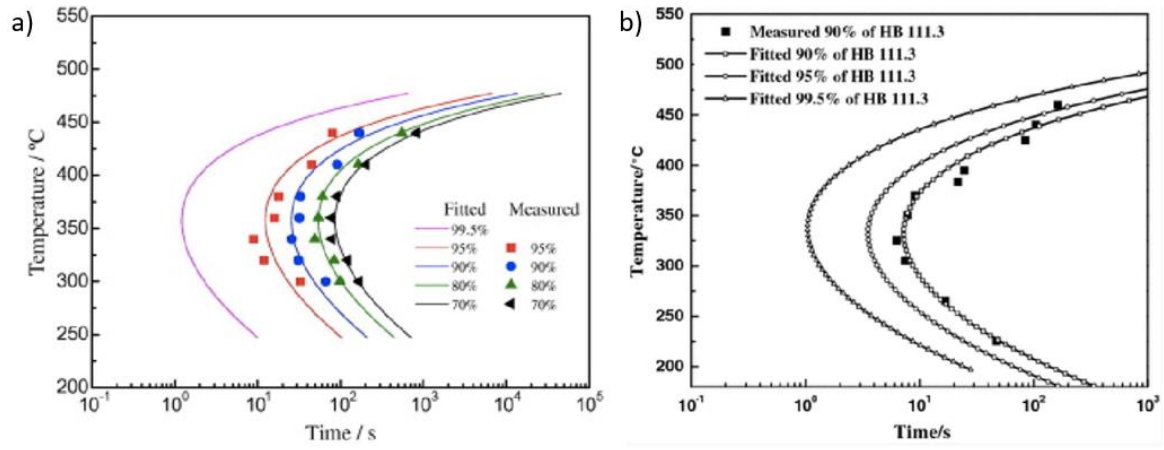

Figure 8: TTP curves for AA6082 obtained by a) Gao, M., et al. [32] and b) Shang, B.C., et al. [33].

The TTP curves in Figure 8 are obtained from AA6082 alloys, but the chemical compositions are somewhat deviating from each other and from the alloy investigated in this project, especially with respect to the Mg content; 0.7wt%Mg for the alloy in curve a and 1.05wt%Mg in b. However, they are quite similar and have a critical (nose) temperature at about 320-400°C. The measured hardness in both curves show that a quenching rate where the nose is reached

within 10 seconds will have small effects on the hardness and precipitation does probably not occur during quenching.

In the specialization project conducted initially to the current project by Myrold, B. et al. [3], the quench delay time was investigated. The samples were air cooled after solution heat treatment to different temperatures before being water quenched and aged. The results are shown in Figure 9, where the temperatures represent the temperatures to which the samples were air cooled before water quenching. The corresponding cooling times are shown in Figure 10. The results indicate that air cooling to a temperature of 500°C will not have a significant effect on the material properties of the AA6082 alloy. Between 500 and 400°C, the hardness decreases slightly. When the samples are exposed to air cooling to below 400°C, the hardness and strength drops drastically. This indicates a cooling rate at which the curve crosses the nose of the TTP curves.

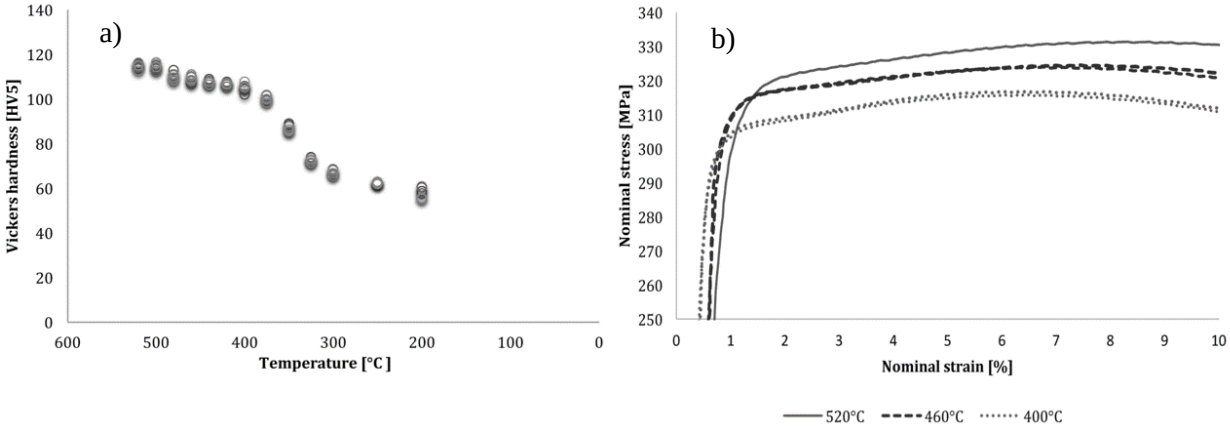

Figure 9: Hardness curve (a) and stress-strain curves (b) as functions of temperature to which the samples were air cooled before water quenching [3].

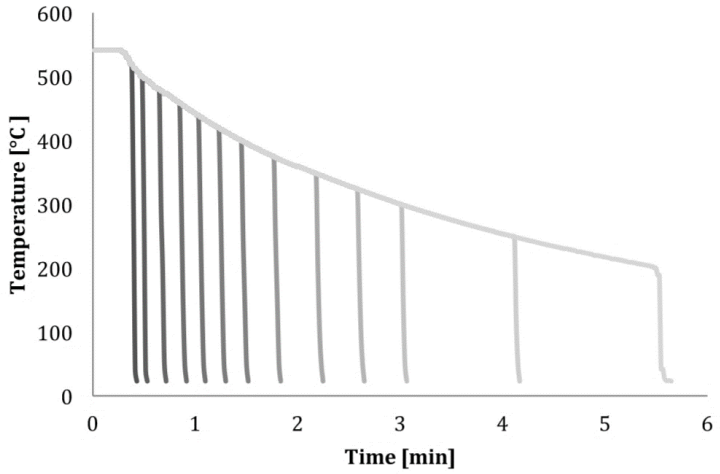

Figure 10: Time-temperature curve of air cooling to room temperature for the experiments from [3] (ref. Figure 9).

2.4.2 Vacancies

At solution heat treatment temperature, the equilibrium concentration of vacancies is high, and decreases with decreasing temperature. During slow cooling, the vacancies will migrate to grain boundaries [34] and, consequently, the concentration will be low as the alloy reaches room temperature. Rapid quenching from high temperatures will cause the vacancies to be quenched-in. These vacancies are metastable and attract each other to form vacancy clusters or sinks at low temperatures. The clusters may collapse into dislocation loops that grow by absorbing more vacancies [34]. Vacancy clusters and dislocation loops act as nucleation sites for the intermediate precipitate phases [34].

Grain boundaries are the main sinks for vacancies and vacancies nearby can easily be lost [34]. Thus, the concentration of vacancies near the grain boundaries can be significantly lower than in remote areas. The areas near the grain boundaries with low precipitate concentration are called precipitate free zones (PFZ). To obtain an even distribution of precipitates, a critical vacancy supersaturation is necessary as the amount of precipitation near the grain boundaries is affected by the distribution of vacancies. PFZs can also be formed at other second phase particles, i.e. dispersoids at which vacancies can be lost in their interfaces with the matrix [34]. Narrow PFZs can be obtained by higher solution heat treatment temperatures, higher quenching rates and lower aging temperatures.

The number of vacancies, n_v, per m^3, at a given temperature is given approximately by the Equation 7 [35]:

$$n_v = nexp(\frac{-Q}{RT}) \tag{7}$$

Where n is the number of lattice points per m^3, Q is the energy required to produce a vacancy, R is the gas constant and T the temperature.

2.4.3 Heat transfer

In the case of in-die quenching and deformation, the quenching is done by water-cooled steel. A requirement for the quench medium is that it does not heat too much during quenching, causing an interrupted quench at higher temperatures. In addition, the heat extraction from the quenchant should be uniform so that the variations in properties along the final product are minimized [36]. An important parameter influencing the cooling rate is the interfacial heat transfer coefficient (IHTC) which is defined as the amount of heat transferred per unit area per temperature difference between the interfaces (W/m^2K) [37]. IHTC should be identified to optimize the production rate, to achieve the critical quenching rate for the alloy and to retain the full mechanical strength of the formed components.

Studies show that the IHTC depends on the contact pressure, i.e. the IHTC increases with increasing contact pressure [37, 38]. The use of lubricant on the tool surface during quenching and deformation leads to increased IHTC as the lubricant fills the vacancies of an uneven contact surface [37].

Figure 11 shows the cooling curve of an AA6082 sheet with a thickness of 4.8mm being press cooled in a pressing tool at AP&T. The tool is semi-automatic and a mineral oil containing

graphite was used as tool surface lubricant. The cooling rate from 520°C is approximately 123°C/s [39].

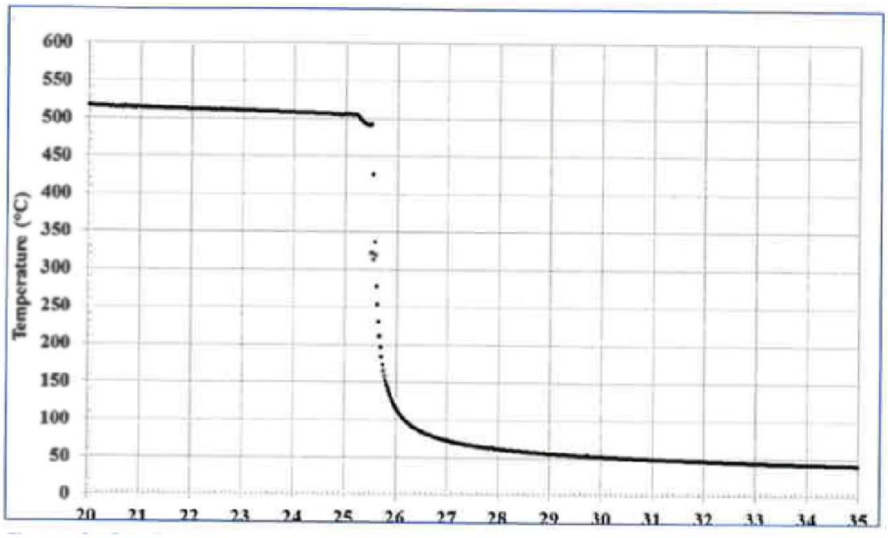

Figure 11: Cooling curve from an AA6082 sheet being formed in an industrial pressing tool [39] .

2.5 The combined influence of quenching and room temperature storage on precipitation hardening in an Al-Mg-Si alloy

For Al-Mg-Si alloys with a solute content of more than 1wt% and a Si/Mg ratio larger than 1, the clusters formed during the storage period have a negative effect on subsequent precipitation during artificial aging [12, 15, 18]. Si has a lower solubility than Mg in Al [19], therefore Si clusters and Si rich Si-Mg co-clusters in combination with quenched-in excess vacancies preferentially form during storage at room temperature [15]. These clusters act as nucleation sites for β- and Si precipitates and consequently causes a reduction in number of strengthening β" precipitates [15, 18, 40]. The Si-vacancy clusters are found to be stable even at artificial aging temperatures due to strong covalent bonds between the Si atoms [13].

As the clusters formed during natural aging is detrimental for subsequent precipitation, it should be beneficial to skip storage at room temperature. During annealing or step quenching at temperatures above 50°C, it has been suggested that Mg-Si-vacancy clusters are formed, these act as nucleation sites for precipitation of β" phase [13, 18]. Yamada, K. et al. [13] found that step quenching of an Al-Mg-Si alloy promotes the formation of Mg-Si-vacancy clusters. The heat treatment sequence involving step-quenching is shown in Figure 12.

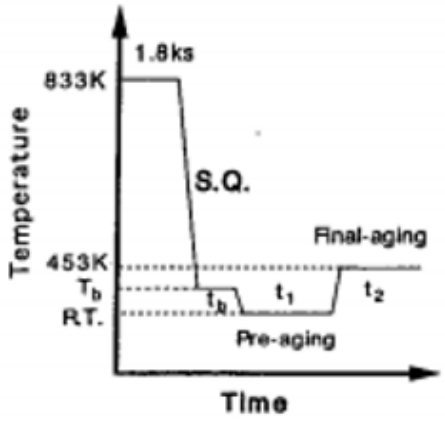

Figure 12: Step-quenching of Al-Mg-Si alloy [13].

The quenching was interrupted, and the samples were held at a temperature, T_b, for a time, t_b, before natural aging (pre-aging) and artificial aging (final-aging). This suggests that formation of the Mg-Si-vacancy clusters occupy the quenched-in excess vacancies so that they won't be trapped by Si-clusters or annihilated at artificial aging temperatures. Thus, the vacancies play an important role in formation of nucleation sites for β" phase and it is therefore beneficial to be able to control the behaviour of vacancies and solutes during heat treatment to achieve good final properties.

The effect of natural aging time in Al-Mg-Si alloys was also investigated by Kovaćs, I. et al. [19] and it was found that one achieves greater hardness the shorter the storage period at room temperature, as shown in Figure 13. At short room temperature storage times, relatively large concentrations of the alloying elements supposedly remains in solid solution [19].

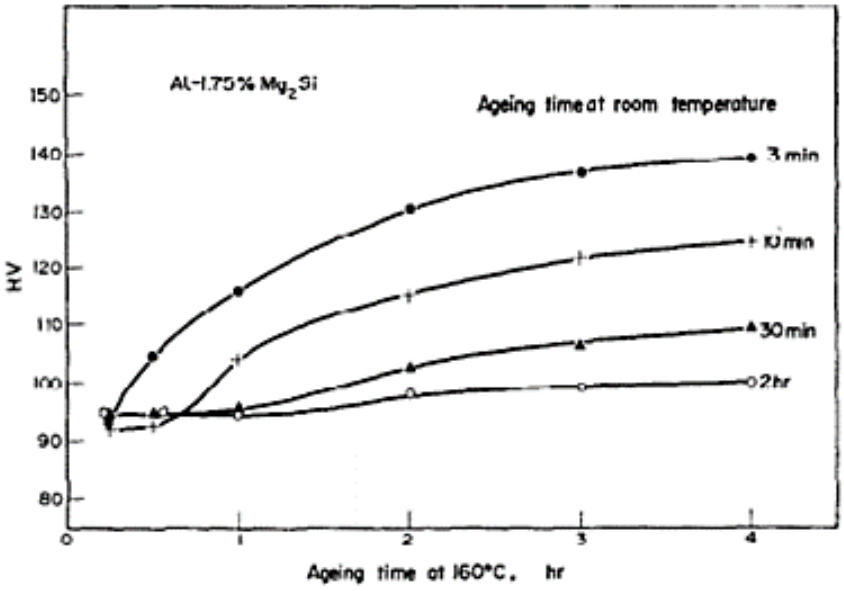

Figure 13: Change of microhardness during aging at 160°C after different pre-aging times at room temperature [19].

To summarize, it is beneficial to avoid formation of Si-clusters that causes a shortage of vacancies for formation of Mg-Si-vacancy clusters. To achieve an optimal strength in the alloy, a sufficient quenching rate is important to obtain a high concentration of quenched-in vacancies

and supersaturated solid solution. Room temperature storage should be avoided and as suggested by Yamada, K. et al [13], an interrupted quench should contribute in the formation of Mg-Si-vacancy clusters. Thus, a high concentration of vacancies and elements in solid solution promotes formation of a high number density Mg-Si-vacancy clusters and, consequently, a high number density of strengthening β" precipitates.

Results from the specialization project [3] indicated that direct artificial aging after quenching from solution heat treatment gives a strength increase compared to storage at room temperature before artificial aging, as shown in Figure 14.

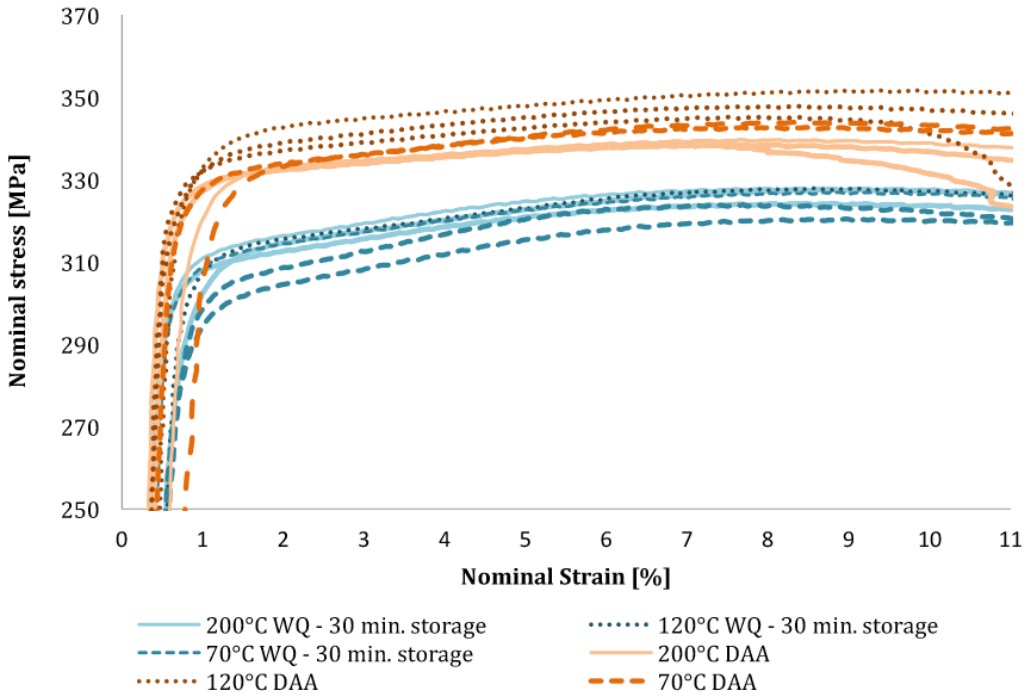

Figure 14: Tensile tests of samples being pressure quenched to selected temperatures with a steel bolt before direct artificial aging (DAA) or water quenched and stored at room temperature for 30 minutes (WQ - 30 min. storage) [3].

The samples being directly artificially aged have an average strength of about 20MPa higher than those being stored at room temperature for 30 minutes.

2.6 Deformation

During deformation, several mechanisms may take place. The most important mechanisms will be presented in this chapter, primarily with focus on hot deformation.

2.6.1 Static recovery and recrystallization

After deformation, there is high elastic energy stored in the lattice of the aluminium alloy and it is in an unstable state. This is mainly caused by dislocation formation and multiplication [6]. The stored energy is released by the thermal activation processes during annealing [6, 41]. Annealing at elevated temperatures or for short times drastically reduces the dislocation density, but the basic deformed microstructure remains. This is called recovery [6].

After recovery, the material still have a high dislocation density, which means that there is still energy stored in the deformed aluminium. This stored energy act as the driving force for recrystallization at high temperatures, and the dislocation energy is further reduced to an equilibrium value [6]. Recrystallization is a process that includes nucleation and growth of new grains. The deformed matrix with high defect density is completely replaced by new grains as the new grains continues growing until they meet each other [6].The new structure contains few dislocations in the grains, therefore, the structure is largely strain free [41]. The recrystallized grains are formed by growth of subgrains in the deformed and recovered structure [41]. An illustration of the recovery and recrystallization sequence is shown in Figure 15.

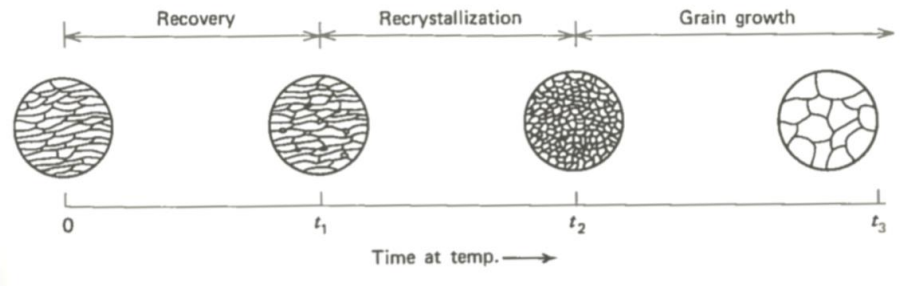

Figure 15: Schematic representation of the recovery, recrystallization and grain growth sequence [35].

The recrystallization rate as a function of temperature is shown in Equation 8 [41].

$$\frac{1}{t} = ke^{\frac{a}{T}} \tag{8}$$

Where *t* is time at temperature *T*, *k* and *a* is material dependent constants unique to each alloy and its condition. *a* may be replaced by *Q/R*, where *Q* is the activation energy and *R* the gas constant. This equation is valid before secondary reactions take place such as precipitation of intermetallic phases [41]. The higher the temperature the higher the rate of recrystallization.

2.6.2 Dynamic restoration

Dynamic restoration refers to dynamic recovery and dynamic recrystallization during deformation. Dynamic restoration causes softening and reduction in flow stress in the material, enabling easier deformation [42]. This process also influences the texture and grain size. The dynamic restoration process during deformation occurs as follows: Initially the flow stress is increased as dislocations interact and multiply. A microstructure of low angle grain boundaries and subgrains develop [42]. At a certain strain rate; work hardening and recovery reach a

dynamic equilibrium and the dislocation density remains constant. Steady state flow stress is achieved. Dynamic recovery occurs rapid during hot deformation of aluminium [42].

Figure 16 shows typical flow curves during cold and hot deformation of aluminium. The peak in the dynamic recrystallization flow curve is due to formation, growth and deformation of new grains, there might also be several peaks in the flow curve of dynamic recrystallization [43].

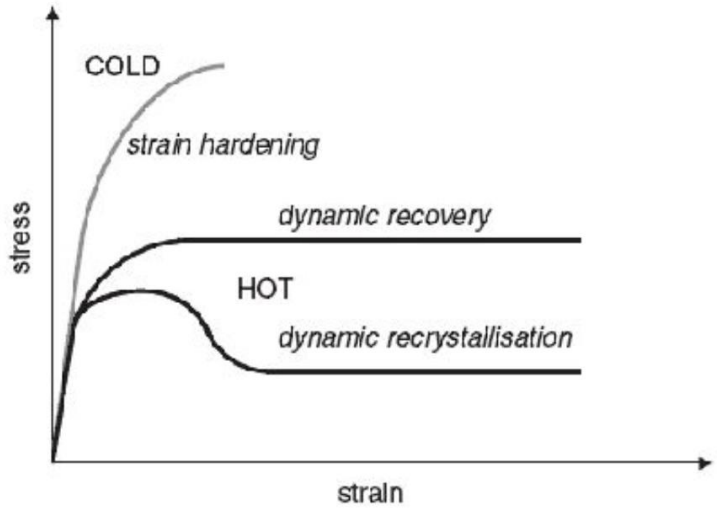

Figure 16: Flow curves during cold and hot deformation of aluminium [43].

At high temperatures, where the restoration processes occur, the microstructure evolution depends on the deformation temperature, strain rate and strain. This relationship is described by the Zener-Hollomon parameter (*Z*), Equation 9 [42]:

$$Z = \dot{\varepsilon} \exp(\frac{Q}{RT}) \tag{9}$$

Where $\dot{\varepsilon}$ is the strain rate, *Q* is the activation energy, *R* is the gas constant and *T* is the temperature. The relationship between the Zener-Hollomon parameter and flow stress, σ, is shown in Equation 10 [42].

$$Z = c_1 \sinh(c_2\sigma)^n \tag{10}$$

c_1, c_2 and *n* is constants. *Z* is closely related to the flow stress and thus the dislocation density in the subgrains as shown in Equation 11 [42].

$$\sigma = c_1 + c_2 G b \rho_i^{\frac{1}{2}} \tag{11}$$

Where ρ_i is the dislocation density within the subgrains, *G* is the shear modulus, *b* is Burgers vector, and c_1 and c_2 are constants. The dislocation density, and thus the strength, is a function of strain rate and temperature.

2.6.3 Texture and anisotropy

Texture is referred to as the distribution of the crystallographic orientations of the crystallites in a polycrystalline aggregate [44]. Plastic deformation of a metal causes the individual grains to rotate so that preferred orientations, or texture, is developed [35]. Due to slip, the lattice rotates with the slip direction towards the rotation axis [26]. In fcc metals, axis-symmetric extrusion results in a mix of <111> and <100> fibre textures [45]. In extrusion of flat profiles, the texture might result in a texture similar to rolling textures due to dominating plane strain deformation. The major texture components in rolled fcc-metals with high stacking fault energy are copper $\{112\}<11\bar{1}>$, S $\{123\}<41\bar{2}>$ and brass $\{110\}<1\bar{1}2>$ [45].

In aluminium, recrystallization may lead to a completely different textures, depending on deformation temperature and strain rate, described by the Zener-Hollomon parameter (Z) [44]. High and low Z leads to different textures. In a recrystallized fcc metal with a high stacking fault energy, the major texture components are commonly cube $\{100\}<100>$ and R $\{123\}<41\bar{2}>$ [44, 45].

Texture is of great interest in a commercial manner as it controls the highly anisotropic physical properties obtained in a deformed material. Anisotropy is defined as the dependence of properties on orientation [20]. The preferred orientation of the grains induced by deformation results in crystallographic anisotropy. Crystallographic anisotropy affects material properties as yield strength, tensile strength and the r-value [20]. The r-value is the ratio between true plastic strain along the width and true plastic strain along the thickness during tensile tests [46]. The yield strength is greater either in the longitudinal or the transverse direction depending of the preferred orientation.

By recrystallization the crystallographic anisotropy may be altered. However, the recrystallization texture can cause reappearance of a different type of anisotropy [20].

2.6.4 Hot forming

Hot forming or hot working is associated to the process where a material is being plastically deformed at a temperature and strain rate such that extensive dynamic recovery occurs during the process [47]. Thus, large strains can be obtained with no strain hardening. The energy required to deform the alloy is decreased and the ability to flow without cracking is increased. Depending on the thickness of the material being deformed, the properties may not be uniform across the cross section. The surface may have more and a different type of deformation than the interior, which can result in a finer recrystallized grain size on the surface. The inner part of large pieces may have higher temperatures longer during cooling than the surface, which can cause grain growth [47]. Thus, understanding the effect of high temperatures on the alloy, in addition to ensuring temperature surveillance and control are of great importance in a hot forming process.

To achieve complex geometrical shapes in sheet metal forming, good formability of the material is crucial. Formability is associated to the ability of an alloy to be plastically deformed without necking or cracking and is strongly influenced by temperature [48]. The formability of a material is influenced by a series of factors, including temperature, stress state, strain rate,

material properties, forming tool, lubrication and so on [48]. However, the formability may be significantly increased with increased temperature.

The temperature necessary to perform hot work on a material is high for rapid deformation and cooling to achieve a high degree of deformation. In general, a maximum temperature for hot working is 50ºC below the melting point due to the possibility of segregated regions of lower-melting-point material [47]. The minimum temperature required for hot forming is $0.5T_m$ [26].

An issue associated to cold forming of aluminium is springback of the material after deformation. Springback is the dimensional change of the formed part after released pressure of the forming tool [20]. Elastic recovery, and therefore the springback, will be great with increased yield stress and plastic strain, and decreased elastic modulus [20]. For a given material and strain, the springback increases with the ratio between the lateral dimensions of the sheet and its thickness [20]. In hot deformation, springback in a deformed material after released force is significantly reduced.

2.6.5 Hot deformation mechanisms

Hot forming includes plastic deformation. While elastic deformation is completely reversible upon stress release, plastic deformation is permanent and irreversible. On an atomic scale, it corresponds to the breaking of atomic bonds to form new bonds with new neighbouring atoms [21]. As the applied stress is released, the atoms do not return to their original positions. In AA6082, the main plastic deformation mechanism is slip [35], which is a permanent change of shape without changing the atom structure (fcc).

During deformation at high temperatures new slip systems are activated. Compared to cold deformation where slip occurs on the {111} slip plane, the {111}, {100} and {211} planes are activated during deformation at temperatures above 260°C [20]. The high temperature creep conditions occur on many slip planes for small slip distances and are suggested to be due to the operation of many dislocation sources [20]. Under low-temperature conditions, the mobility of dislocations is reduced, which impacts the nucleation of new dislocation loops at the source due to the repelling stress from other dislocations [20]. At high temperatures, the loops can climb and annihilate each other and there is a constant stream of new dislocations from several sources [20].

Lattice bending near grain boundaries may occur during creep, which results in the formation of excess dislocations of equal signs. Dislocation climb cause the dislocations to arrange into low-angle grain boundaries, thus they form a cell structure or a subgrain structure [20]. The subgrain size depends on stress and temperature. Large subgrains are formed during high temperatures and low stress or creep rates [20].

The main creep deformation mechanisms that occur during deformation of AA6082 at high temperatures are dislocation glide and dislocation creep. Dislocation glide occurs at high stress levels ($\sigma/G > 10^{-2}$) and involves dislocations that moves along slip planes and overcome barriers by thermal activation [20]. Dislocation creep occur for $10^{-4} < \sigma/G < 10^{-2}$, involving movement of dislocations overcoming barriers by thermally assisted mechanisms such as diffusion of vacancies [20].

2.6.6 Press Form Hardening

The most commonly used method for high production volume sheet metal forming is press forming, driven by either mechanical or hydraulic action. A convex punch and a matching concave die are basic tools for a metal working press [20], where the punch is the moving part as illustrated in Figure 17.

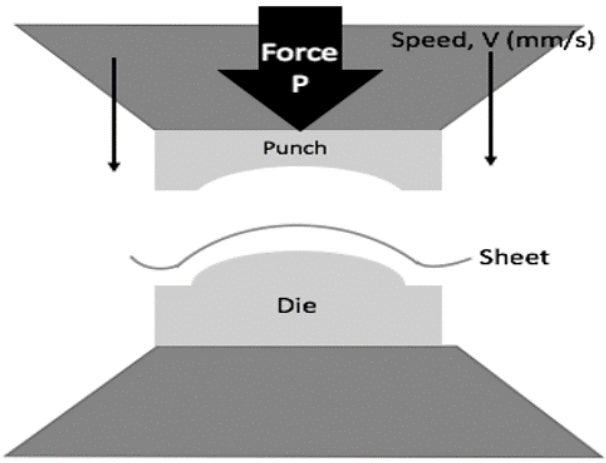

Figure 17: Press forming of high strength aluminium alloy sheet.

Press hardening or die quenching is a method originally applied on high strength steel to produce light weight components for the automotive industry. The method combines forming, hardening and heat treatment in one single process step and induce good formability and weak springback. Other advantages associated with this technology are lower die pressure, high dimensional accuracy, cost effectiveness and the ability to control the material properties by for example tailored tempering or quenching. Challenges associated with hardening of steel are the complex physical phenomena involved such as plastic deformation, heat transfer and microstructural changes [38, 49]. An illustration of a typical process chain in direct press hardening of steel is shown in Figure 18.

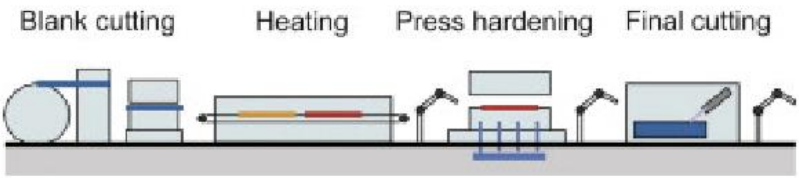

Figure 18: Process chain for press hardening of steel blanks.

The press form hardening method for aluminium applications is quite new and still under development. The method permits integrated hardening and forming of complex geometries. Hot forming of aluminium is beneficial compared to cold forming in terms of formability, ductility, springback and microstructural control.

In practice the aluminium sheet is solution heat treated before it is brought directly from the furnace to a water cooled pressing tool, that ideally holds a temperature below room temperature. The forming starts slightly below solution heat treatment temperature due to air

cooling as the sheet is transported from furnace to the press. The sheet is formed and quenched simultaneously before the component is brought out of the press and stored at room temperature. After a period at room temperature, the component in its final shape is artificially aged at an elevated temperature. The reduction of process steps that is introduced by press form hardening makes the application aluminium components time saving, cost effective and therefore more competitive in the automotive industry.

3. Experimental work

The experimental work in this project has been conducted with a flat pressing tool attached to an MTS 311 - 1000kN hydraulic driven press. The intention was to simulate the industrial forming process of aluminium car components. As the pressing tool was new, and the method not yet developed, a practical and accurate procedure had to be developed before conducting the planned experiments. Therefore, some attention will be directed towards the development of the method in the following sections. Initially to the deformation experiments the material was characterized as delivered. Subsequently, strength and hardness measurements were done to analyse the effect of different quenching conditions and direct artificial aging in combination with deformation during testing. The methods used to conduct the experiments are described in this chapter.

The terminology used to address planes and directions in the hot-extruded flat profile is shown in Figure 19.

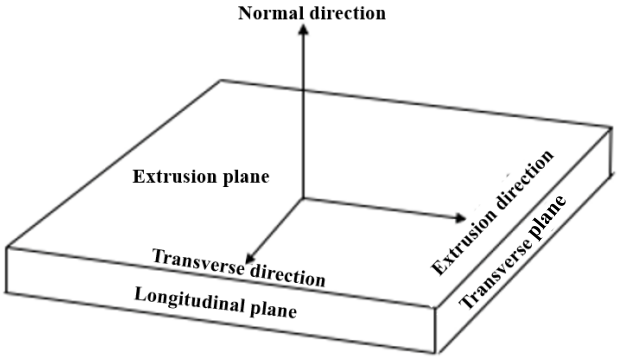

Figure 19: Terminology used to address the planes and directions in the extruded profile.

The alloy investigated in this thesis is delivered by Hydro Karmøy (billet) and extruded at HAP Raufoss. The alloy is classified as 6082.25. The flat profile was produced by direct extrusion in a 2200-ton press with a billet temperature of 510°C and air cooled from the extrusion temperature. The billet was extruded to a flat profile with a cross section of 152x4.6mm, which gives an extrusion ratio of 1:47. The profile was homogenized at 575°C for 2.25 hours.

The chemical composition of the extruded profile is shown in Table 2.

Table 2: Chemical composition of the extruded profile of 6082.25 given in weight percent.

6082.25	**Si**	**Fe**	**Cu**	**Mn**	**Cr**	**Mg**	**Zn**
Wt%	0.92	0.17	0.01	0.55	0.15	0.64	0.02

3.1 Microstructure characterization

The as-extruded base material was characterized to study the properties of the alloy as delivered. Some characterization of the material after treatment were also performed to observe any changes. The material properties were studied by different analysis methods such as light optical microscopy, SEM and EBSD, as summarized in Table 3.

Table 3: Analysis methods.

Property	Analysis method	Instrument	Preparation
Grain structure	Light Optical Microscopy	Leica MEF4M Optical Microscope	Grinding > 2.4μm Polishing > 1μm Anodized
Particle structure	SEM	FE-SEM Zeiss Ultra 55	Grinding > 2.4μm Polishing > 1μm
Texture	SEM (EBSD)	FE-SEM Zeiss Ultra 55, NORDIF	Grinding > 2.4μm Polishing > 1μm Electropolished

3.1.1 Grain structure

The grain structure in the extrusion plane, longitudinal plane and transverse plane was studied by light optical microscopy. Sample preparation included grinding to 2.4μm with SiC grinding paper and polishing with polycrystalline diamond suspension down to 1μm. Anodizing forms an oxide layer on the surface that changes the reflection of the different grains under polarized light. The anodizing was done with a voltage of 20kV for 120s with 5%HBF_4 – 95%H_2O electrolyte. Polarized light was used, and a sub-lambda plate was inserted to reveal the grain structure.

The grain structure was analysed as-extruded, after solution heat treatment and after deformation and quenching from solution heat treatment. The latter was done to determine any effects of the grain structure on the subsequent tensile testing and hardness measurements.

3.1.2 Particle structure

The particle structure was examined by scanning electron microscopy (SEM) in the extrusion plane, longitudinal plane and transverse plane. Sample preparation included grinding to 2.4μm with SiC grinding paper and polishing with polycrystalline diamond suspension down to 1μm. The pictures were taken with a working distance of 20-25mm, magnification of 350X and a voltage of 20kV. Detection of secondary electrons (SE2) was used as imaging mode. A detailed investigation of the particle structure was not intended.

3.1.3 Texture

Texture of the base material was gained by using electron back-scattered diffraction (EBSD) to get an indication of mechanical anisotropy. Sample preparation included grinding to 2.4μm with SiC grinding paper and polishing with polycrystalline diamond suspension down to 1μm.

Electropolishing was done with A2 electrolyte at a voltage of 20kV for 20s. The temperature of the cooling unit was set to be -30^{o}C.

The EBSD patterns were obtained from the fibrous grain structure area in the longitudinal plane with a magnification of 200X, accelerating voltage of 20kV, aperture of 300 μm, high probe current and a tilt angle of 70^{o}. Detection of secondary electrons (SE2) was used as imaging mode. EDAX Orientation Imaging Microscopy software was used to index and analyse the patterns.

The texture was obtained from as-extruded samples and after deformation and quenching from solution heat treatment. The texture analysis was done to obtain an indication of any changes in texture during hot forming and in-die quenching, and of the degree of mechanical anisotropy in the material. A detailed investigation of texture or texture evolution was not intended. The scan was obtained from an area of 0.16mm^2, shown in Figure 20.

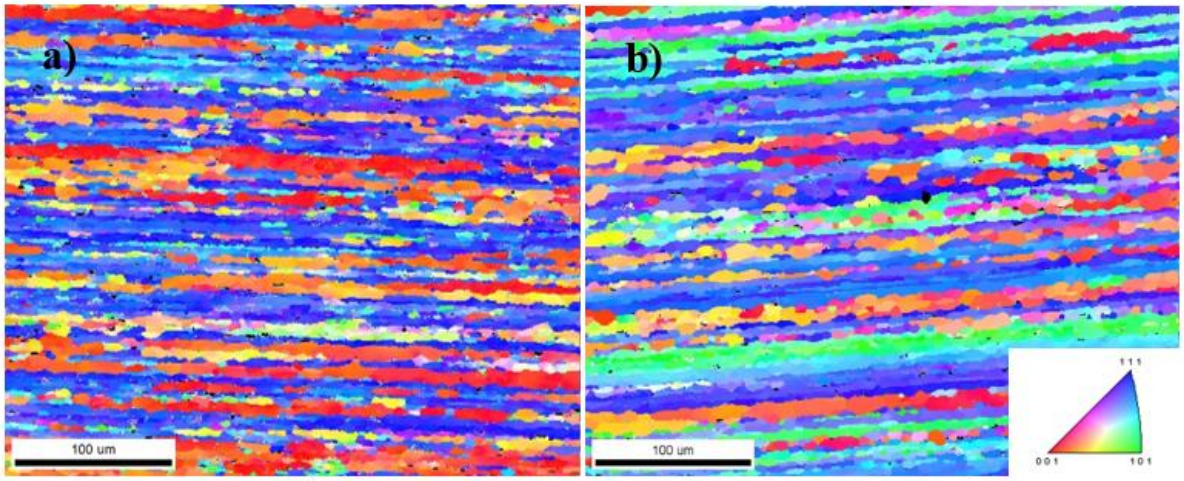

Figure 20: Scan area in EBSD with corresponding inverse pole figure. The scans areas are obtained from the longitudinal plane of samples a) as-extruded and b) after solution heat treatment and deformation.

3.2 Integrated hot forming and in-die quenching

The test set-up included solution heat treatment in a Naberterm N15 air circulation furnace, deformation in a flat pressing tool attached to a MTS 311 - 1000kN hydraulic driven press and artificial aging in oil bath as shown Figure 21. The design, function and purpose of the pressing tool, as well as the method development and final test procedure, are presented in the following sub-sections.

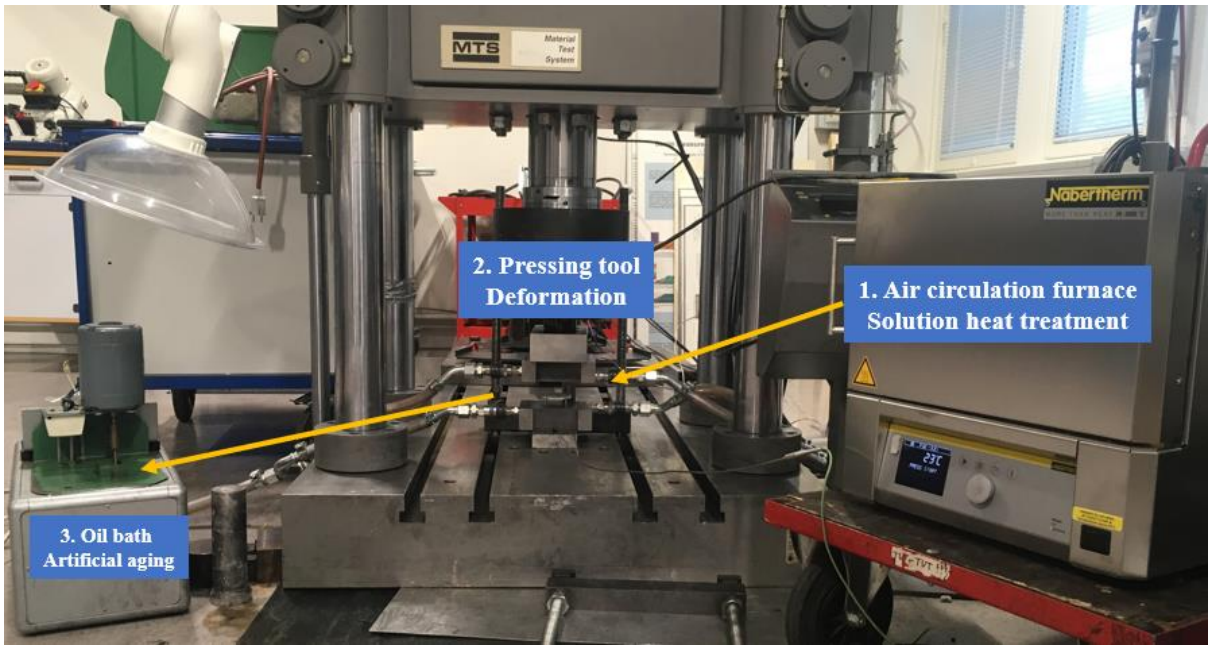

Figure 21: The test set-up including (1) air circulation furnace for solution heat treatment, (2) pressing tool for hot deformation and quenching, and (3) oil bath for artificial aging.

3.2.1 Design, purpose and function of the pressing tool

To introduce deformation of the material to the quenching sequence, a flat pressing tool was designed and built by AP&T. The tool is shown in the picture in Figure 22. To get a fast and reproducible cooling rate, the upper and the lower dies were built with water channels with inlet on one side and an outlet on the opposite side at which water hoses were attached to provide a waterflow through the dies. That way, the tool can be constantly water-cooled during testing. Four spikes are attached to the lower die, standing on springs, with the purpose of holding the sample a certain distance above the lower die to avoid heat transfer and excessive cooling of the hot sample before compression. During testing, the upper die presses the sample and spikes until the sample comes into contact with the lower die. As the upper die is raised, the sample is lifted by the spikes and separated from the lower die, which reduces the cooling rate of the samples after abrupt compression and cooling at elevated temperatures.

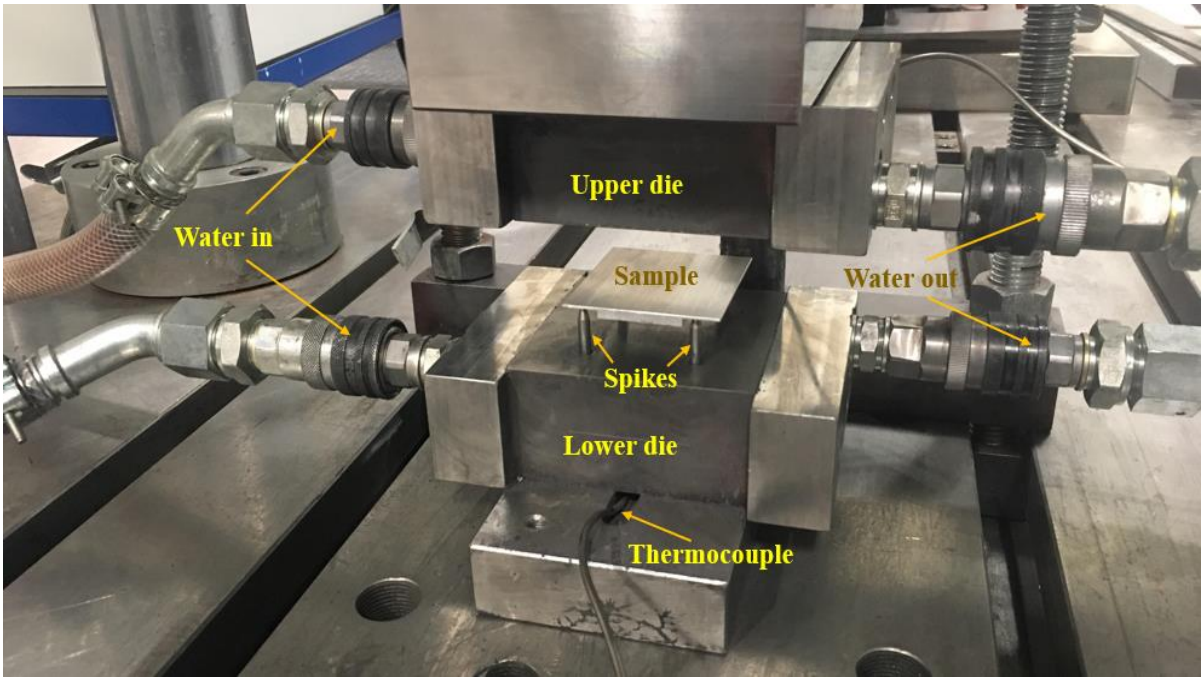

Figure 22: A picture of the pressing tool showing the different components and functions.

The centre distance between the spikes are 60 and 46mm, and the samples were placed freely on top of the spikes. The dimensions of the samples were therefore decided to be 70x55mm. However, the surface area of the samples proved to be too large as the force required to achieve the desired amount of deformation exceeded the capacity of the press. Therefore, the test area of the samples had to be reduced, but at the same time be large enough to fit on top of the spikes without sliding off. The area reduction of the samples was done by milling "wings" on the samples as shown in Figure 23.

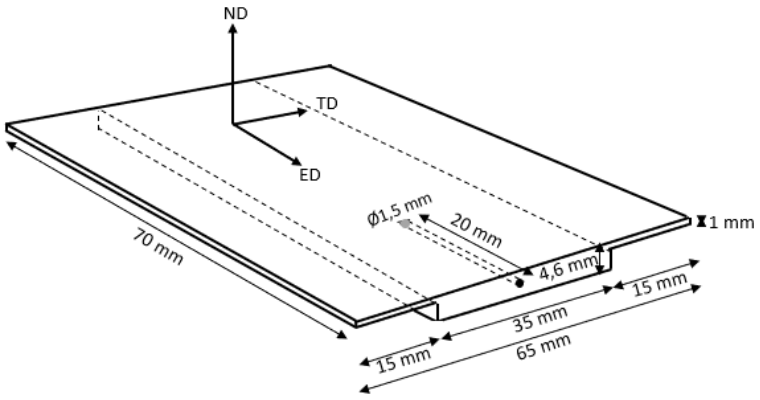

Figure 23: Sample dimensions and directions used for hot forming and in-die quenching experiments.

Lubricant was used to reduce the friction during testing as well as assuring an even heat transfer as the lubricant fills vacant surface unevenness. Molykote G-Rapid Plus was sprayed as a thin layer on the tool surfaces. This is a lubricant with mineral oil that provides low friction, high pressure absorption and prevents stick-slip, scoring, seizing and fretting corrosion.

3.2.2 Method development

To achieve reproducible and accurate experiments some initial adjustments had to be done prior to the planned experiments. The method had to be developed from scratch as the tool had not before been used. Software parameters for the hydraulic press also needed iterations in order to obtain a well-functioning deformation sequence.

Deformation speed, degree of deformation, deformation temperature, cooling rate and lubrication were important parameters to customize to get valid and accurate results. The intention was to simulate the industrial process as close as possible. The deformation is preferentially performed in the higher temperature range of the cooling curve for increased formability and reduced springback issues. This requires a high deformation speed and strain rate as the sample is quenched to room temperature in few seconds.

The maximum speed of the press-piston was 25mm/s. The null position of the tool, i.e. the distance between the upper and lower tool surfaces, was set to be equal to the original sample thickness, thus the distance was approximately 4.5mm. The start position in the experiments was 50mm above zero, hence the time from start position to null position was 2 seconds. As contact was reached between the tools and the sample, the speed was reduced to 5mm/s for deformation. The desired degree of deformation was 15%, and therefore a thickness reduction of 0.675mm, i.e. from 4.5mm to 3.825mm. The deformation time was calculated to be 0.135s, which should be sufficient to finish deformation in the higher temperature range. The speed reduction was necessary to assure small variations in thickness after deformation. A deformation speed higher than 5mm/s resulted in uncertainties regarding the final degree of deformation.

As for the degree of deformation, some challenges were encountered with respect to the position at which the upper tool should stop. It was set to be -1.3mm relative to the null position, as this resulted in a thickness reduction of about 15%. However, the reduction was not consistent for each test. On the lower tool, two cylindrical columns were mounted, which in combination with 3.825mm thick shims, were designed to provide mechanical stop for the press to get an accurate deformation for each experiment. The tool was designed to outstand the applied load, but still, did not have the tolerance for the force it was subjected to during testing, and the upper tool failed. A new plate for the upper tool was built, and mechanical stop was not further used in the experiments. As an alternative, more parallels were tested for those samples with high deviations in thickness reduction.

The temperature during cooling was logged for each test with intervals of 0.1 seconds. A thermocouple was attached to a hole in the sample with a diameter of 1.5mm and a depth of 20mm. As previously mentioned, water channels were built near the surface in both the upper and lower die, and tap water was supplied through an inlet and lead through the tool to the outlet to provide a continuous cooling of the tool. However, at constant water flow during the experiments, the cooling rate was too high to provide reproducibility to the experiments due to difficulties in the practical execution of the experiments. To get a somewhat lower cooling rate, the tool was water cooled until the start of the tests. This resulted in more heating of the tool surfaces during pressing, however not of a detrimental degree as the cooling rate was concluded to be sufficient to avoid precipitation. This allowed for a greater tolerance for operator delays

causing more decrease in temperature before starting the test. A slower cooling rate increases the possibility of stopping the cooling at the predetermined temperatures from which the samples should either be air cooled or brought directly to artificial aging.

To ensure low friction during testing and avoiding damages to the tool and sample, lubrication was used during the experiments. The lubrication was applied to the tool before starting the test. As for which lubrication should be used, two alternatives were tested. First, a thin layer copper paste spray was applied to the tool. Copper paste reduces the friction significantly as well as it has a high temperature tolerance. However, the high viscosity of the copper paste caused the sample to stick to the upper tool after deformation. This was unfavourable to the experiments as the contact between sample and tool after interrupted cooling would cause excessive cooling due to heat transfer.

Molykote G-rapid Plus spray was the second alternative. After application, the lubricant dries and becomes solid and powder-like, which eliminates the viscosity issues. The sample remained at the spikes when opening the tool after deformation. Molykote has a maximum temperature tolerance of 450^{o}C. The samples had a temperature of about 500^{o}C when reaching contact with the lubricated tool, however, only for milliseconds, and the Molykote seemed to not suffer for being exposed to these temperatures for such short times. Therefore, the Molykote was considered to be the best option for lubrication during testing.

The project experiments include samples being pressure cooled to selected temperatures between 70-200^{o}C before interrupting the quenching by raising the upper die. The high cooling rate caused challenges managing to open the press at the exact temperatures. Two options were considered; raising the upper die manually from the software or programming a pressure holding time of the upper die before it being raised automatically. Either way, it would result in deviations in temperatures at which the cooling was interrupted. However, it was concluded that the reaction time raising the upper die manually would cause larger uncertainty. A cooling curve was obtained by pressure cooling a sample to room temperature. From the cooling curve the cooling times to the different temperatures were obtained. The upper die was successfully raised at the highest chosen quench interruption temperature with a variation of about 200±5^{o}C. This variation decreased as the temperatures at which the quenching was interrupted decreased.

The press-cooling experiments are time sensitive, and after solution heat treatment, the temperature decrease of the samples need to be controlled in order to avoid sources of errors. A practical set-up of the equipment was necessary to achieve an effective and reproducible procedure for the experiments. The furnace and the oil bath were placed on either side of the press to ensure as short time as possible needed for transportation of the samples. For practical and safety reasons, two operators were needed to carry out the experiments. Operator 1 was handling the samples, while operator 2 was operating the software controlling the press.

3.2.3 Integrated hot forming and in-die quenching test procedure

Before executing the experiments, some preparations were necessary. A thermocouple was attached to the hole in the sample using a punch at the hole opening. The two ends of the conductors were joined by welding to ensure that the temperature was measured in the contact between the thermocouple and the end of the sample hole. Lubrication was sprayed on to the tool surfaces in a thin layer and the tool was water cooled shortly before starting the press. The upper tool was placed in start position, 50mm. The test matrix for the planned experiments is shown in Appendix A.

The following test procedure was established and applicated:

1. Solution heat treatment in air circulation furnace for 30 minutes at 540^{o}C.
2. The sample was brought out of the oven by operator 1 using a bent nose plier.
3. The moment the sample was out of the oven, a timer was started by operator 2, counting 6 seconds until test start.
4. The sample was placed on top of the spikes by operator 1.
5. After 6 seconds the press was started by operator 2, and simultaneous deformation and quenching of the samples were conducted.
6. a) For the samples being directly brought to artificial aging: The press was opened automatically as the sample reached the predetermined temperature. Operator 1 removed the sample from the spikes, cut off the thermocouple, attached a steel wire to the sample using a paper clip and lowered the sample into the oil bath for artificial aging for 3 hours at 190^{o}C. This part of the procedure is illustrated in Figure 24.
   b) For the samples stored at RT for 30 minutes: The press was automatically opened as the sample reached the predetermined temperature. It was left on the spikes allowing further cooling in air exposure. After 30 minutes, the thermocouple was cut off, a steel wire attached by paper clip and the sample were lowered into the oil bath for artificial aging for 3 hours at 190^{o}C. This part of the procedure is illustrated in Figure 25.
   c) For the samples cooled to room temperature: The press was opened manually as the sample reached a temperature of 30-40^{o}C. The thermocouple was cut off, a steel wire was attached, and the sample was either stored at room temperature for 30 minutes or brought directly to oil bath for artificial aging.
7. After artificial aging, the samples were brought out of the oil bath and quenched in water before being washed and cleaned to remove any remains of oil and lubricant.

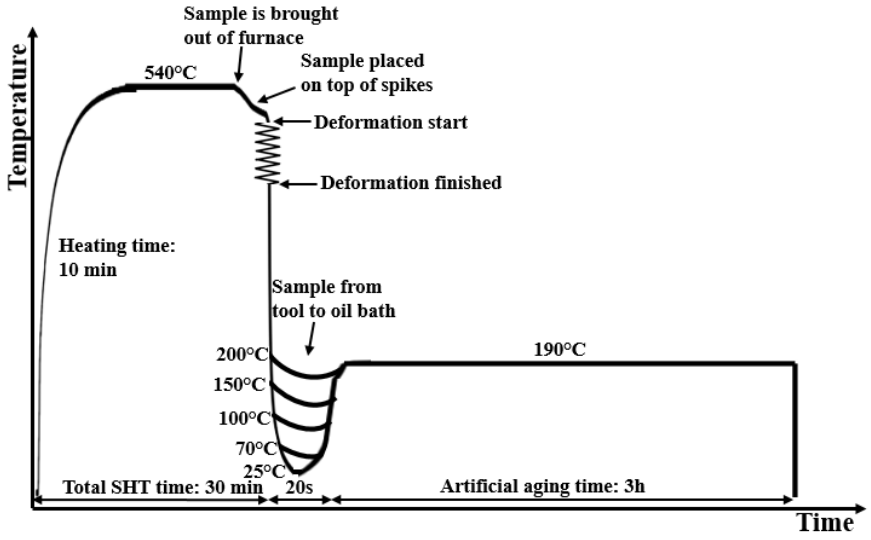

Figure 24: An illustration of the integrated hot forming and in-die quenching heat treatment sequence for samples being directly artificially aged.

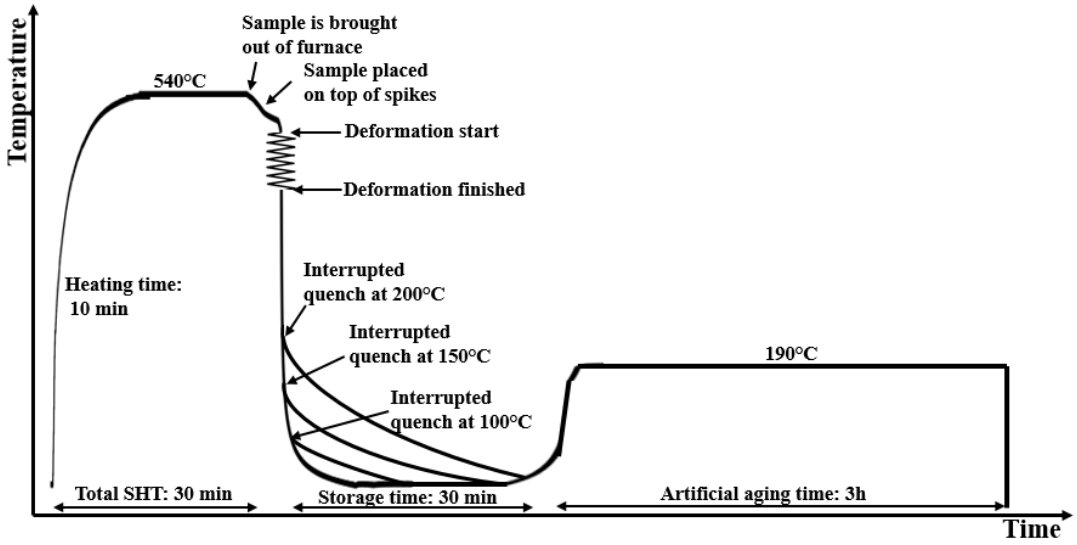

Figure 25: An illustration of the integrated hot forming and in-die quenching heat treatment sequence for samples being stored at room temperature before artificial aging

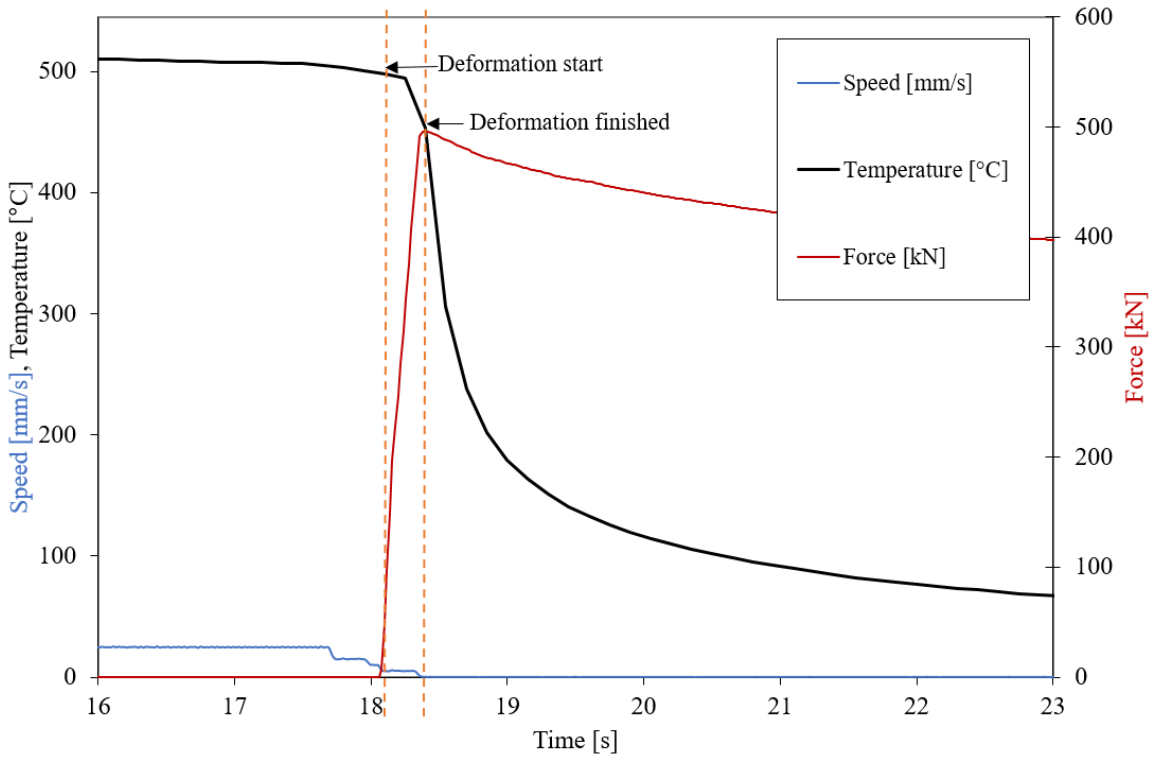

Figure 26: Experiment data from sample deformation. Temperature, die speed and force as functions of time.

Figure 26 shows data obtained from one test with forming and quenching to room temperature. The blue line represents the speed of the upper die. The black line is the cooling curve. And the red line shows the force applied by the piston. From a distance 50mm to 5mm the speed was set to 25mm/s. From 5mm, as the tool pushes down the sample and spikes, the speed is reduced to 15mm/s and 10 mm/s until zero position (sample thickness) is reached. Then the sample is deformed at a speed of 5mm/s until the tool reaches position -1.3mm. The upper die is kept at this position with force until the sample reaches the desired temperature, before the die is raised, and the test is finished. The force required to deform the sample is about 500kN, which equals 50 tons. The temperature during deformation decreases from about 505°C to 450°C.

3.3 Mechanical test methods

The effects of the experiments on the mechanical properties was measured by hardness measurements, tensile tests and electrical conductivity measurements.

3.3.1 Hardness measurements

An Innovatest Nova 360 micro-macro Vickers & Brinell hardness tester was used to measure Vickers hardness of the material, i.e. a measure of the ability of the material to resist plastic deformation. A load of 5 kg was used to set the indentation with a holding time of 10 seconds. The samples were initially grinded to get distinct indentations in the material surface. The hardness was measured on the extrusion plane with 10 measurements per sample, and with 3 parallels for each case. A total of 30 hardness measurements were done per case.

3.3.2 Tensile testing

Tensile tests were conducted with a Zwick Roell Z2.5 micro tensile testing machine. Three samples were obtained from the longitudinal plane (cross section) in the extrusion direction as illustrated in Figure 27, together with the dimensions of the tensile specimens. 3 parallels for each case equals 9 parallel tensile specimens per case. The results from the tensile tests will be discussed by terms and definitions obtained from [50], as shown in Figure 28.

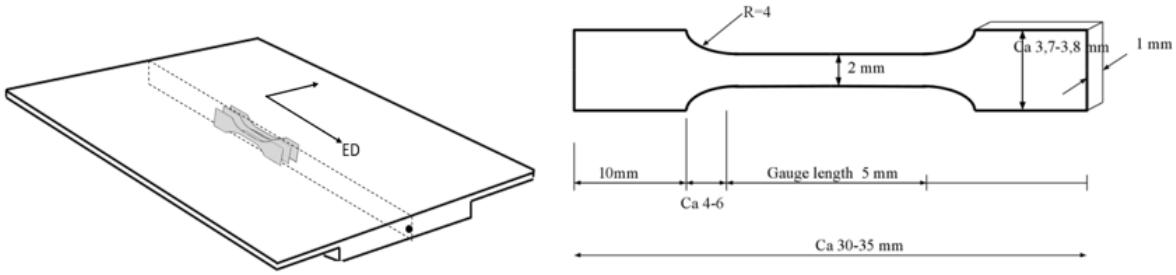

Figure 27: Tensile specimen dimensions and the position in the sample from which they were obtained.

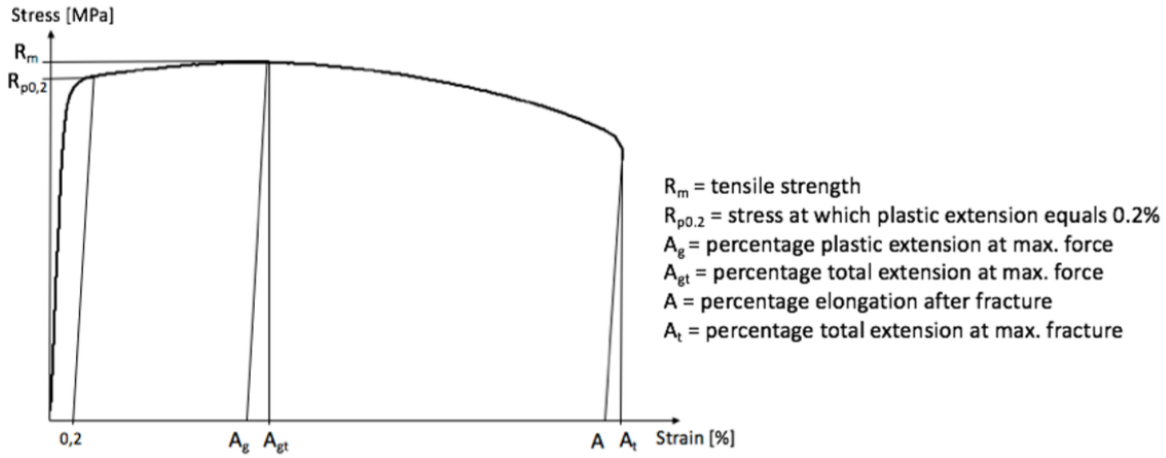

Figure 28: Terms and definitions used to address the results from the tensile tests.

3.3.3 Electrical conductivity

The peak hardness, and thereof the artificial aging time of 3 hours, of the 6082.25 alloy was found in the specialization project [3] and applied to this project. Due to differences and variations in time and temperatures in the heat treatment sequence, the hardness curve might have shifted in some cases, causing need of adjustments in artificial aging time to achieve T6. Electrical conductivity can give an indication of the degree of precipitation in the alloy as it decreases with increasing precipitation or aging time. The electrical conductivity was measured in the extrusion plane of all samples with Foerster Sigmatest 2.069 after treatment.

4. Results

The results from the experiments described in Chapter 3 is presented in this chapter. This includes images obtained from microstructure characterizations, and hardness measurements and stress-strain curves from the samples being subjected to the hot deformation and in-die quenching experiments. Additional results from light optical microscopy are shown in Appendix B and values obtained from the tensile tests are listed in Appendix C.

4.1 Microstructure characterization

The images obtained from grain structure, particle structure and texture analysis of the base material are presented in the following sections. Characterizations for the different treatments were conducted for comparison.

4.1.1 Grain structure

The grain structure was examined for the alloy, as-extruded and after the hot deformation and in-die quenching experiments. The latter was done to determine any changes in the grain structure after subjection to solution heat treatment and deformation. Figure 29 - Figure 31 show images of the extruded plane, longitudinal plane and transverse plane for as-extruded samples and is compared to solution heat treated samples.

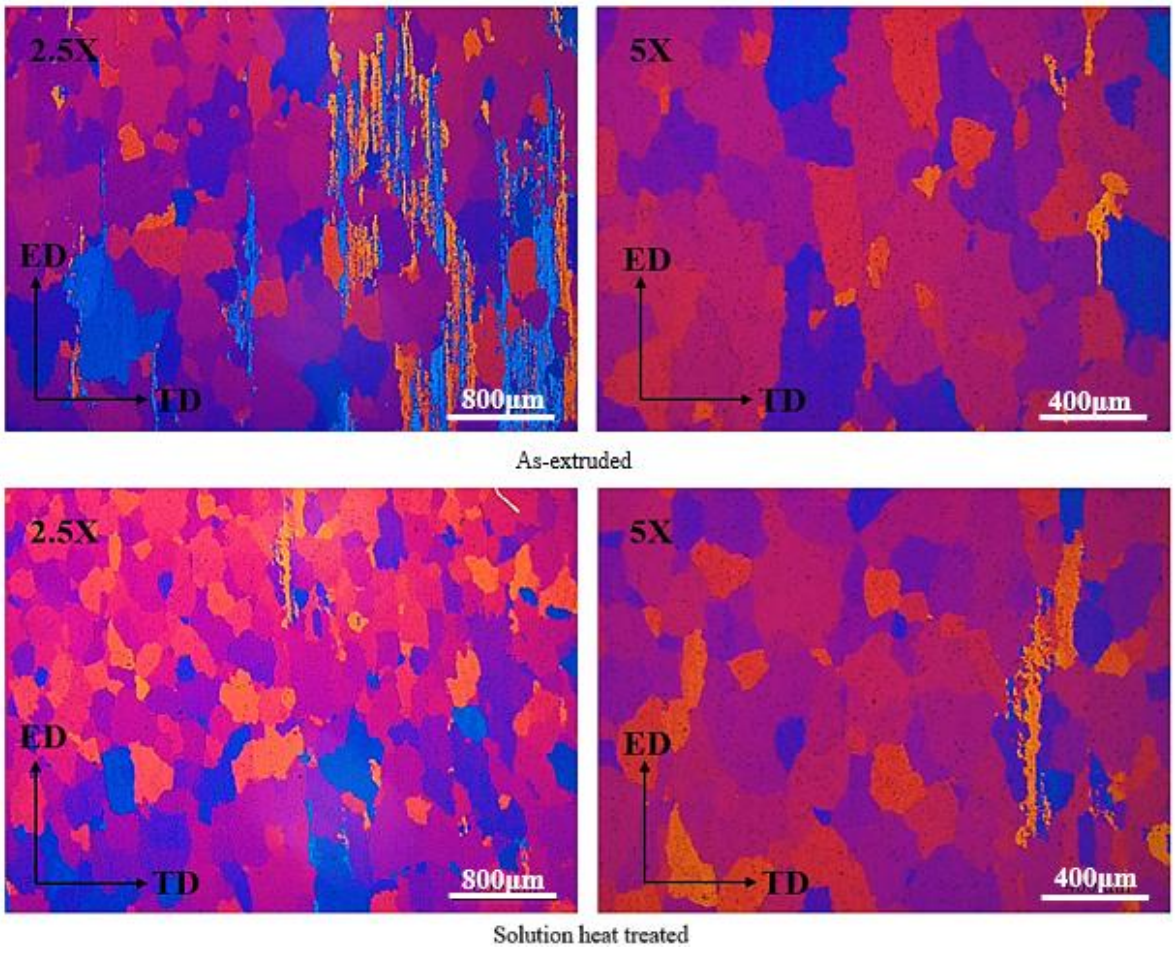

Figure 29: The grain structure in the extrusion plane (the surface) as-extruded and after solution heat treatment. The left images have magnifications of 2.5X and the right images have magnifications of 5X.

In Figure 29, the grain structure in the extrusion plane shows recrystallized grains in the surface of the samples both before and after solution heat treatment. This is recognized by large equiaxed grains. The unrecrystallized as-extruded grain structure is easily recognized by a fibrous grain structure. During sample preparation the sample surface was grinded and polished, and in some places, the fibrous grain structure has become visible from underneath the sample surface recrystallized layer.

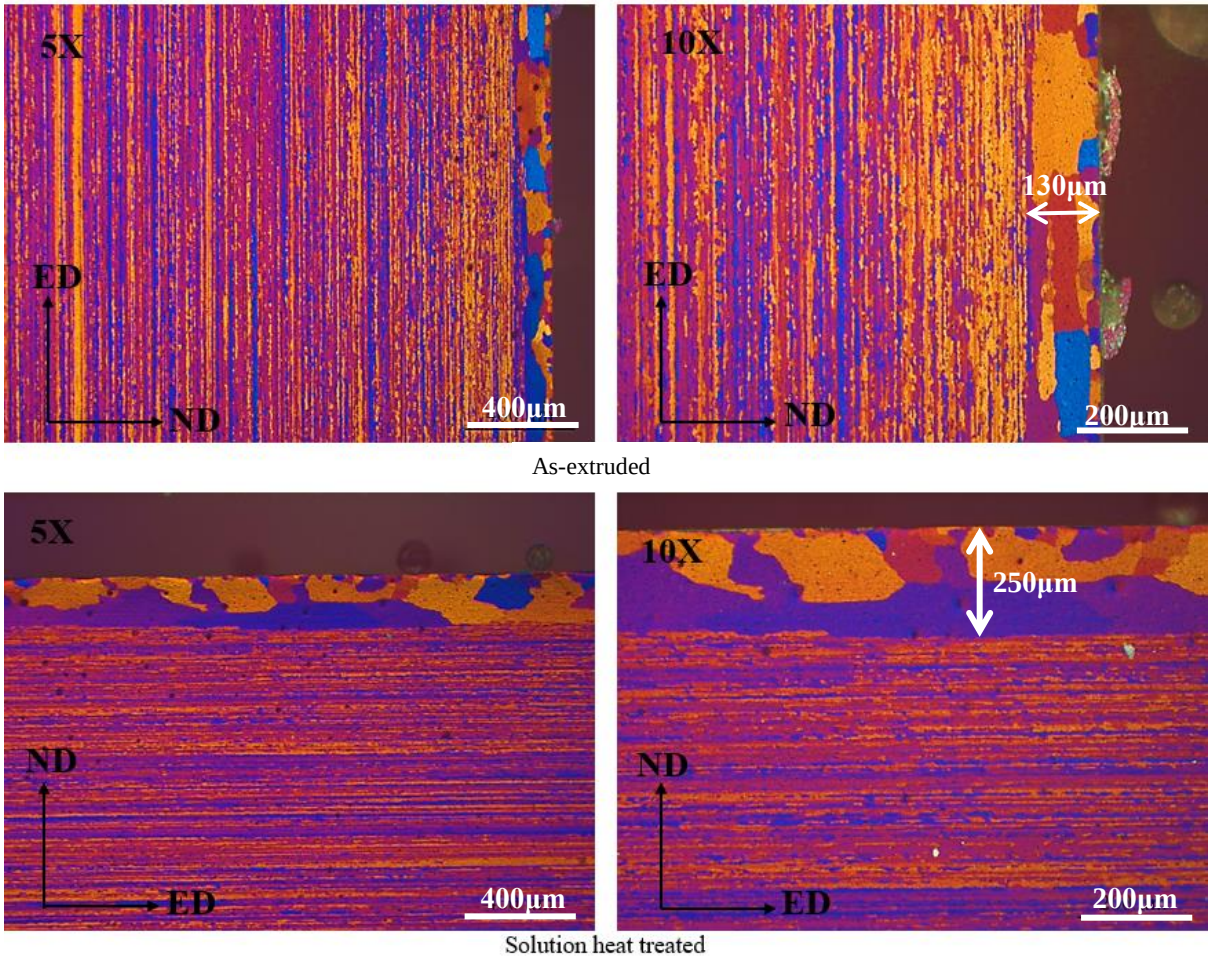

Figure 30: The upper images show the grain structure in the longitudinal plane in an as-extruded sample at two magnifications, 5X and 10X. The lower images are obtained from a sample after solution heat treatment at magnifications 5X and 10X.

In Figure 30, it is visible that recrystallization has occurred as a thin surface layer. The thickness of the layer can be approximated to be 130µm in the as-extruded sample and 250µm in the solution heat treated sample. The fibrous structure beneath the recrystallized surface shows no sign of recrystallization. The recrystallized surface in the solution heat treated sample is thicker than for the as-extruded sample.

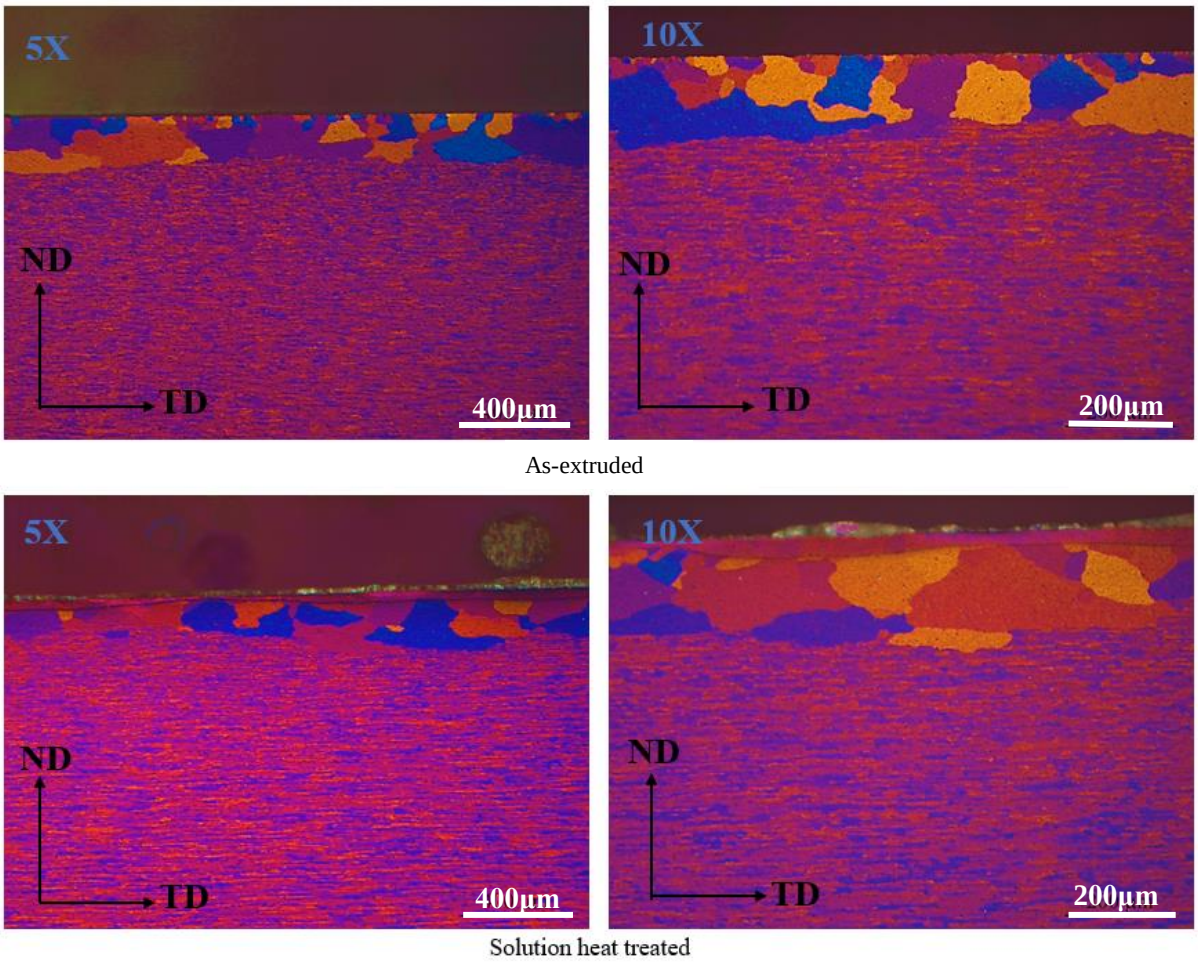

Figure 31: Images of the grain structure in the transverse plane. The upper images show the grain structure in an as-extruded sample at two magnifications, 5X and 10X. The lower images are obtained from a sample after solution heat treatment at magnifications 5X and 10X.

The images from the transverse plane in Figure 31 shows the recrystallized layer on the surface, as-extruded in the upper images and after solution heat treatment in the lower images. The thickness for the two cases also appears to be similar. However, some variation in the thickness can be observed from the images. A thicker recrystallized surface of the solution heat treated sample is not observed here.

As the thickness of the recrystallized layers appears to be varying along the extruded profile, additional characterization was done on selected samples from the delivered profiles. This was done to observe any severe changes in the recrystallized surface thickness along the profile. While exceeding a certain thickness, the recrystallized layer may have detrimental effects if included in the tensile specimens.

The width of the tensile specimens was 2mm (=2000µm) and the original sample thickness was approximately 4.5mm. A critical thickness of the recrystallized layer would be the tensile specimen width subtracted from the thickness of the sample the specimen was obtained from, divided by two surfaces, i.e. (4.5mm – 2mm)/2 = 1.25mm. The thicknesses of the deformed samples were 3.8mm which give a critical thickness of the recrystallized layer of 0.9mm in order to avoid inclusion of the recrystallized surface in the tensile specimens.

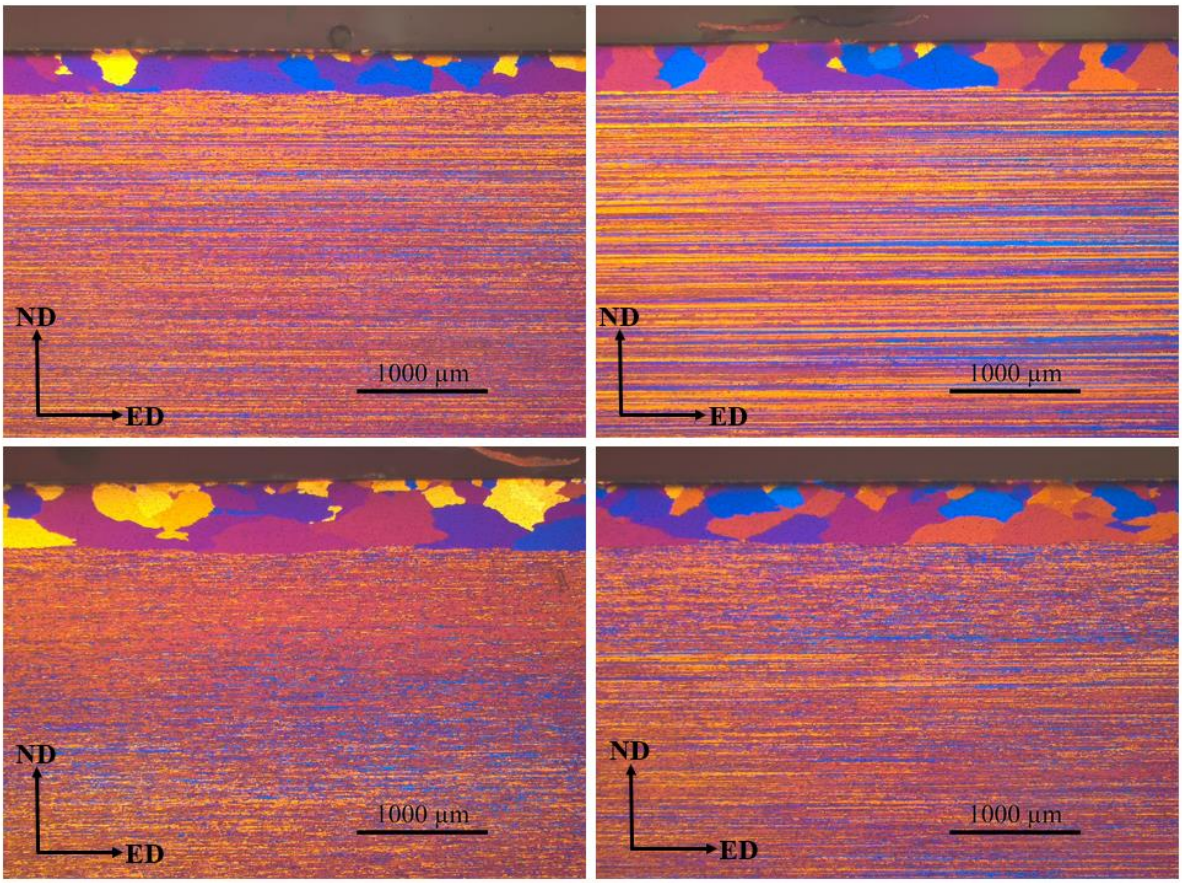

Figure 32: Selected samples obtained randomly from areas along the profile, as-extruded.

A representative selection of the images obtained randomly from the delivered profile is shown in Figure 32. More images from the initial grain structure investigations are shown in Appendix B1. The most severe cases of the recrystallized surface observed in the delivered profile are shown in the figure. The maximum thickness of the samples was measured to be 600µm.

Due to deviations in tensile test results in the sample parallels within one case, selected samples within the same case were studied in light optical microscopy subsequent to deformation and quenching from solution heat treatment, and artificial aging. The intention was to determine whether the recrystallized surface might have been the cause of the deviations. Three parallel samples within the same treatment are shown in Figure 33.

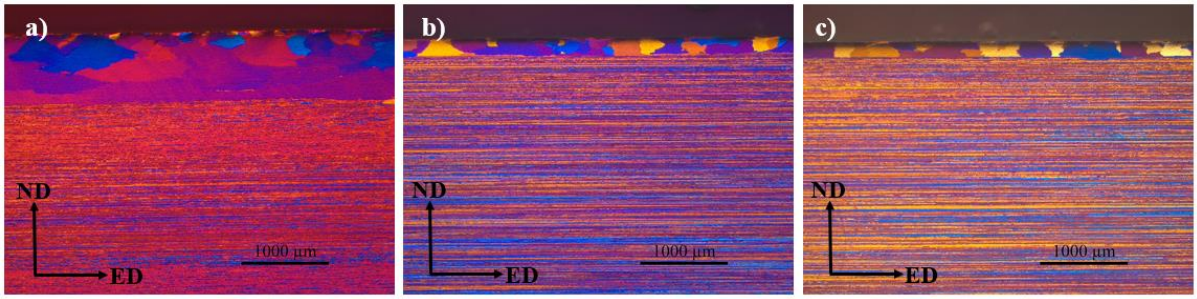

Figure 33: Samples being tool quenched after solution heat treatment and artificial aging. The samples are parallels of the same treatment. Image c) is obtained from a sample having high deviations in the tensile tests (high strength) compared to its parallels a) and b).

The images in Figure 33 show the recrystallized layers of samples after solution heat treatment, tool quenching and artificial aging. Sample a, b and c are the three parallels within one case where the tensile tests from sample c showed a significantly higher strength than the specimens obtained from sample a and b. Sample a have the thickest recrystallized surface layer of 1000µm and sample b and c have layer thicknesses of 200µm.

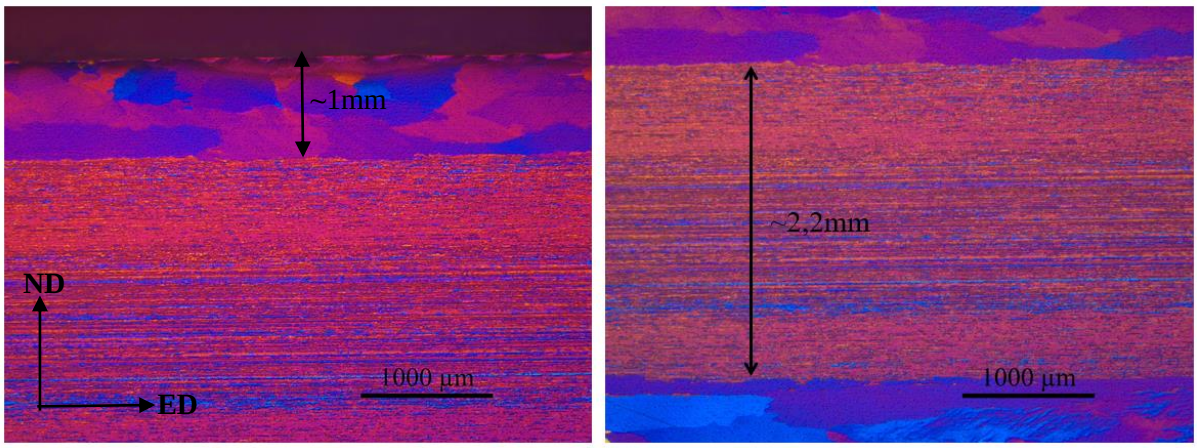

Figure 34: Sample a) showing the recrystallized layer on both surfaces and a measurement of the width of the original fibrous grain structure (ref. Figure 33).

Figure 34 shows measurements of the recrystallized layer of sample a from Figure 33. The recrystallized layer has a thickness of approximately 1mm, and the thickness of the fibrous grain structure layer is approximately 2.2mm. As compared to the 2mm thick tensile specimens, this indicates that the recrystallized layer is avoided in the tensile specimens.

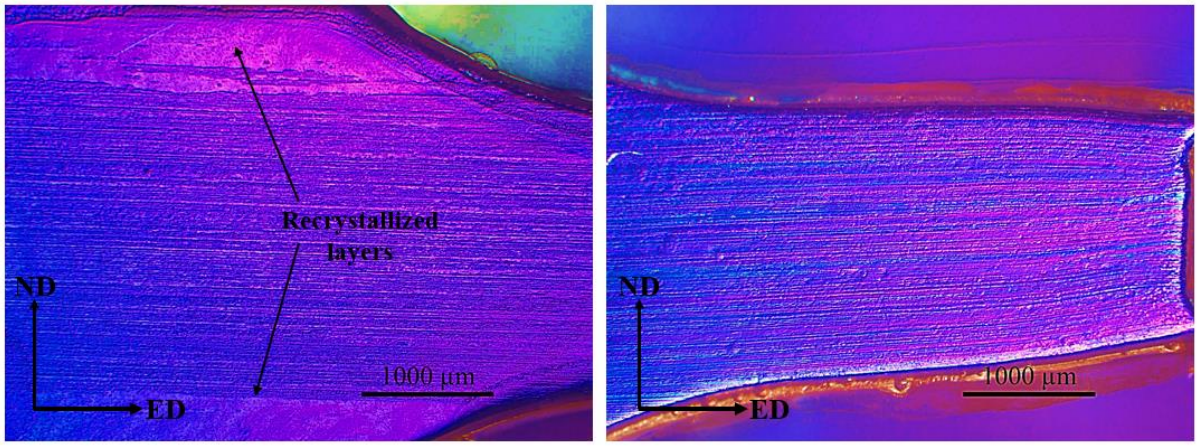

Figure 35: Images of the a tensile specimen from parallel a) (ref. Figure 33).

Figure 35 shows a tensile specimen obtained from sample a, ref. Figure 33. Due to small specimen dimensions, the anodization and resulting grain structure visible in light optical microscopy was not optimal. The recrystallized surface can be observed in the left image on the specimen grip section, and in the right image the test area does not appear to contain any part of the recrystallized layer.

Several samples were studied in light optical microscopy after treatment to observe any changes in the recrystallized surface after heat treatment and deformation. Two samples showing the thickest surface layers are shown in Figure 36. The images after deformation not included in this chapter are shown in Appendix B2.

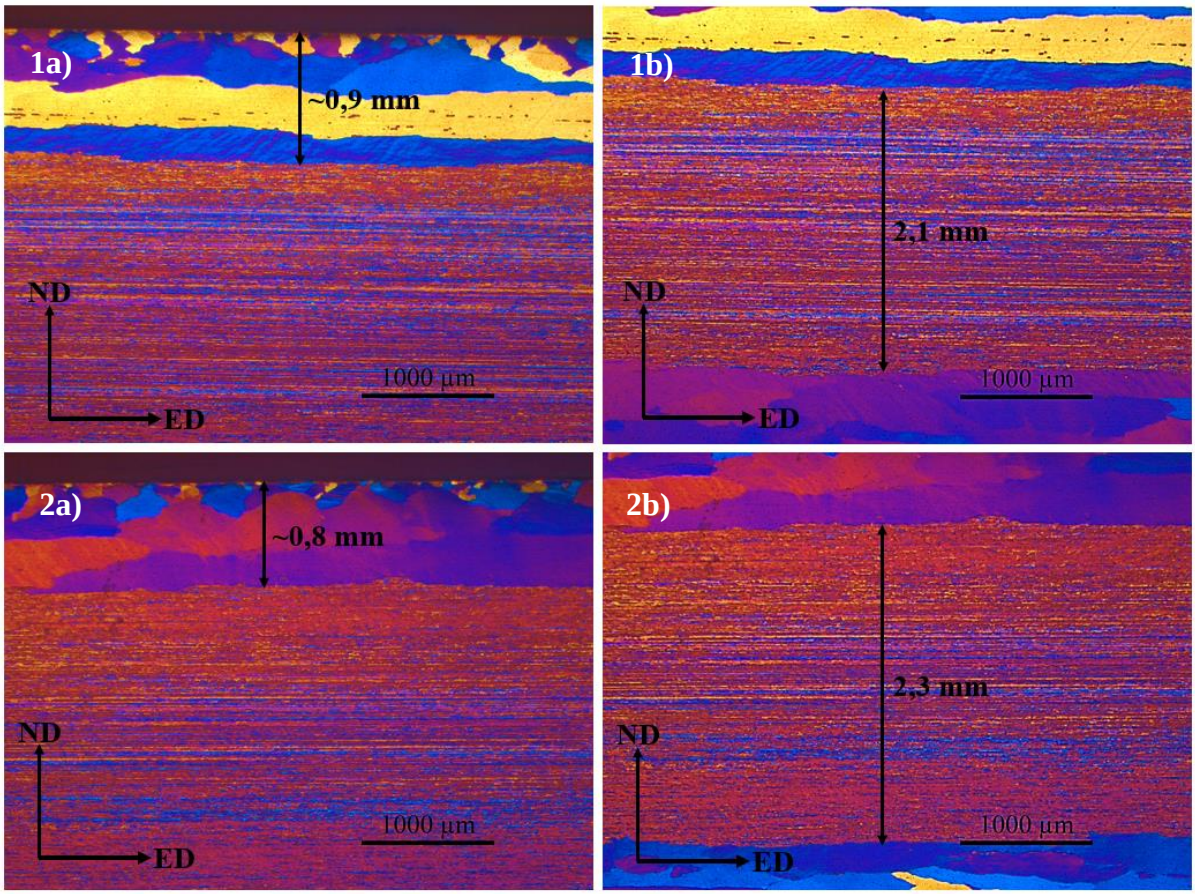

Figure 36: The grain structure of deformed samples referred to as 1 and 2 showing deviations in the tensile test results, i.e. lower tensile strength and yield strength compared to their parallels. The thickness of the surface layers are measured in 1a and 2a. The thickness of the interior fibrous grain structure are measured in 1b and 2b.

Figure 36 show the recrystallized layers of two selected samples after being simultaneously deformed and quenched to room temperature. These two samples showed the thickest recrystallization layers of the samples being controlled after heat treatment and deformation. In addition, these samples showed some deviations in the tensile tests with lower yield and tensile strength than their parallels. The sample thickness after deformation was approximately 3.8mm. Rough measurements of the recrystallization layers and the area between not being recrystallized indicate that the recrystallized layer is not included in the tensile specimen test area with a width of 2mm.

At the bottom of the surface layers, large elongated grains exceeding the image can be observed. The length of the grains cannot be measured as the magnification is too high, and the whole grain is not visible. In addition, it is not possible to determine whether the grain is pancake shaped or rod shaped as the grains only are captured from the longitudinal plane. This effect has not been further investigated in this project and will therefore not be discussed in detail.

4.1.2 Particle structure

The particle structure in the as-extruded profile was examined in the extrusion plane, longitudinal plane and the transverse plane. The results are shown in the SEM images in Figure 37 - Figure 40.

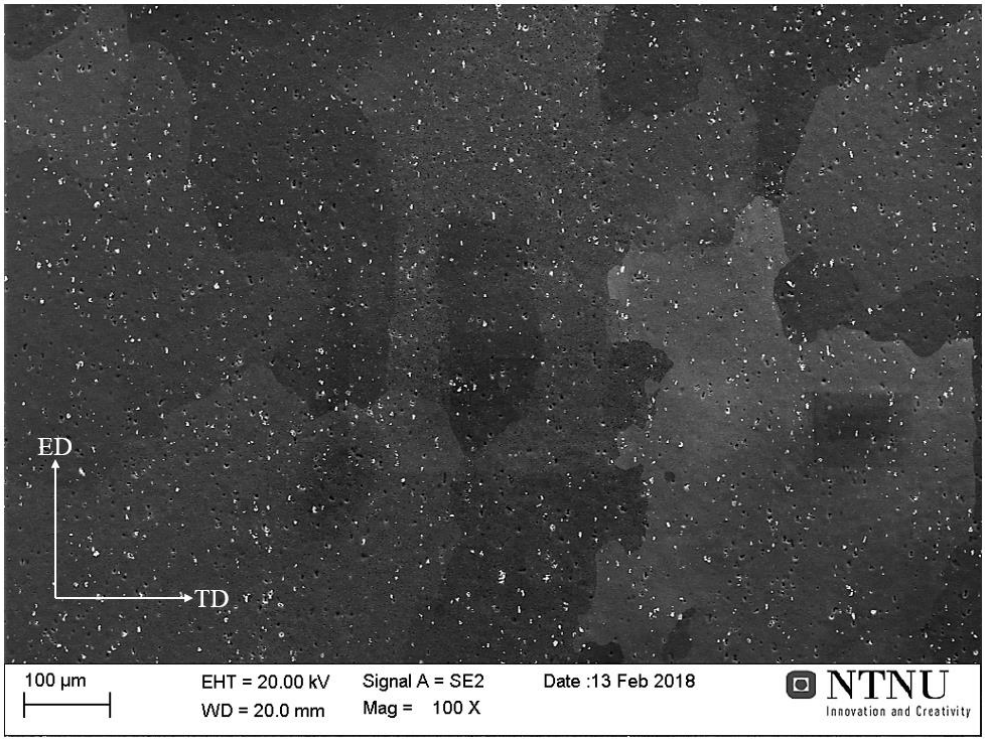

Figure 37: The particle structure in the extrusion plane at low magnification, 100X.

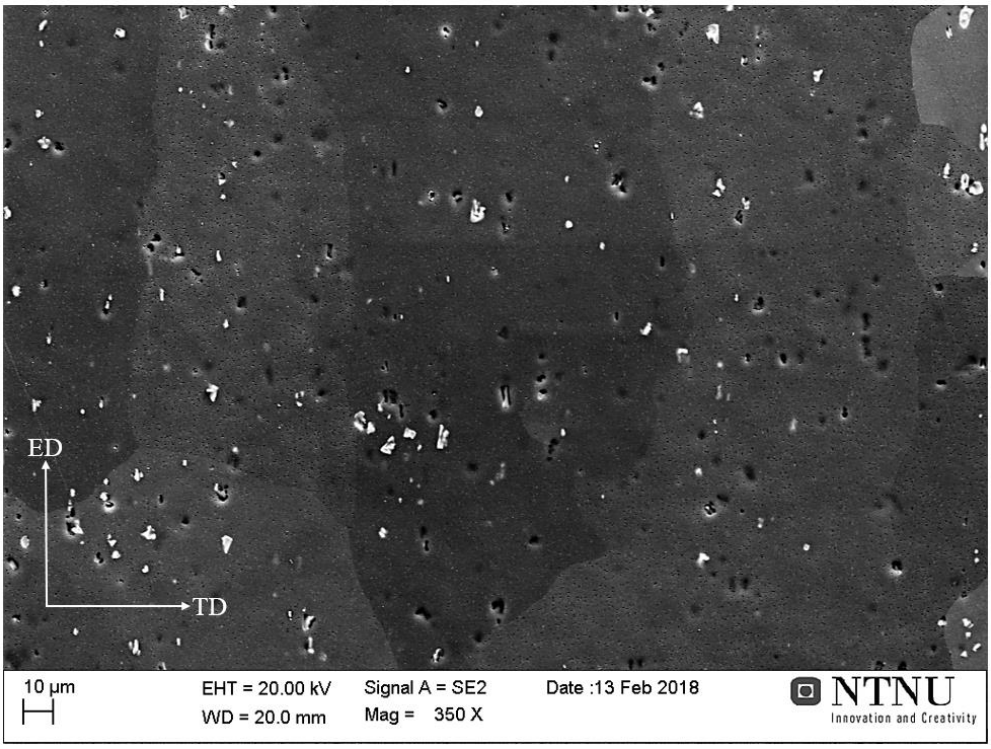

Figure 38: The particle structure in the extrusion plane, i.e. the surface, in an as-extruded sample with a magnification of 350X.

An image with relatively low magnification of 100X obtained from the extrusion plane is shown in Figure 37.

The image gives an indication of the particle density and distribution. The particles visible in the image are primary intermetallic particles of sizes between 2-5μm. The dispersoids are presumably too small to be visible at low magnifications. The particles seem to be homogeneously distributed. The surfaces of the extruded profile are recrystallized, which is visible in the extrusion plane in this image.

The particle structure in the extrusion plane is shown in Figure 38 at a higher magnification of 350X. The cavities are likely left after particles that was grinded or polished away during sample preparation. At some spots one can observe slight accumulations of particles. Due to the recrystallized surface, it is difficult to determine whether the accumulations are concentrated at the original grain boundaries.

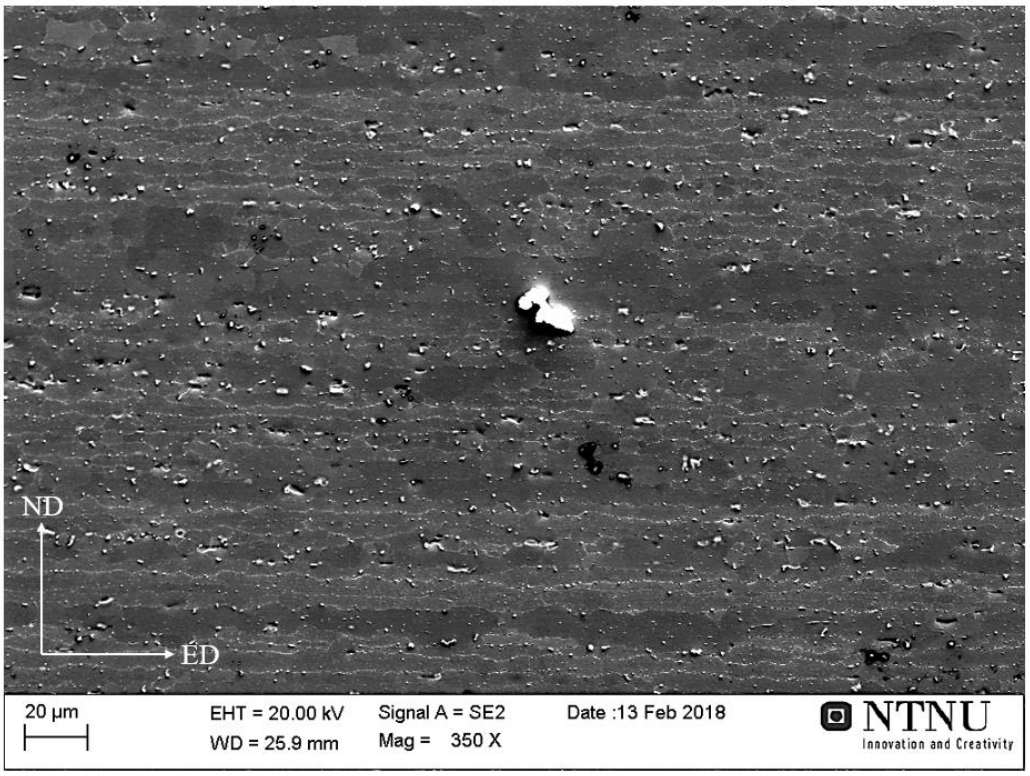

Figure 39: The particle structure in the longitudinal plane in an as-extruded sample with a magnification of 350X.

The particle structure in the longitudinal plane is shown in Figure 39. The particle distribution is dense, and the larger particles are elongated in the extrusion direction. Small particles aligned and concentrated at the grain or subgrain boundaries are barely visible. The sizes of the small particles are approximately 1μm.

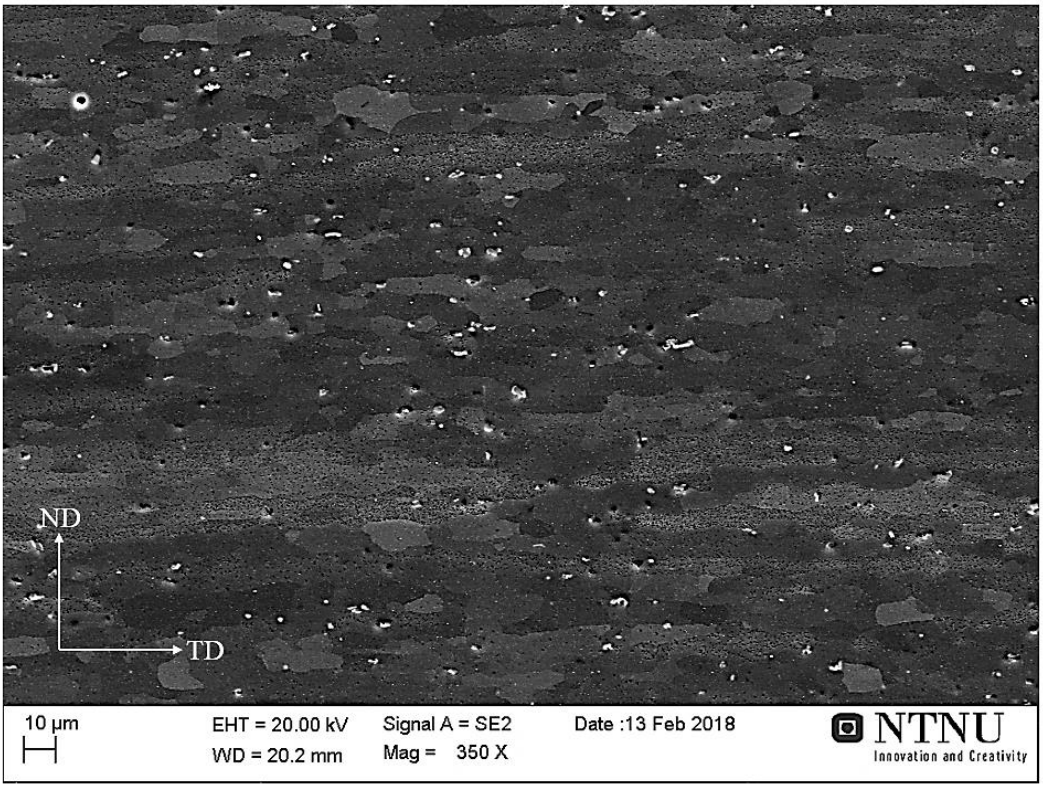

Figure 40: The particle structure in the transverse plane, i.e. the surface, in an as-extruded sample with a magnification of 350X.

Figure 40 shows the particle structure in the transverse plane. The larger particles seem to be of sizes 2-5µm. The particles do not have as significant elongated shapes as in the previous planes due to the extrusion direction being normal to the paper plane. Compared to the particle structure in the longitudinal plane, accumulations of small particles along the grain boundaries are not visible in this image.

4.1.3 Texture

The 111 and 100 pole figures obtained from the longitudinal plane of an as-extruded sample and from a sample after solution heat treatment and hot deformation are shown in Figure 41.

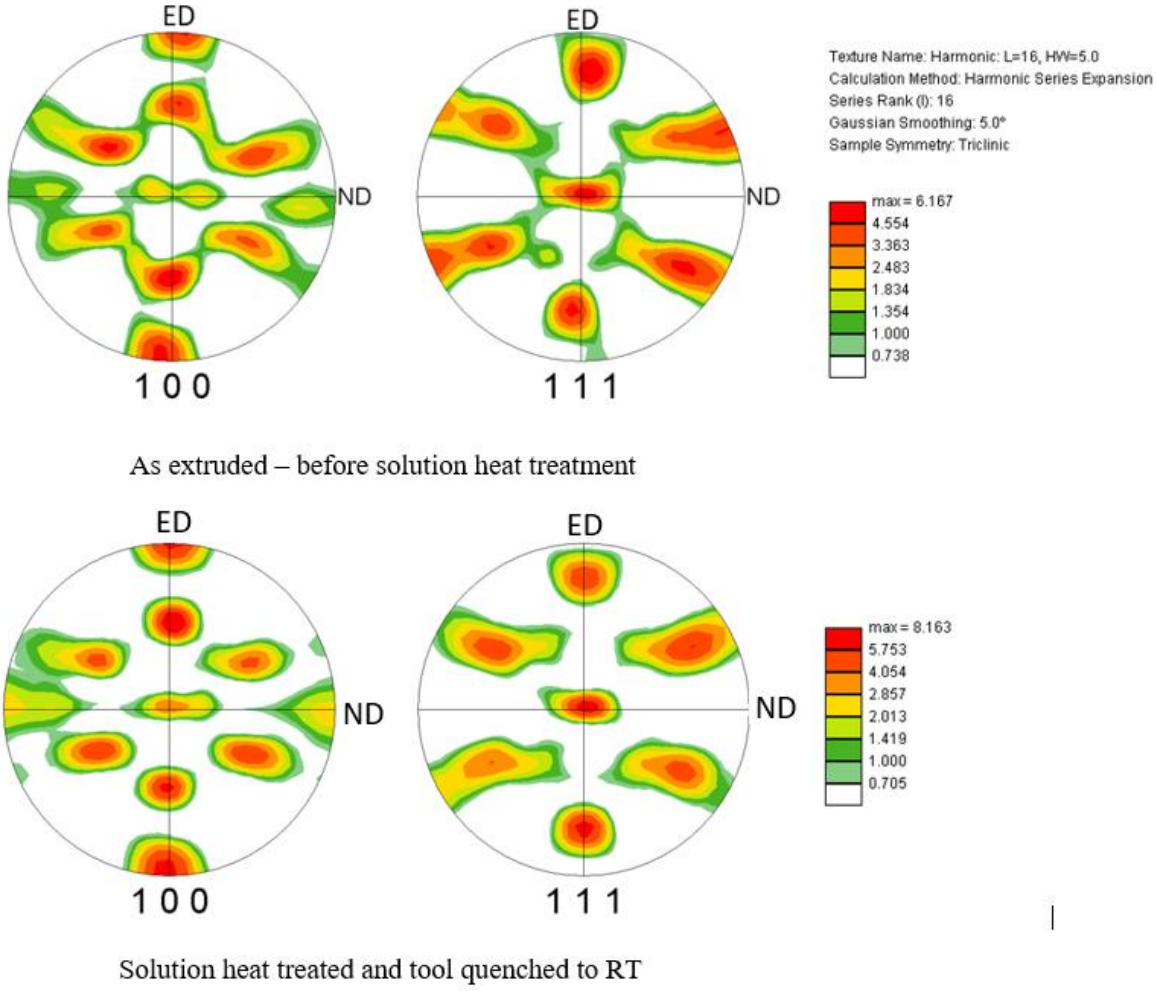

Figure 41: 100 and 111 pole figures obtained from the fibrous grain structure in the longitudinal plane, as-extruded and after deformation and quenching from solution heat treatment and artificial aging.

The texture in both pole figures show traces of cube {100}<100> and brass {110}< $1\bar{1}2$>. These are components normally expected in recrystallized materials. Comparing the two cases, as-extruded and after deformation, it can be observed that the texture components have not changed during deformation.

The maximum intensity for the as-extruded sample is 6.2 times random and for the solution heat treated and artificially aged sample the maximum intensity is 8.2.

4.2 Electrical conductivity

The results from the measurements of electrical conductivity are shown in Figure 42.

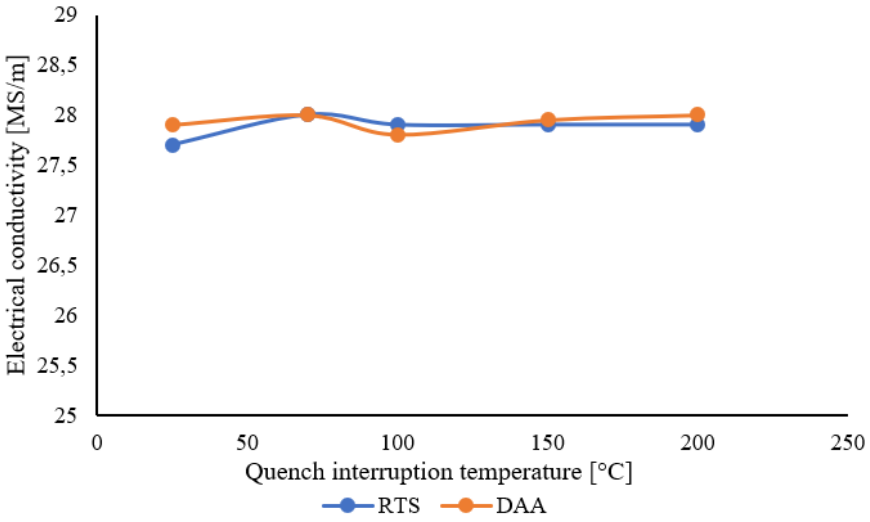

Figure 42: Electrical conductivity as a function of quench interruption temperature for samples being stored at room temperature or directly artificially aged.

As shown in Figure 42, all samples had a conductivity between 27.7 and 28MS/m, which means that the hardness curve is equal for all treatments, and are not affected by the variations in parameters throughout the experiments.

4.3 Integrated hot forming and in-die quenching

The results of the tensile tests and hardness measurements from the integrated hot forming and in-die quenching experiments are presented in this chapter. The effect of deformation, pre-cooling of tool, quench interruption and direct artificial aging have been investigated.

4.3.1 Effect of in-die quenching, pre-cooling of tool and deformation

The effect of die quenching was studied by conducting tests where the samples were die quenched in the dies from solution heat treatment without deformation. A pressure of approximately 10MPa of the upper die was held until the sample reached room temperature. The sample was either stored at room temperature for 30 minutes or directly artificially aged. Reference samples were water quenched after solution heat treatment before being stored at room temperature for 30 minutes or directly artificially aged. The hardness results are shown in Figure 43 and the corresponding tensile test results are shown in Figure 44 - Figure 46.

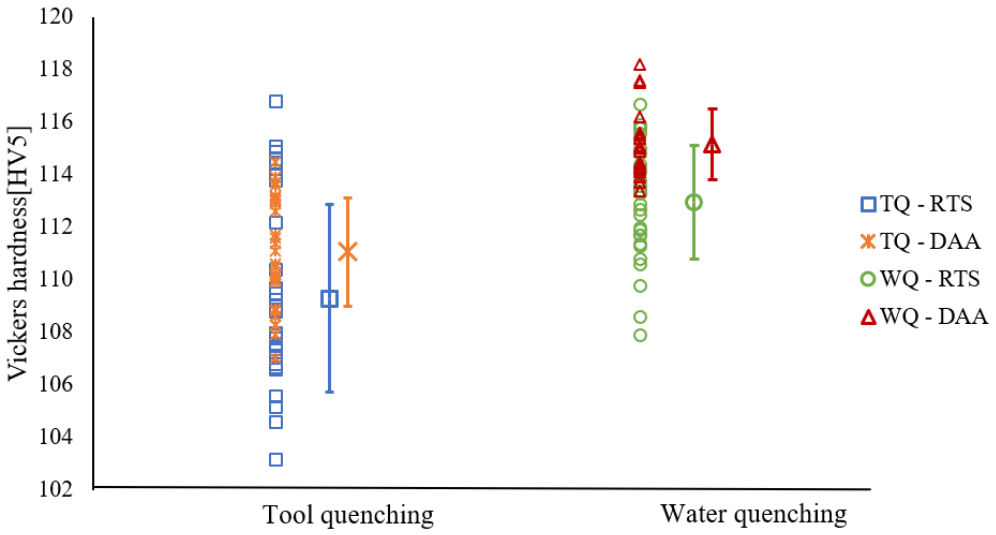

Figure 43: Tool quenching (TQ) and water quenching (WQ) with no deformation. Direct artificial aging (DAA) and room temperature storage (RTS).

The hardness results in Figure 43 show that the water-quenched samples have the highest hardness, especially those being water quenched and directly artificially aged. There is a greater spread in the results for both cases of samples that were stored at room temperature for 30 minutes.

The water quenched and directly artificially aged samples have the highest average hardness and a relatively small standard deviation. The average hardness of the tool-quenched and directly artificially aged samples is higher than for the samples being tool quenched and stored at room temperature. Both cases of the water-quenched samples have higher average hardness than the two cases being tool quenched. However, the measurements from the samples being water quenched and stored at room temperature seem to overlap the measurements from both of the sample sets being tool quenched.

The tensile test results from the cases of water quenching and tool quenching are shown in Figure 44, Figure 45 and Figure 46.

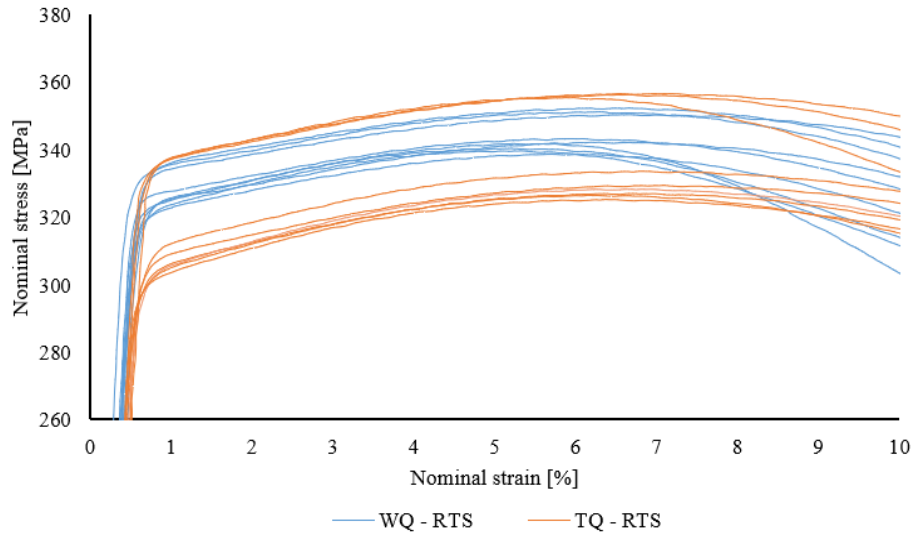

Figure 44: Stress – strain curves of samples being tool quenched (TQ) or water quenched (WQ) before room temperature storage (RTS) for 30 minutes.

Figure 44 compares the stress-strain curves for the samples being tool quenched and the samples being water quenched before storage at room temperature for 30 min. There are some spread in the results and the results for the two cases seem to overlap. However, the curves for the samples being water quenched have the highest average strength.

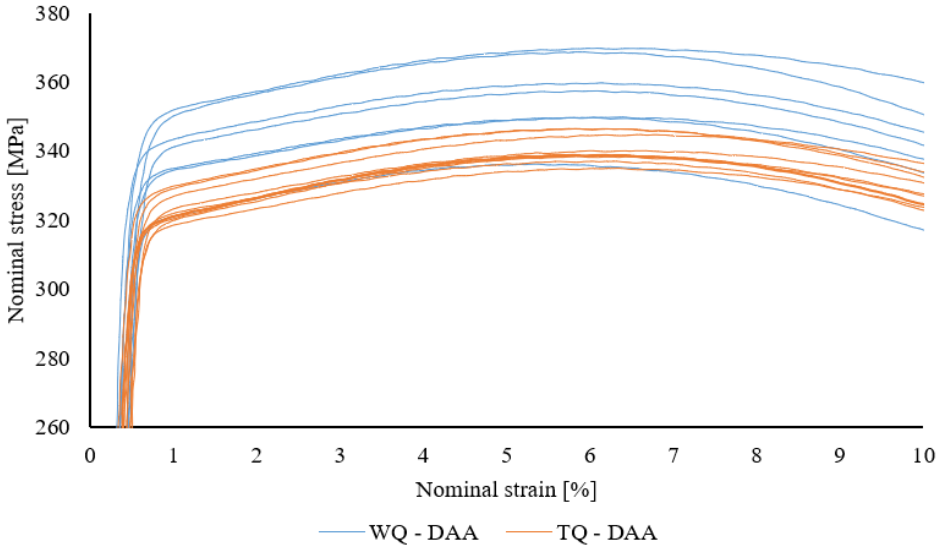

Figure 45: Stress-strain curves of samples being water quenched (WQ) or tool quenched (TQ) and directly artificially aged (DAA).

Figure 45 shows the tensile test results from samples being water quenched or tool quenched before direct artificial aging. The water quenched samples have higher tensile strength than those being tool quenched. A reasonable approximation of the difference in average tensile and yield strength is 20MPa.

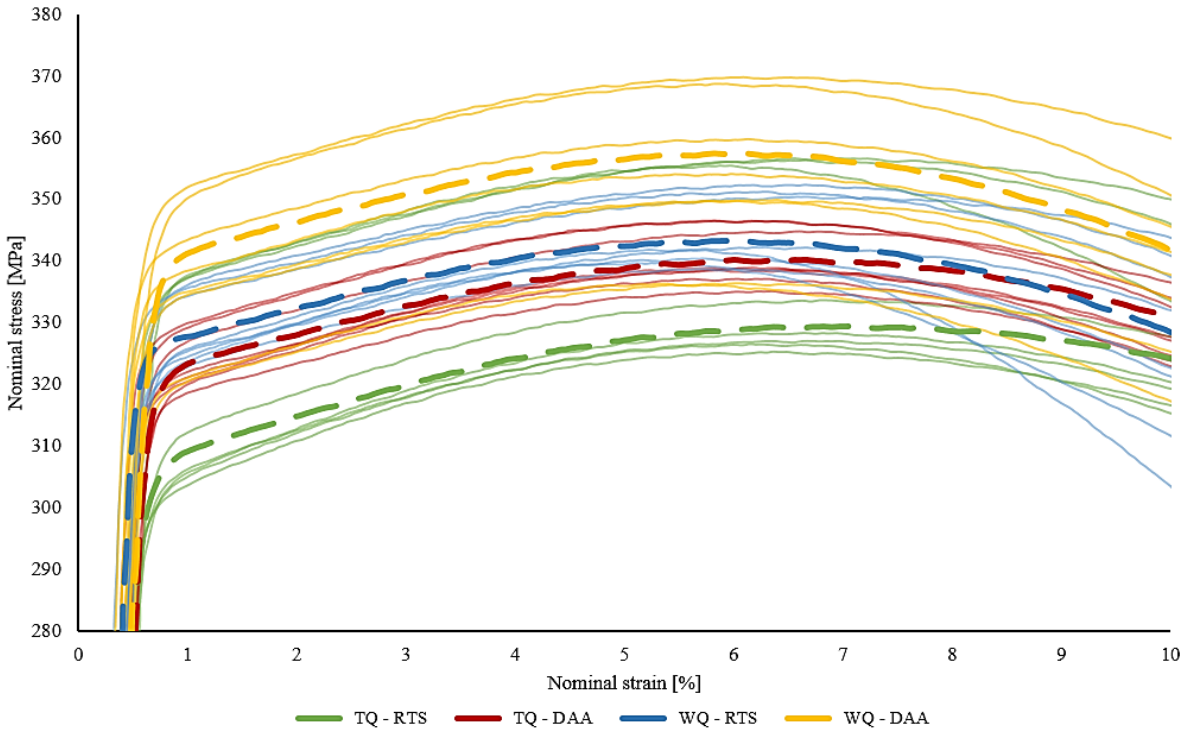

Figure 46: Tool quenching (TQ) or water quenching (WQ) before room temperature storage (RTS) or direct artificial aging (DAA).

The tensile test results from the four different cases of tool quenching and room temperature storage, tool quenching and direct artificial aging, water quenching and room temperature storage and water quenching and direct artificial aging are plotted in Figure 46. The dotted, highlighted lines are approximated average stress-strain curves representative for their case. A trend is difficult to observe. However, both cases including direct artificial aging seem to have higher tensile strength and yield strength than for those being stored at room temperature.

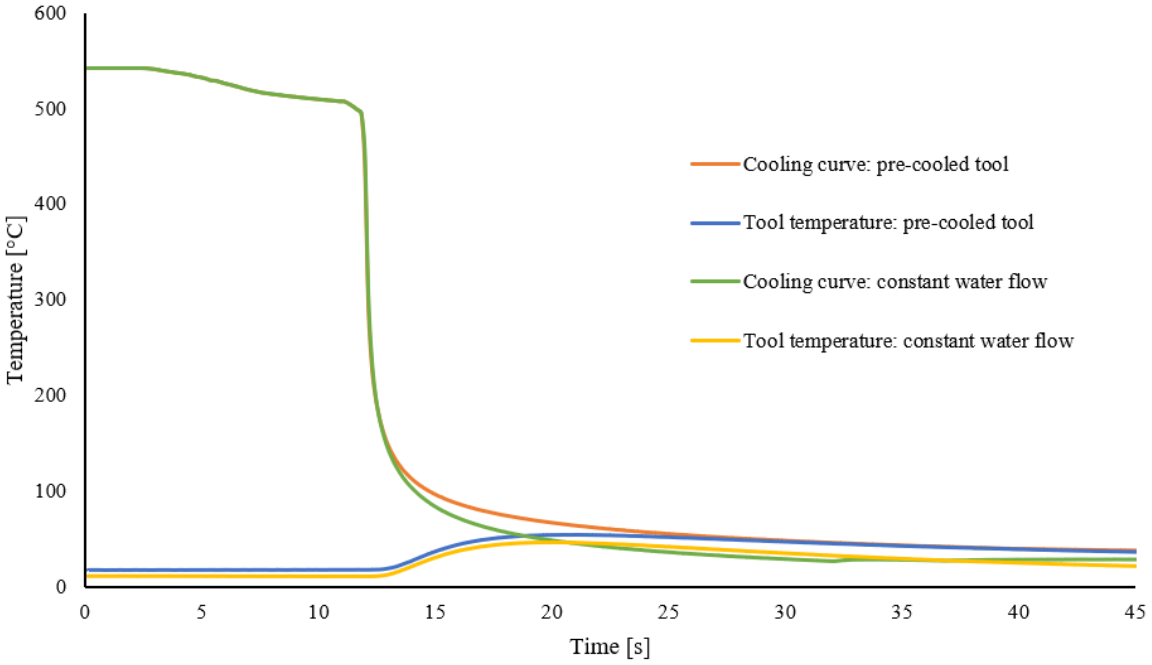

Figure 47: Cooling curve for the samples being quenched with pre-cooled tool and the samples being quenched by a constantly water-cooled tool. Including the temperature measured close to the lower tool surface for pre-cooling and constant cooling.

Figure 47 shows the temperature of the samples during quenching with pre-cooled tool and with constantly cooled tool. The temperature of the tool during quenching is also included for the pre-cooled tool and the constantly cooled tool during quenching and deformation. The tool temperature is measured by a thermocouple being attached from underneath the lower die, close to the tool surface.

The sample temperature during quenching and deformation in a pre-cooled tool have the same cooling rate as the samples being quenched and deformed in a constantly cooled tool until they reach a temperature of approximately 150°C. Here, the cooling rate decreases more for the samples quenched in the pre-cooled tool than for those being quenched in the constantly cooled tool. The time until the sample reaches room temperature is longer for the samples quenched in the pre-cooled tool.

For the tool surface temperature, the pre-cooled tool heat more than the constantly cooled tool. The temperature of the pre-cooled tool matches the sample temperature of 66°C after approximately 12 seconds after quench start before both the sample and the tool cool slowly until they reach room temperature. The constantly cooled tool matches the sample temperature at 50°C after 7 seconds, and both have a higher cooling rate to room temperature than for the case of the pre-cooled tool.

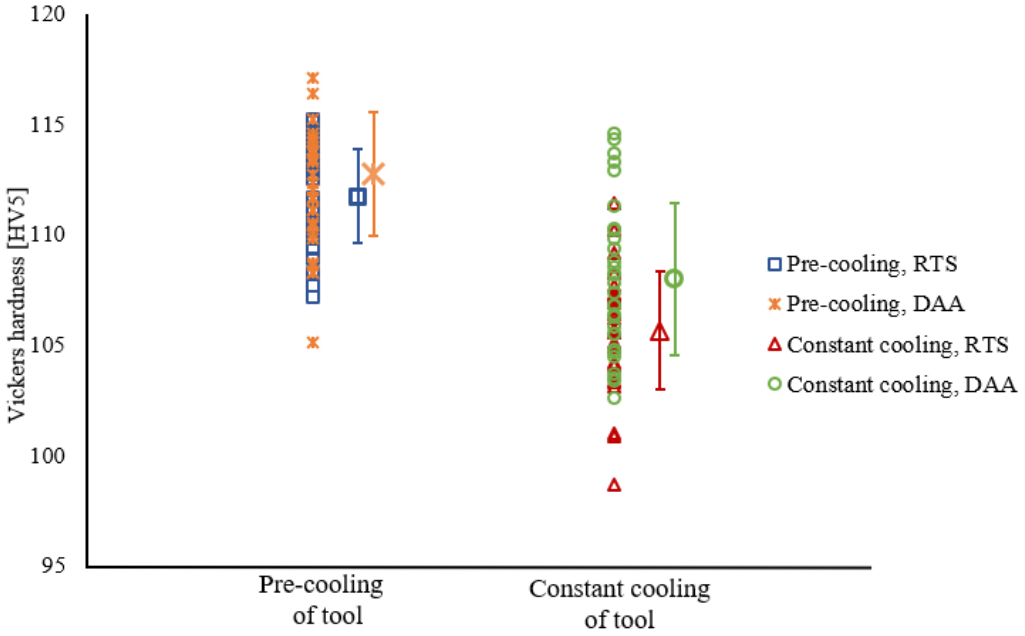

Figure 48: Vickers hardness of pre-cooled tool and constantly water-cooled tool before room temperature storage (RTS) or direct artificial aging (DAA). The average hardness with standard deviations as error bars are included.

Figure 48 shows the hardness measurements of the samples being deformed 15% and quenched to room temperature in a pre-cooled tool and constantly cooled tool before room temperature storage or direct artificial aging. The samples being quenched and deformed in the pre-cooled tool have a higher hardness than those being quenched and deformed in the constantly cooled tool. However, there is a larger spread and standard deviation for the samples being quenched in the constantly cooled tool. The difference in average hardness for the samples being quenched and deformed in the pre-cooled tool and the constantly cooled tool before room temperature storage is about 5 Vickers hardness units, and for the directly artificially aged samples the difference is approximately 4 Vickers hardness units.

The results also show that the samples being directly artificially aged after quenching and deformation have higher hardness than those being stored at room temperature. This is true for both the case of quenching and deformation in the pre-cooled tool and in the constantly cooled tool. The difference in hardness after direct artificial aging and room temperature storage is the most significant for the samples being quenched and deformed in the constantly cooled tool.

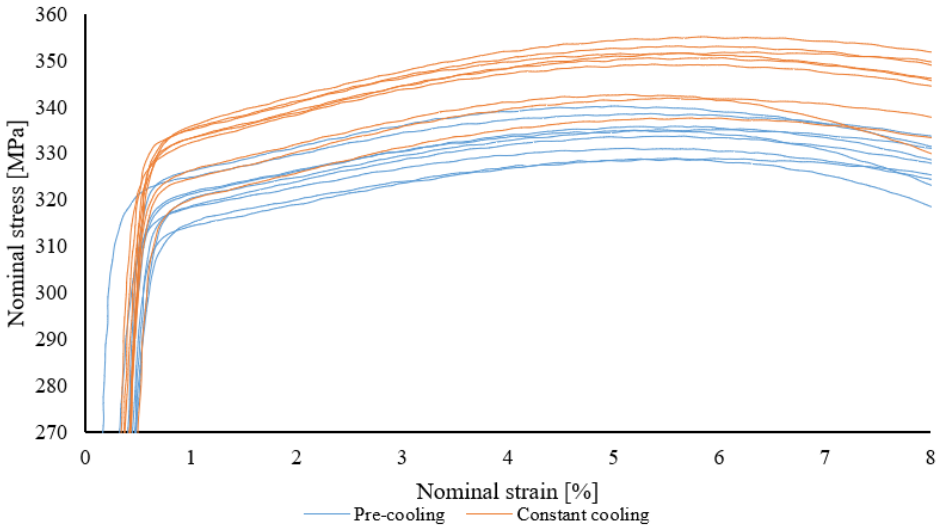

Figure 49: Stress-strain curves of samples being deformed and quenched in constantly water-cooled tool or pre-cooled tool before room temperature storage.

The results from the tensile tests for the samples being deformed and quenched in pre-cooled tool and constantly cooled tool before room temperature storage are shown in Figure 49. These results contradict the hardness results as the samples being quenched and deformed in a constantly cooled tool show higher strength than those being quenched and deformed in the pre-cooled tool. There is an overlap between the two cases. However, the three specimens deviating from the other samples being quenched and deformed in the constantly cooled tool were obtained from the same parallel.

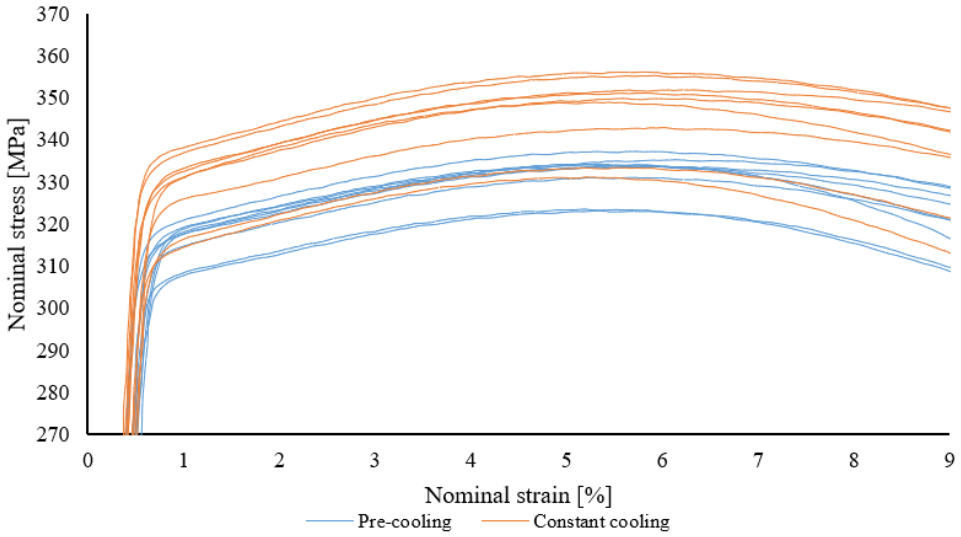

Figure 50: Stress-strain curves of samples being deformed and quenched in constantly water-cooled tool or pre-cooled tool before direct artificial aging.

The results from the tensile tests for the samples being deformed and quenched in pre-cooled tool and constantly cooled tool before direct artificial aging are shown in Figure 50. The samples being quenched and deformed in the constantly water-cooled tool have the highest strength. The three specimens showing the lowest strength obtained from the samples being quenched and deformed in the constantly cooled tool were all obtained from the same parallel.

The effect of deformation was investigated by comparing samples being simultaneously quenched and deformed with samples being tool quenched without deformation. A set of samples were deformed 15% in the tool and simultaneously quenched to room temperature in the dies. The reference samples were die quenched, where a pressure of approximately 10MPa was held on the sample during quenching without introducing deformation. Both cases included storage at room temperature for 30 minutes and direct artificial aging. The hardness results are shown in Figure 51 and the corresponding tensile test results are shown in Figure 52, Figure 53 and Figure 54.

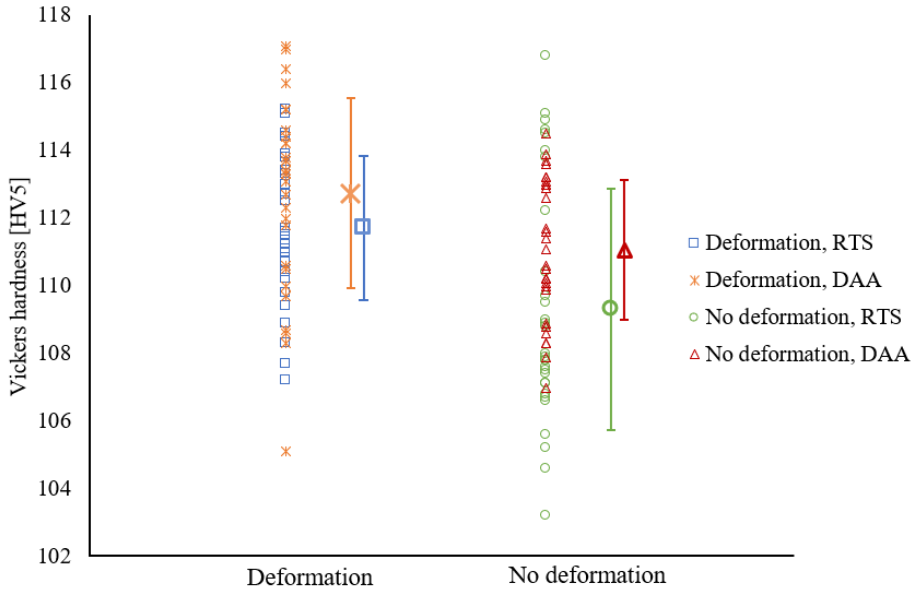

Figure 51: The effect of deformation. Average Vickers hardness is shown with standard deviation represented by error bars.

The hardness results from the simultaneously quenched and deformed samples, and tool quenched samples without deformation, before room temperature storage or direct artificial aging, are shown in Figure 51. The samples being deformed and directly artificially aged have the highest average hardness, followed by the samples being deformed and stored at room temperature. For the samples being tool quenched without deformation, the samples being directly artificially aged are about 2 Vickers hardness units higher in average hardness than those being stored at room temperature. The spread and standard deviations are relatively high, especially for the samples being tool quenched without deformation and stored at room temperature.

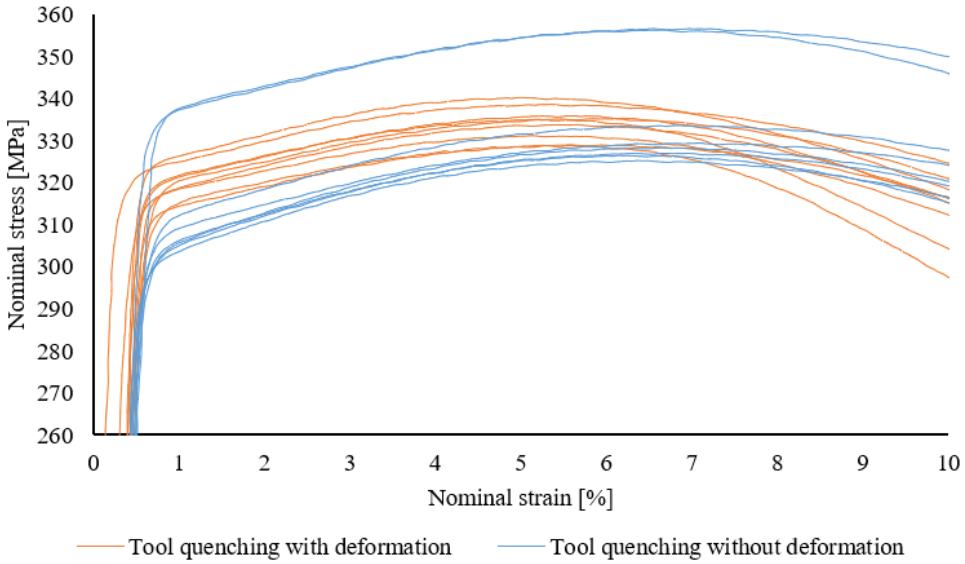

Figure 52: Tool quenching with or without deformation before storage at room temperature.

Figure 52 shows the stress-strain curves for the samples being stored at room temperature for 30 minutes after tool quenching with or without deformation. The deformed samples seem to have the highest tensile and yield strength. However, there are two parallels from the samples being tool quenched without deformation that shows higher values than for the rest of the parallels from the actual case and for those being deformed. These tensile specimens are obtained from the same sample, which may indicate that this sample is deviating from the rest, this is also the case for the hardness measurements obtained from this sample.

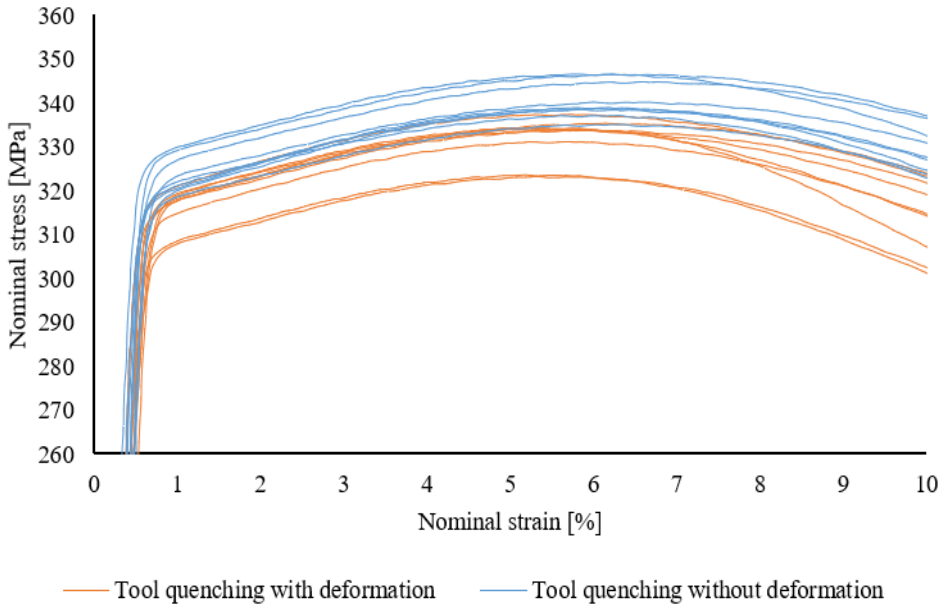

Figure 53: Tool quenching with or without deformation before direct artificial aging.

The results from the samples directly artificially aged after tool quenching with or without deformation are shown in Figure 53. The strength of the samples without deformation are higher than for the deformed samples. There is a slight overlap for the two cases.

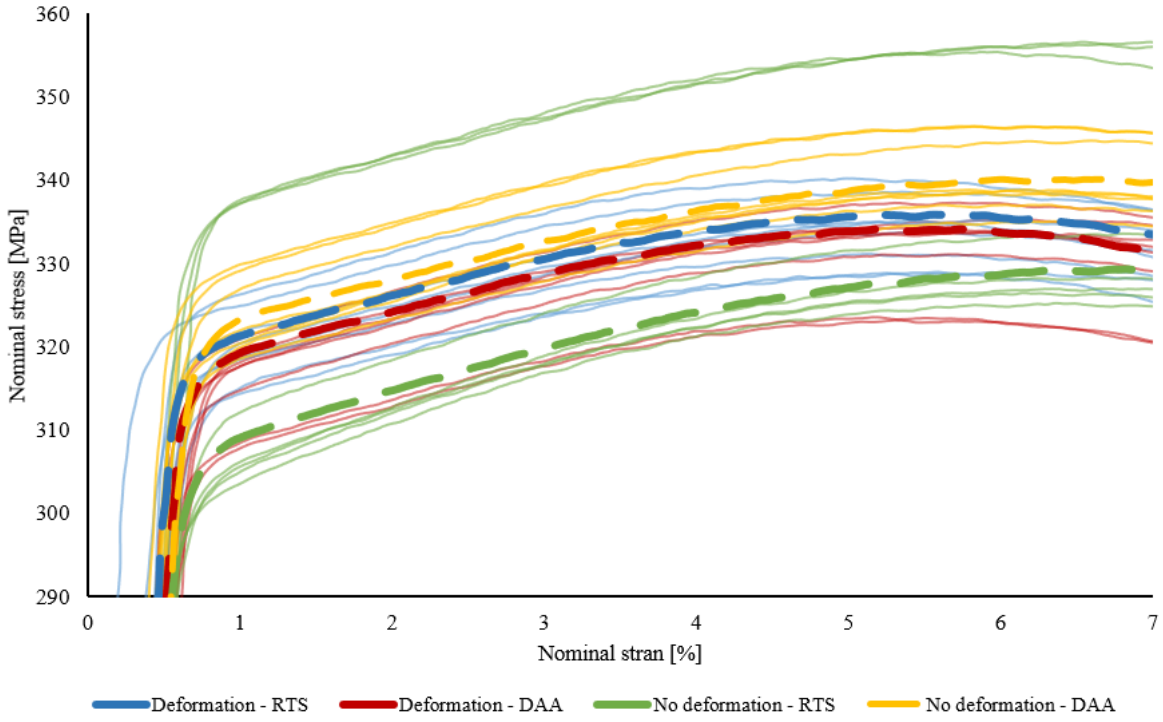

Figure 54: Stress-strain curves of samples being tool quenching with or without deformation before room temperature storage (RTS) or direct artificial aging (DAA).

The tensile test results for the previous four cases are plotted in Figure 54. The dotted, highlighted lines are approximated average stress-strain curves representative for their case. The samples without deformation and directly artificially aged seem to have the highest average strength. However, there are a few parallels with deviating results from the cases of room temperature storage, with and without deformation, where the strength is higher than the majority of the parallels.

4.3.2 Effect of interrupted quenching

The effect of interrupted quenching was tested by quenching and deforming the samples after solution heat treatment. The upper die was lifted before the sample reached room temperature. The following quench interruption temperatures were selected: 70, 100, 150 and 200°C. The samples were either brought directly to oil bath for artificial aging or stored at room temperature for 30 minutes after the interrupted quenching.

The hardness and tensile test results from the quench interruption experiments are shown in Figure 55 - Figure 58.

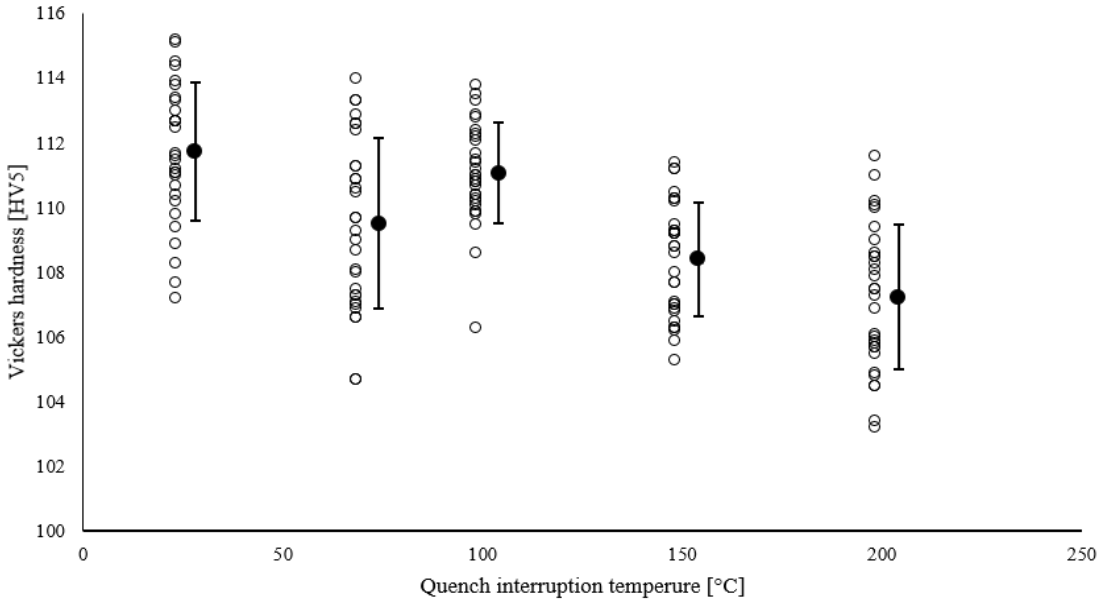

Figure 55: Vickers hardness measurements for interrupted quenching at quench interruption temperature and room temperature storage before artificial aging. The corresponding average hardness is plotted with standard deviations.

Figure 55 shows the Vickers hardness results of the quench interruption experiments for the samples being air cooled from the quench interruption temperature and stored at room temperature for a total of 30 minutes before artificial aging. The average hardness with standard deviations are included. All samples were subjected to a deformation of 15%. Reference samples being deformed and quenched to 25°C before room temperature storage are included in the results for comparison. The samples quenched to room temperature have the highest hardness, while the samples quenched to 100°C before air cooling to room temperature obtained the approximate same hardness and have less standard deviations. For the samples quenched to 70°C, 150°C and 200°C, the hardness decreases with increasing quench interruption temperature.

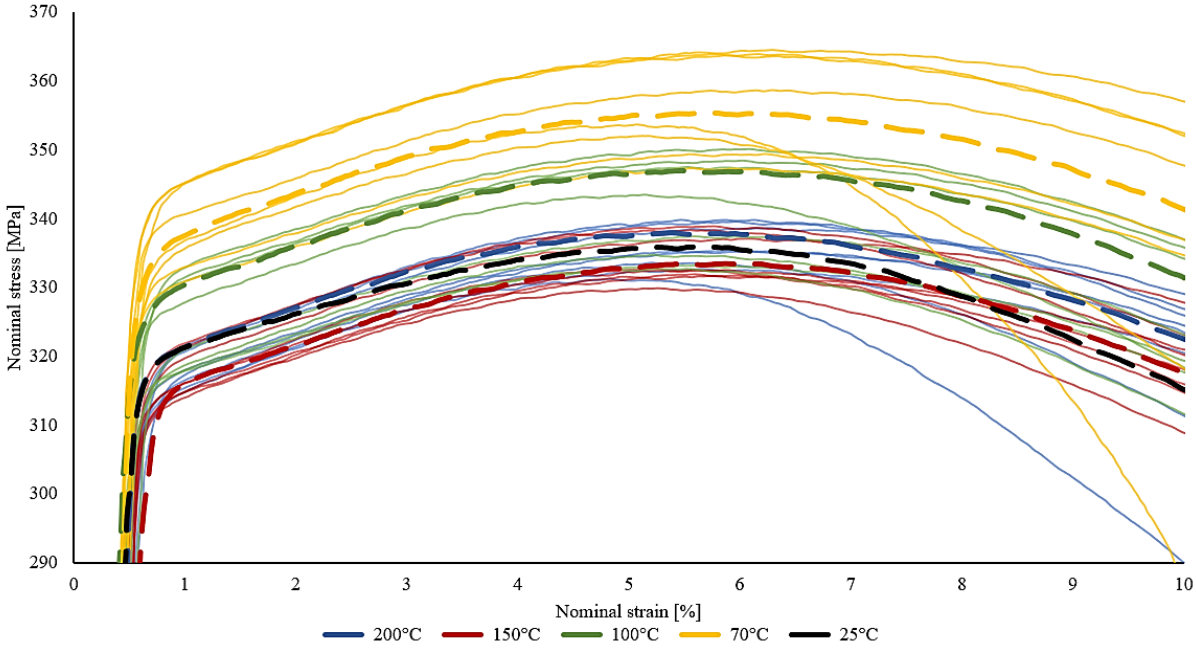

Figure 56: Quench interruption and subsequent air cooling and storage at room temperature. The temperatures represent the temperatures to which the samples were quenched before air cooling and storage.

The stress strain curves for the samples being quenched to selected temperatures before room temperature storage are shown in Figure 56. The dotted, highlighted lines are approximated average stress-strain curves representative for their case. There are some spread in the results. The same tendency is shown for the tensile tests as for the hardness measurements; the higher the quench interruption temperature, the lower the strength. The results for the samples being quenched to 200°C, however, seem to have higher strength than the samples being quenched to 150°C.

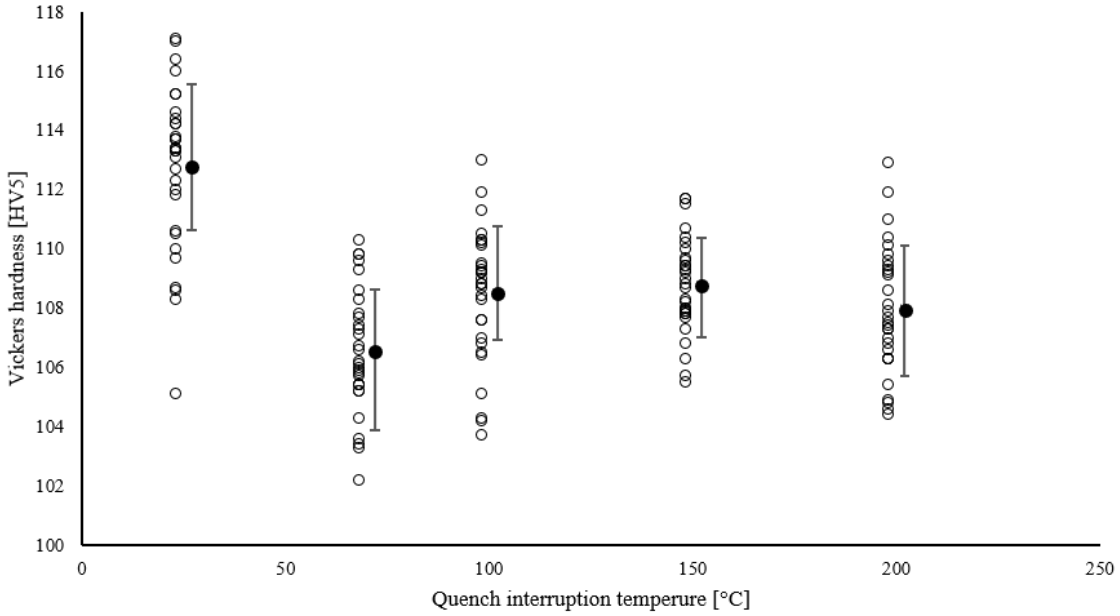

Figure 57: Vickers hardness measurements for interrupted quenching at quench interruption temperature and direct artificial aging. The corresponding average hardness is plotted with standard deviations.

Figure 57 shows the hardness results for the quench interruption samples that were brought directly to oil bath for artificial aging. The average hardness with standard deviations are included. The samples quenched to room temperature have the highest hardness. There are some spread for all the measurements, especially for those quenched to 100°C and 200°C. The samples quenched to 70°C before direct artificial aging show the lowest average hardness. The samples quenched to 100°C, 150°C and 200°C before direct artificial aging show approximately the same average hardness and the standard deviations show an almost complete overlap in hardness of the three cases.

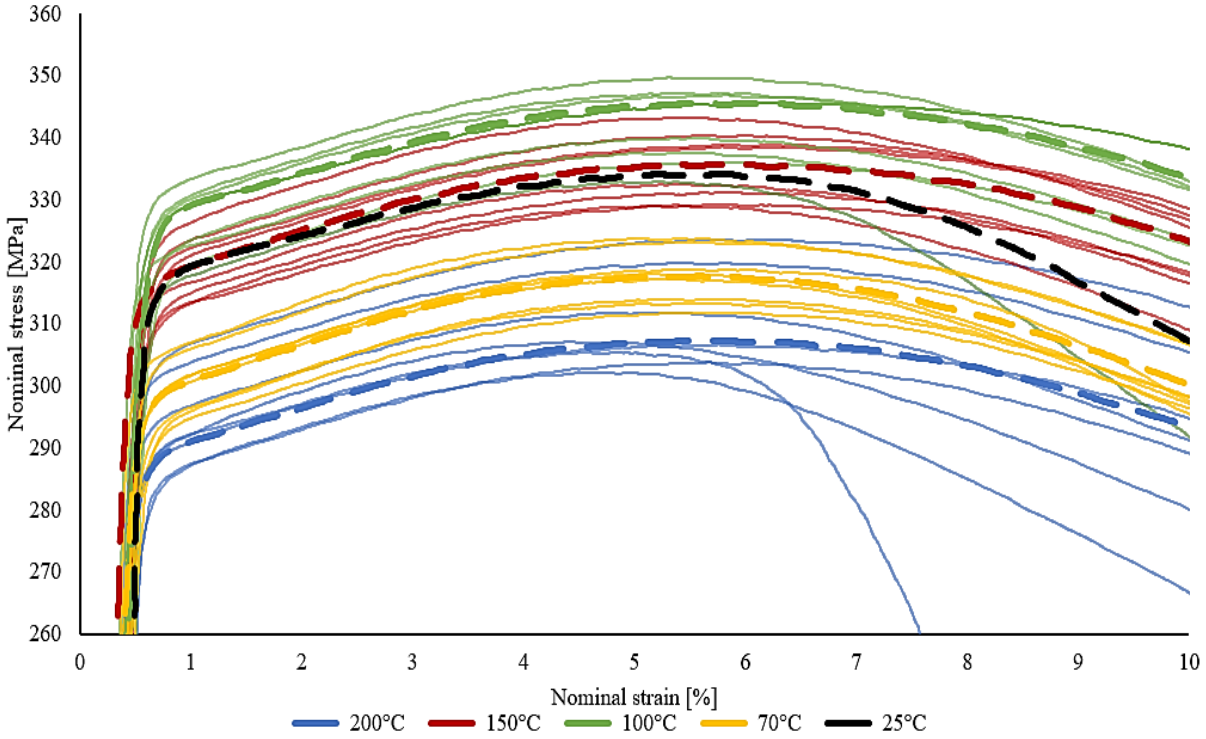

Figure 58: Quench interruption at different temperatures and direct artificial aging.

Figure 58 shows the stress-strain curves for the samples being deformed and quenched to selected temperatures before direct artificial aging. The dotted, highlighted lines are approximated average stress-strain curves representative for their case. The samples being quenched to 100°C have the highest strength followed by the samples being quenched to 150°C. The samples quenched to 200°C have the lowest strength. However, a couple of parallels is strongly deviating from the others, both specimens are obtained from the same sample.

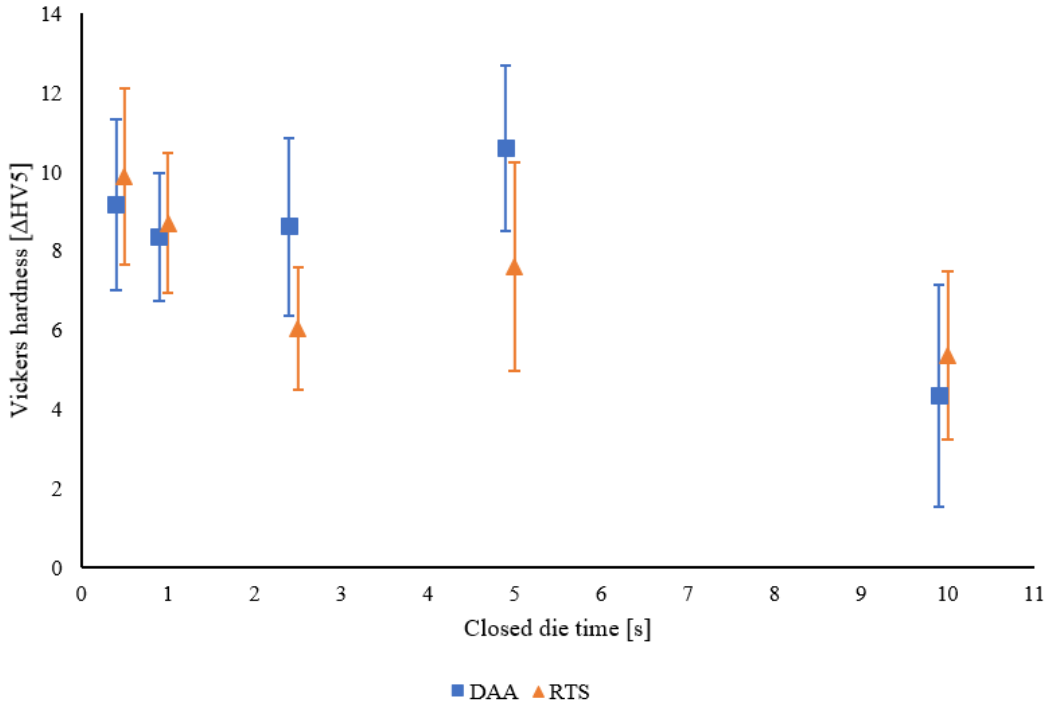

Figure 59: The difference of the Average Vickers hardness (ΔHV5) and the peak hardness as a function of closed die time, i.e. the die pressure time required to cool the samples to the selected temperatures. Subsequent to deformation, the samples were directly artificially aged (DAA) or stored at room temperature for 30 minutes (RTS) before artificial aging.

Table 4: The applied pressure time required to reach the quench interruption temperature.

Quench interruption temperature [°C]	200	150	100	70	25
Closed die time [s]	0.5	1	2.5	5	10

Figure 59 shows the difference between the average Vickers hardness and the peak hardness obtained for the alloy in this project as a function of closed die time. The peak hardness of HV5 = 117 was measured for the samples being simultaneously deformed and quenched to room temperature before direct artificial aging. This hardness is referred to as the maximum hardness for this figure. The lower ΔHV5, the higher the hardness. The closed die time is the time the press was programmed to apply pressure to the samples after deformation to reach the quench interruption temperature before air cooling and room temperature storage or direct artificial aging. Table 4 shows the quench interruption temperatures and the corresponding closed die times.

A closed die time of 10 seconds gives the hardness closest to the maximum hardness, especially for the samples being directly artificially aged. Also closed die times of 2.5 and 5 seconds seem to be beneficial for the samples being stored at room temperature for 30 minutes after quenching. Closed die times of 0.5 and 1 seconds, and for the samples being directly artificially aged with closed die times of 2.5 and 5 seconds, the hardness difference from the maximum hardness is 8 or higher, which means that these closed die times are the least beneficial for the resulting hardness.

4.3.3 Effect of direct artificial aging

To investigate the effect of direct artificial aging, two sets of samples were tested for each case. After quenching and/or deformation, one set of samples were stored at room temperature for 30 minutes and the other brought directly to oil bath for artificial aging. In this section, the results from the two sets of different cases are plotted together for comparison. The results are shown in Figure 60 - Figure 64.

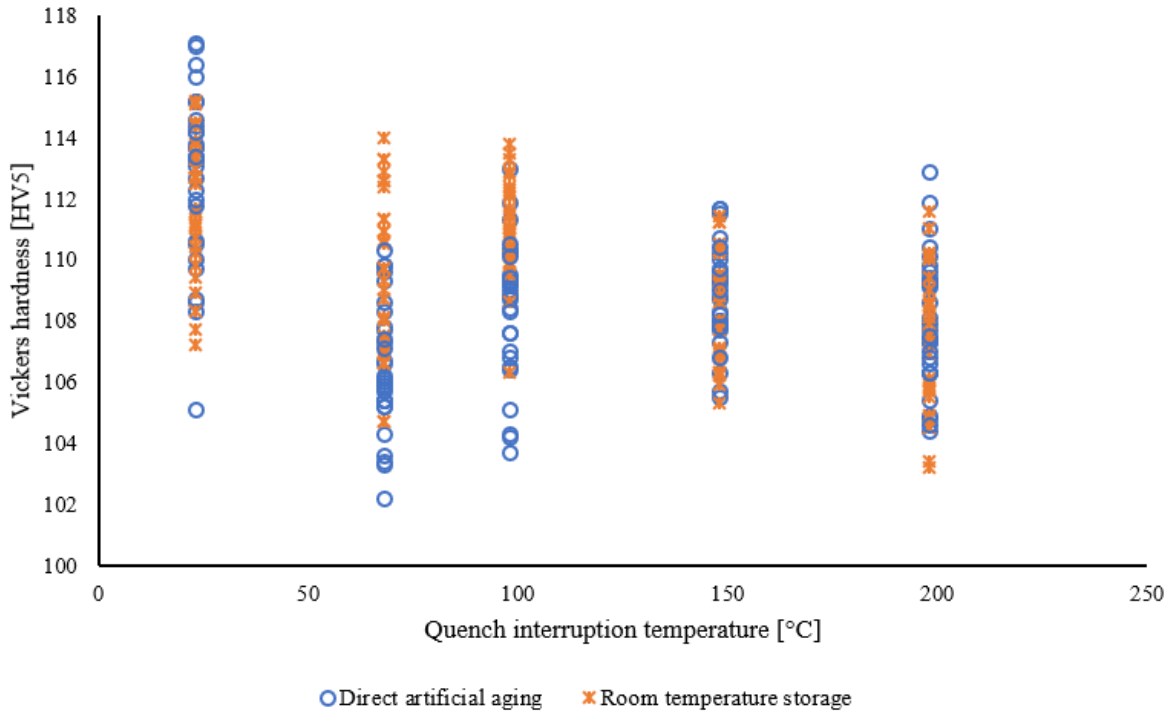

Figure 60: Hardness measurements of samples being quench interrupted before direct artificial aging or room temperature storage.

Figure 60 shows the Vickers hardness results from the quench interruption experiments, both from the directly artificially aged samples and those being stored at room temperature for 30 minutes. It is difficult to observe an obvious trend in hardness for the two cases as there is a great overlap of the measurements. Overall, the samples being stored at room temperature seem to have slightly higher hardness than the samples being directly artificially aged.

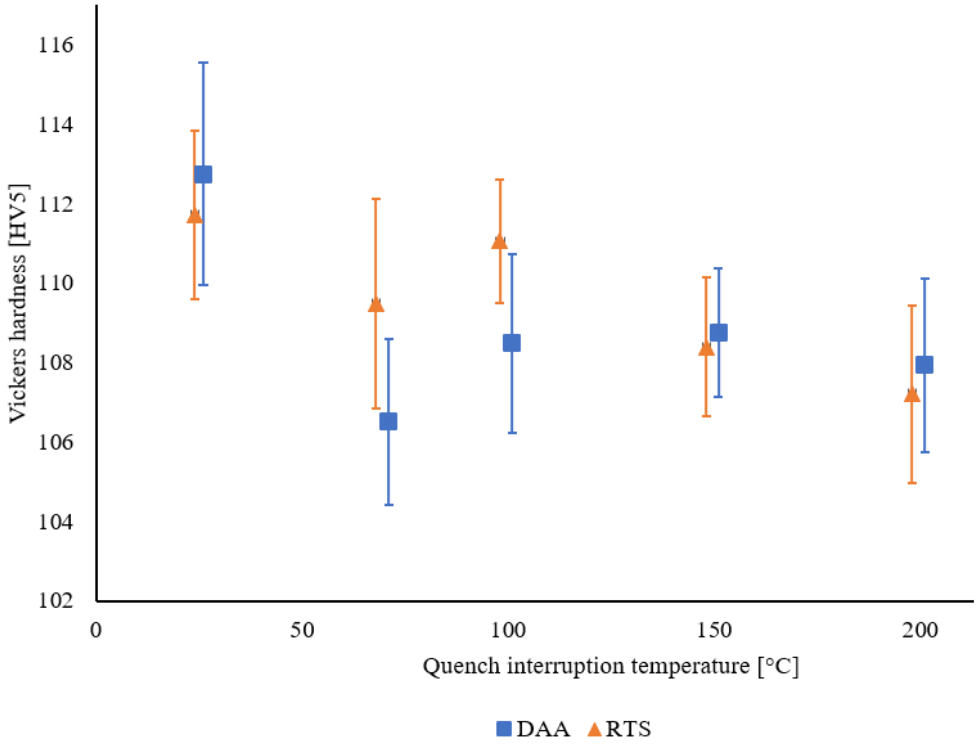

Figure 61: The average Vickers hardness for samples being quench interrupted and directly artificially aged (DAA) or stored at room temperature (RTS). The standard deviations are represented by error bars.

The average of the results in Figure 60 are plotted in Figure 61 with standard deviations as error bars. The reference samples quenched to room temperature has the highest average for the samples being directly artificially aged. From the error bars, one can observe that there is an overlap of the direct artificial aging samples and the samples stored at room temperature for 30 minutes. As for the quench interruption experiments, the samples being quenched to 70 and 100°C and stored at room temperature have the highest hardness. There are some overlaps between these and the samples being directly artificially aged. The differences in these cases are the most significant. For the samples being quenched to 150 and 200°C, direct artificial aging samples have the highest hardness. However, there is a significant overlap with the samples stored at room temperature, and the differences in average hardness are small.

Overall, the effect of direct artificial aging does not seem to be significantly beneficial regarding these results. The samples being deformed and quenched to room temperature obtain higher hardness than the samples being quench interrupted.

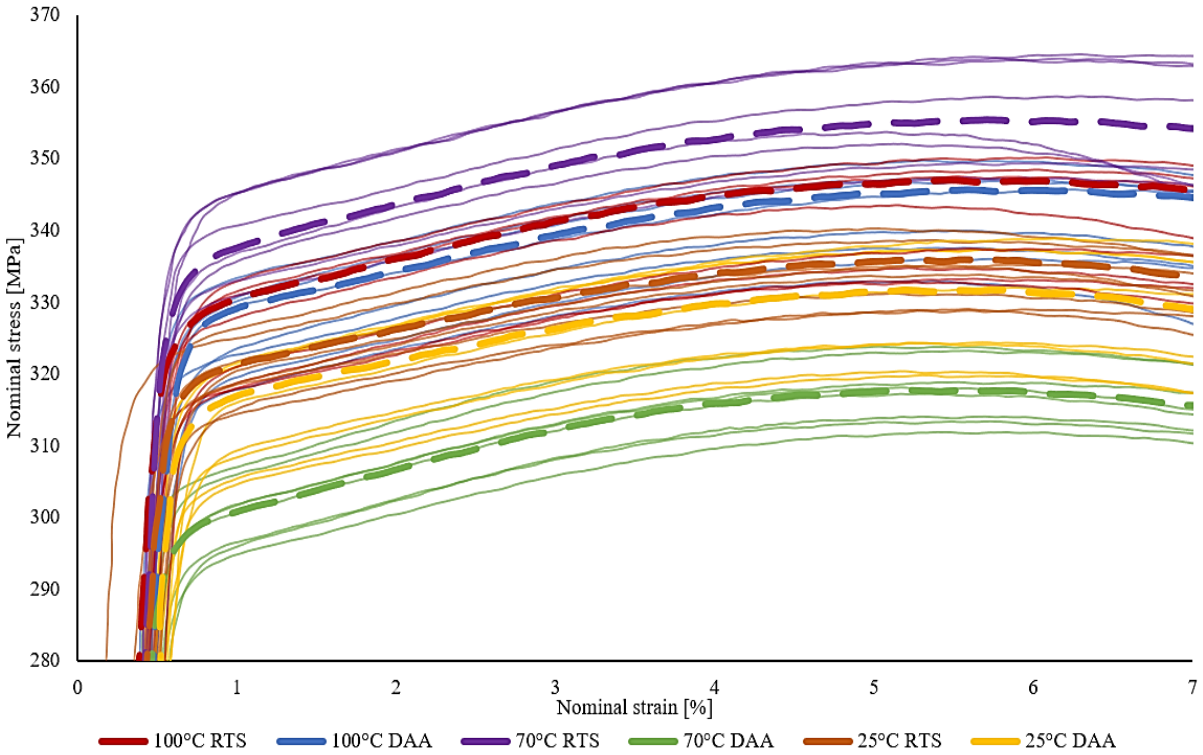

Figure 62: Stress-strain curves for samples being quench interrupted at different temperatures before room temperature storage (RTS) and direct artificial aging (DAA).

Figure 62 shows selected stress-strain curves for the quench interruption experiments in the cases of both direct artificial aging and room temperature storage. The selected cases are obtained from those samples that showed the highest strength with the intention of getting a readable presentation of the results. In contradiction to the hardness results, the reference samples being quenched to room temperature show intermediate to low strength in relation to the others. The samples being quenched to 70°C before storage at room temperature has the highest strength followed by the samples being quenched to 100°C before direct artificial aging or room temperature storage. The samples with the lowest strength are those quenched to 70°C before direct artificial aging.

As there is a spread for the parallels in the tensile tests, simpler representations of the results are shown in Figure 63 and Figure 64. Average tensile strength and average yield strength are plotted with standard deviations.

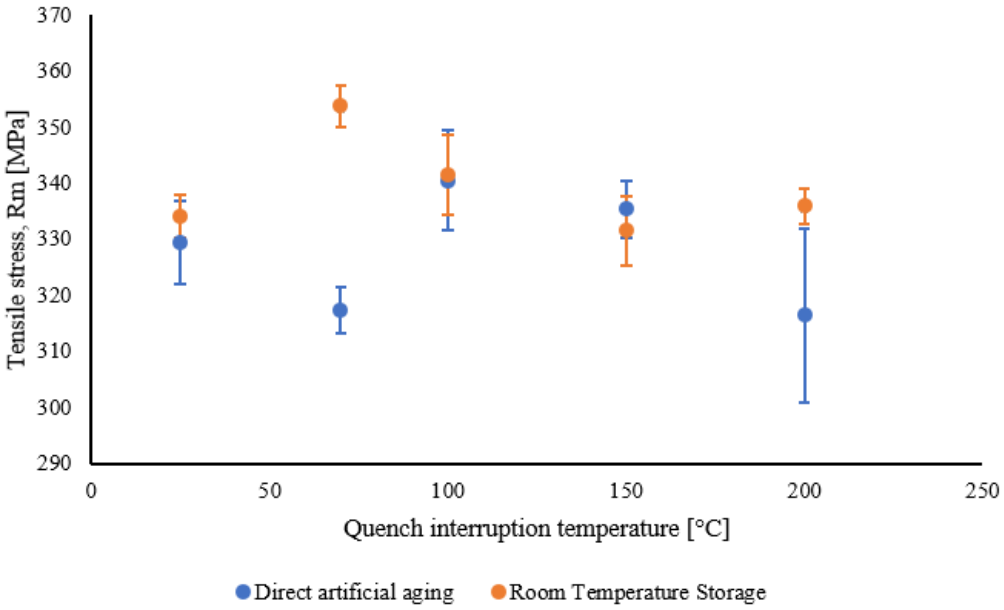

Figure 63: The average tensile strength as a function of quench interruption temperature for samples being stored at room temperature or directly artificially aged. Standard deviations are represented by error bars.

Figure 63 shows the average tensile strength (maximum strength), of the samples being quench interrupted before direct artificial aging or room temperature storage. Standard deviations are represented by error bars. As seen in Figure 62, the samples being quenched to 70°C and stored at room temperature have the highest strength, and the samples quenched to the same temperature before direct artificial aging have the lowest strength. There are insignificant differences in the average tensile strength between the directly artificially aged samples and the samples stored at room temperature after quenching to 25, 100 and 150°C. The difference between the room temperature stored samples and the directly artificially aged samples quenched to 200°C is about 20MPa. There is a large standard deviation of the samples quenched to 200°C and directly artificially aged.

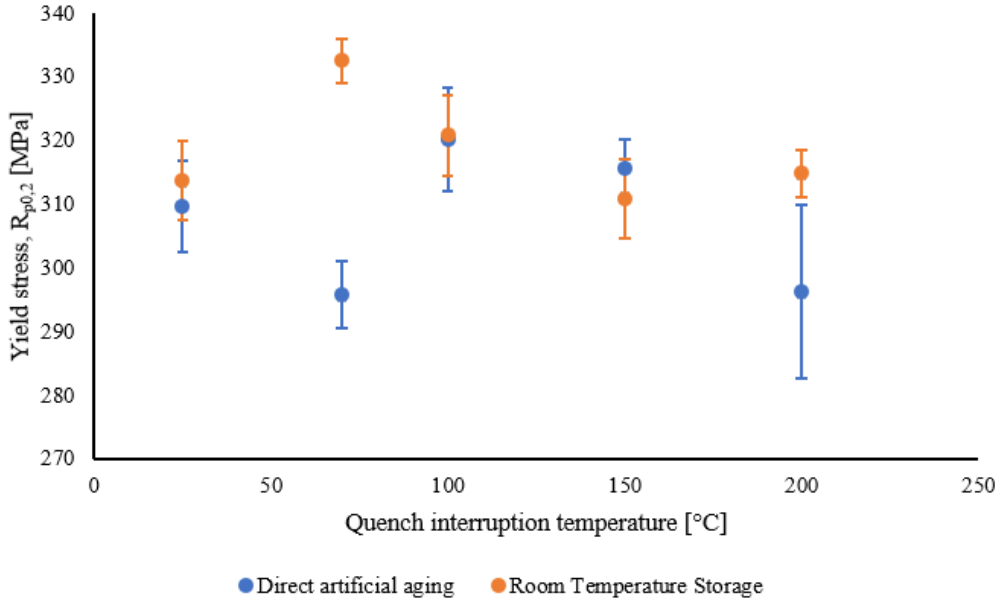

Figure 64: The average yield strength as a function of quench interruption temperature for samples being stored at room temperature or directly artificially aged. Standard deviations are represented by error bars.

Figure 64 shows the average yield strength for the quench interruption experiments. The standard deviations are represented by error bars. The average yield strength for the different cases corresponds to the tensile strength in Figure 63. The samples quenched to 70°C and stored at room temperature has the highest yield strength, while the samples quenched to the same temperature before direct artificial aging has the lowest yield strength. The difference in average yield strength between the directly artificially aged samples and the room temperature stored samples is insignificant for those quenched to 25, 100 and 150°C.

To further observe the effect of direct artificial aging compared to storage at room temperature, some of the previous experiments are presented as a function of direct artificial aging and room temperature storage. The effect of direct artificial aging is illustrated with respect to water quenching, tool quenching and tool quenching with deformation.

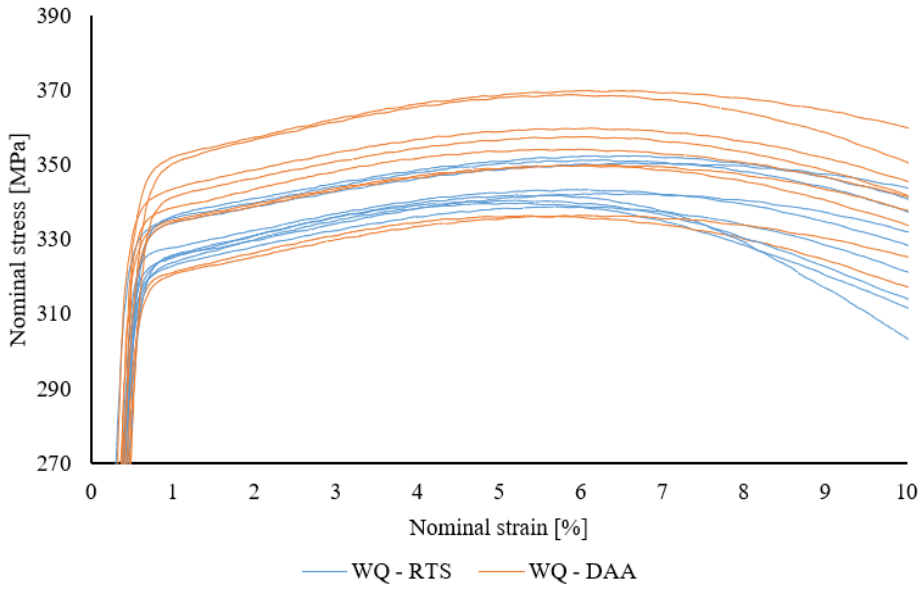

Figure 65: Water quenching (WQ) from solution heat treatment before room temperature storage (RTS) or direct artificial aging (DAA).

Figure 65 shows the stress strain curves for the samples being water quenched to room temperature before direct artificial aging or storage at room temperature for 30 minutes. The directly artificially aged samples show a higher strength than those stored at room temperature.

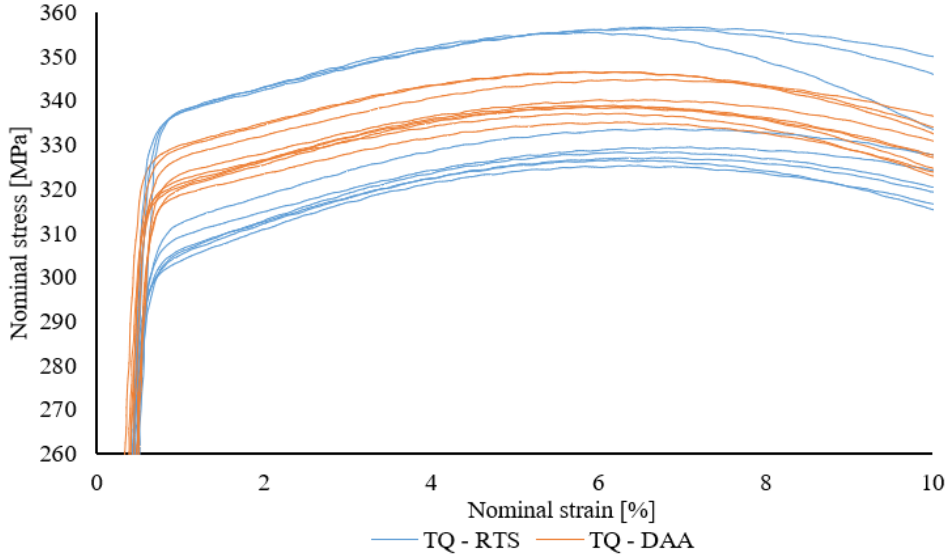

Figure 66: Tool quenching (TQ) from solution heat treatment before room temperature storage (RTS) or direct artificial aging (DAA).

The stress-strain curves in Figure 66 represents the samples being tool quenched without deformation before direct artificial aging or storage at room temperature for 30 minutes. Any strength difference is difficult to observe as the curves seem to completely overlap.

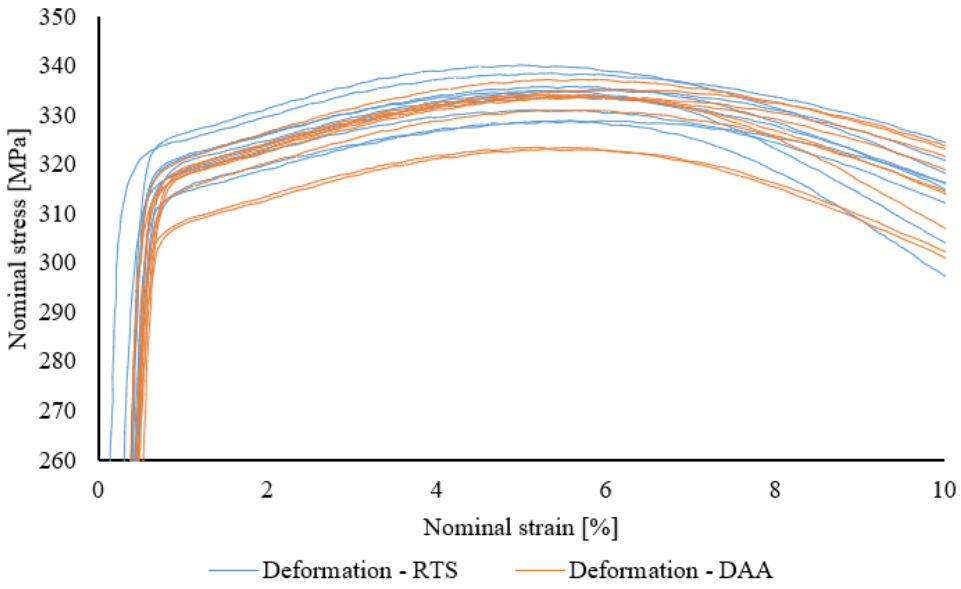

Figure 67: Tool quenching (TQ) and deformation before room temperature storage (RTS) or direct artificial aging (DAA).

Figure 67 shows the stress-strain curves for the samples being simultaneously tool quenched from solution heat treatment and deformed before direct artificial aging and storage at room temperature for 30 minutes. There is a great overlap, which indicate that neither direct artificial aging or room temperature storage have a significant effect on the strength. However, the samples being stored at room temperature seem to have a slightly higher average strength.

5. Discussion

In this chapter, the results presented in Chapter 4 will be discussed and related to the theory presented in Chapter 2. The microstructure evolution and its influence on the experiments and subsequent mechanical testing will be addressed. The method development was a significant aspect of the project; therefore, the feasibility and relevance of the method is evaluated. Finally, a discussion of the effect of quench interruption and direct artificial aging on final mechanical properties, and its relevance to the industry, is presented.

5.1 Microstructure

The recrystallized surface layer is difficult to avoid during extrusion of this alloy as high temperatures and large strains enhance recrystallization. The temperature and strain conditions may change during extrusion. This results in an inhomogeneous thickness of the recrystallized surface layer along the flat profile. As shown in the images of the grain structure both before and after extrusion, the thickness of the recrystallized layer varies strongly, and in some extreme cases, the layer thickness is just below the critical thickness. None of the samples studied in light optical microscopy exceed the critical thickness of the recrystallized layer, thus, it is reasonable to assume that the test area of the tensile specimens was not affected. However, a complete overview of the grain structure along the profile was not obtained.

The changes across the as-extruded profile should have been more thoroughly investigated initially to the hot forming and in-die quenching experiments to ensure equal test conditions and reliable results. The material quantity and the scope of the experiments set against the corresponding time frame, did not provide sufficient time or capacity to perform more comprehensive analysis of the delivered material.

The images showing the particle structure in the base material showed a relatively dense distribution of particles of various sizes. Smaller particles can be observed concentrated along the grain boundaries and possibly subgrain boundaries. It is reasonable to assume that these particles are dispersoids with sizes of approximately 1μm. The dispersoid size depends on time and temperature of homogenization. The size of the dispersoids in a 6082.25 alloy homogenized at 540°C are found to be 0.1μm [51]. However, the alloy investigated in this project is homogenized at 575°C, which leads to larger dispersoids. The dispersoids normally consist of Al_3Cr and Al_6Mn in the 6082.25-alloy [52]. Cr have a tendency to precipitate in precipitate free zones (PFZ). Cr and Mn are added to the alloy in relatively large amounts, which leads to high dispersoid density as can be observed in Figure 39.

Larger particles are aligned along the grain boundaries and along the extrusion direction. These are primary intermetallic particles. The primary particles consist of intermetallic phases such as iron separated from the melt during solidification. These remain stable through subsequent heat treatment processes due to high melting points. The reason to why the large particles are aligned along the extrusion direction may be that they during extrusion are crushed and spread linearly along the extrusion direction. The elongated particles rotate and orientates towards the extrusion direction during extrusion.

The 100 and 111 pole figures show that the texture consist of cube and brass components. Cube is most commonly observed in recrystallized materials [44]. Due to time limits, more thoroughly investigations were not done regarding this observation. An observation from the pole figures show that the texture remains the same after deformation in the hot forming and in-die quenching experiments. An alteration of the anisotropy in the bulk could have inflicted negative effects on the properties and on the subsequent tensile tests. However, the scan area is small ($0.16mm^2$), and includes relatively few grains. Hence, a general conclusion or any statistics cannot be obtained regarding the global texture of the bulk.

5.2 Evaluation of the hot deformation and in-die quenching experiment procedure

The test procedure seems to be efficient in terms of achieving a small degree of deformation. The test set-up proved to be compatible with the time and temperature restrictions involved to achieve a reproducible and accurate experiment procedure. The method developed for simulating integrated hot forming and die quenching does inflict some uncertainties to the results. Whether this is due to the test conditions, errors in the subsequent hardness measurements or tensile testing is not clear. However, certain considerations should be taken into account for future application of the pressing tool.

The hot forming and in-die quenching test procedure is time and temperature sensitive. Variations in execution time of handling the sample during testing may alter the final mechanical properties of the samples as the temperature may decrease too much before deformation starts. A critical factor is the transportation time from furnace to tool when opening the oven door. As the door is open, cold air is let in and may cause cooling of the sample in various amounts depending on the time it takes to grip the sample with a plyer.

The MTS hydraulic press is not capable of exceeding a force of 800 kN. The force required to deform the samples used in this project was maximum 600 kN, which gave a degree of deformation of 15%. If a larger degree of deformation is desired, the sample geometry may be altered to obtain a lower maximum force during the experiments. In addition, to avoid complicated machining of samples, a sample holder fitting the spikes should be designed, and consequently, smaller samples could be used.

Another issue that arose during the experiments was the inhomogeneous deformation obtained by deformation in the tool. The deformation was not homogeneous along the sample due to a small angle in the upper die. Mechanical stop may be introduced, as attempted in the current project. Alternative solutions to the uneven upper die could be found to achieve homogeneous deformation along the samples. As for variations of the degree of deformations for different samples, other conditions in the software for terminating the deformation could be tested. In this project, the deformation stop was programmed by distance, alternative parameters to provide deformation stop might be force or time.

Preferentially, the sample dimensions should be increased to enable larger tensile specimens and avoiding deviations because of small volume tensile tests. In addition, even more parallels can be used to ensure greater certainty as to which results are more likely to be valid. The place at which the hardness is measured on the samples should be carefully considered to avoid deviations caused by surface effects, i.e. recrystallized surface.

In summary, the test method and procedure proved to be applicable to simulate a simultaneous hot deformation and quenching process. Using the tool attached to the press in combination with the air circulation furnace enabled deformation in the form of compression of samples with high temperature. The water supply in the upper and lower die provides a sufficient quenching rate and the feathered spikes made it possible to avoid excess cooling before and after deformation. However, further development and improvement is necessary to ensure identical experiments so that deviations and biases caused by the in-die quenching and deformation experiments may be eliminated.

5.3 The effect of tool quenching and deformation

The samples simultaneously deformed and quenched from solution heat treatment in the pressing tool show lower strength and hardness compared to samples being quenched in water. There are several possible explanations to this effect.

According to the TTP diagrams in Figure 8, the quenching rate obtained during quenching in the pre-cooled tool should be sufficient to avoid any precipitation during quenching. The curve passes the nose at approximately 350°C within the time margin of 10 seconds as the sample reaches 200°C in less than 1 second. However, according to Figure 6, precipitation of GP-zones may occur at low temperatures between 70-110°C. The cooling curve for the tool quenching shows the sample holding temperatures in this range for a time of 10-15 seconds. This might have caused precipitation of zones providing less strength than the β” precipitates formed during subsequent artificial aging. The GP-zones may act as strengthening precipitates. However, the strength achieved by certain precipitates depends on the quantity. And the amount of present GP zones may not be sufficient to achieve the strength corresponding to the strength otherwise achieved by the β” precipitates.

Another possible reason for the decrease in hardness by tool quenching is a decrease in vacancy concentration. The vacancy concentration strongly depends on temperature, and as shown in Equation **7**, the equilibrium concentration decreases with decreased temperature. During water quenching, the quenching rate is high, and by the time the sample reaches room temperature, the vacancies have had no time to disappear, and excess vacancies are therefore quenched in. During tool quenching, the lower quenching rate from 200°C may have affected the vacancy concentration as the diffusion rate of atoms still are elevated and therefore providing a lower equilibrium concentration of vacancies. The vacancies may have migrated to grain boundaries and other vacancy sinks to no longer be available for further clustering and precipitation nucleation.

When introducing deformation at high temperatures during quenching from solution heat treatment, the results are ambiguous. The hardness measurements indicate that the alloy is hardened by deformation, while the tensile tests indicate that slightly lower strength is obtained after deformation. However, due to deviations and overlap in both tensile tests and hardness results, it is reasonable to believe that there are no detrimental effects on the final properties when deformation is introduced.

5.4 The effect of quench interruption and direct artificial aging

The results from the quench interruption experiments indicate that there are no significant effects on neither hardness nor strength after quench interruption at elevated temperatures. The hardness is highest for the samples quenched to room temperature before direct artificial aging or room temperature storage. The yield and tensile strengths are highest for the samples being quench interrupted at 70°C before room temperature storage and artificial aging. As for direct artificial aging, there are no significant differences between direct artificial aging and room temperature storage. However, for the samples quench interrupted at 70°C, there is a severe strength difference between the samples being directly artificially aged and those being stored at room temperature. Figure 68 show the average hardness and yield strength with standard deviations for the samples being quench interrupted at the different temperatures before direct artificial aging or room temperature storage.

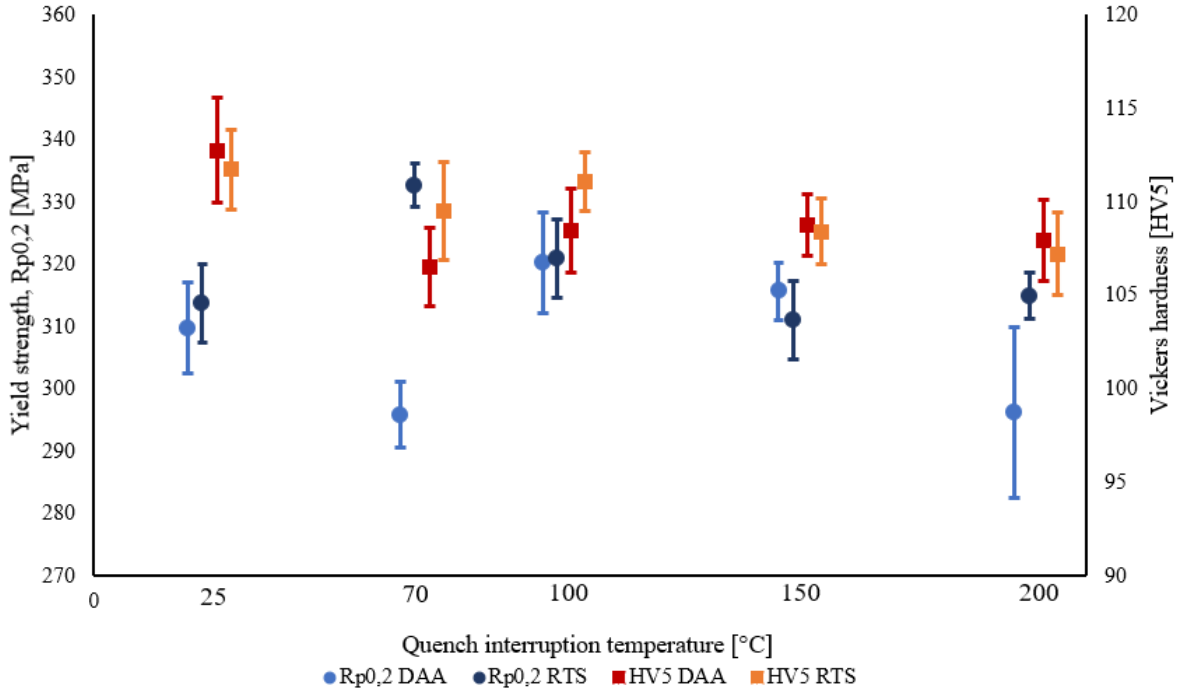

Figure 68: Average yield strength and average hardness with standard deviations for the samples being quench interrupted at quench interruption temperature before direct artificial aging (DAA) or room temperature storage (RTS).

The primary yield strength axis equals the secondary Vickers hardness axis multiplied by three so that the magnitude of standard deviations for both cases can easily be compared.

The most significant differences can be observed between the hardness results and the tensile test results. The results from the tensile tests show more variations in strength between the different cases than the hardness results. The relative standard deviations, i.e. the ratios of standard deviations to the averages, are between 2-5% for all cases of hardness and yield strength. The exception is quench interruption at 200°C before direct artificial aging, which is 9% for the yield strength. The standard deviations are defined as the average distance of the measurements from the average. Therefore, full scatters are not represented in the figure. If the percentage of deviation should be calculated for the interval between maximum and minimum

value, the deviations in hardness are larger than for the yield strength; 8-9% in Vickers hardness and 5-6% in yield strength.

As previously discussed, there is a possible surface effect caused by the recrystallized layer that may introduce deviations to the results. The images of the grain structure in the samples suggested that the tensile specimens are not affected by the recrystallized surface. Therefore, the possibility of interruption from recrystallized grains will not further be counted as a source of error in the result analysis of the tensile tests. The hardness, however, was measured on the surface of the samples. This inflicts a risk of misleading hardness results as there is a large possibility that the indentations were applied on the recrystallized surface. In addition, the scattering of the hardness measurements is larger than for the tensile test results. Consequently, further discussion will primarily be based on the tensile test results.

A hot forming and in-die quenching process would commonly be carried out by deformation and quenching to room temperature from solution heat treatment, and storage at room temperature before artificial aging. The yield strength results propose that introducing direct artificial aging and quench interruption at temperatures lower than 150°C should not be disadvantageous to the final strength of the material. The strength might even be increased compared to the original production process. However, there is one exception to this statement. The samples quench interrupted at 70°C before direct artificial aging show a significantly lower strength than the others; a difference in average yield strength of approximately 35MPa compared to those being stored at room temperature. The results are quite unambiguous as the deviations are low and there is no overlap.

The reason why the difference in strength between direct artificial aging and room temperature storage after quench interruption at 70°C is so significant in this case compared to the others is difficult to explain without performing more comprehensive investigations. One possible theory concerning the high strength of the room temperature storage sample, might be formation of clusters occurring during air cooling to room temperature. The slow cooling rate from 70°C can possibly be compared to the study done by Yamada, K. et al. [13] where step quenching, i.e. interrupted quenching and holding time at an elevated temperature, promoted the formation of Mg-Si-vacancy clusters that act as nucleation sites for β” precipitates, these experiments also included storage at room temperature before artificial aging. The slow cooling from quench interruption at 70°C might have been sufficient for formation of these clusters.

As for samples being directly artificially aged after quench interruption at 70°C, the significantly low strength differs from the other cases of direct artificial aging after quench interruption. This makes it difficult to find a reasonable explanation as it would be arguable that the same effect should have been seen for the samples being quench interrupted at for example 100°C before direct artificial aging. For the samples being quench interrupted at 70°C and directly artificially aged, the distinct parameter is the temperature at which the quenching was interrupted in combination with direct artificial aging. The clusters that possibly form during air cooling has not been formed when the sample is directly heated to artificial aging temperature, i.e. the clustering must have been suppressed as the time was not sufficient for these to form. Thus, the vacancies will not be occupied by these clusters, and neither are they quenched in at room temperature. A possible reason to the strength reduction may therefore be

a significant reduction in number of vacancies for subsequent clustering of nucleation sites. The vacancies might have been lost during the exposure to elevated temperatures, i.e. 70°C at quench interruption and direct heating to 190°C.

The hypothesis presented above cannot be established as valid as it has not been further investigated, and is not supported by any similar research found on this subject. In addition, it cannot be explained why this case deviate in such extent from the other quench interruption and direct artificial aging experiments. When including the hardness results, the difference between direct artificial aging and room temperature storage after quench interruption at 70°C is contradicted. The hardness results show that slightly greater hardness is achieved for the case of room temperature storage, but not to such an extent as the tensile test results indicate. Thus, the strength difference cannot be established as a truth and further experiments should be conducted to be able to confirm this effect.

As suggested by Myrold, B. et al. [3] and Kovaćs, I. et al. [19], skipping room temperature storage after quenching from solution heat treatment should result in increased strength and hardness of AA6082. This effect is not observed in the results from the hot forming and in-die quenching experiments. The major difference between this project and the mentioned studies is the introduction of deformation to the quenching sequence.

The dislocation density is a function of strain rate and temperature as shown in Section 2.6.2. During the hot deformation experiments, the temperature and strain rate change rapidly. The motion of dislocations may have an influence on the vacancy concentration. The dislocations can act as vacancy traps. If this is the case also during high temperature dislocation motion, the dislocations trap the vacancies and take the vacancies along in the annihilation. As a result, the vacancy concentration after ended deformation would be lower than during quenching with no deformation. Therefore, fewer vacancies are available for clustering and precipitation nucleation during subsequent age hardening.

Hence, the introduction of dislocation motion in deformation may affect the final strength by altering the dislocation density or the vacancy concentration after ended procedure. These mechanisms may be supressing the mechanisms causing the distinguished properties observed by direct artificial aging compared to room temperature storage for non-deformed samples. Thus, insignificant differences are observed in strength and hardness in the cases of direct artificial aging and room temperature storage.

In summary, quench interruption at temperatures below 150°C after deformation is according to the tensile test results beneficial to the final strength of the product. Direct artificial aging may also be introduced to the process as it would not be detrimental to the properties, except for the case of quench interruption at 70°C. The results from this project suggest that an increase in efficiency in the industrial hot forming in-die quenching process is possible by reducing the closed-die time and skipping room temperature storage, without inflicting negative effects on the final product properties.

The experiments conducted in this project is intended to be of relevance for the industrial production of aluminium components produced by press form hardening of extruded 6082.25 profiles for car applications. The most significant difference between the experiments

conducted in a laboratory and industrial production is the dimensions, where the dimensions in the industry are significantly larger than on the laboratory. The material volume and tooling are increased resulting in different cooling rates and temperature distribution through the material and the tool, in addition to time consume and limitations. However, the results should provide a sufficient indication of the material behaviour under similar conditions and show the essence of the effects of the different treatments on the material properties as it would in an increased scale.

The quench interruption experiments are intended to give an indication of the possibilities and limitations of a reduced closed-die time. Even if the time required to quench a larger part is longer in an industrial press, the effect of temperature to which the parts are quenched to before air cooling or direct artificial aging should be quite similar to the laboratory experiments. A reduction of closed-die time may spare few seconds of the production of one component. However, industrial production of large quantities means significant time saved in the process, and thus, increased efficiency and reduced costs.

The effect of direct artificial aging investigated in this project should also be of relevance for the industry. The storage period in the industry is a bottleneck in the production line of car components. If the room temperature storage period can be avoided without suffering diminished strength and hardness, significant time can be spared, that is, several minutes per part produced. This may provide large reductions in production costs and increased production efficiency.

The results showing the most promise in terms of time reductions without suffering decrease in the final product strength are achieved from the samples being quench interrupted at 100°C after deformation and quenching from solution heat treatment before direct artificial aging. Implementing this in an industrial production line would provide significant reductions in closed-die time as well as time savings from skipping the room temperature storage period. In addition, the time it takes heating the components from room temperature to artificial aging temperature in air circulation furnaces is also reduced.

6. Conclusion

The aim of the project was to investigate the influence of quench interruption, i.e. closed-die time, and direct artificial aging on the mechanical properties of a 6082.25 aluminium alloy in a hot deformation and in-die quenching process.

The method developed for simulating the hot forming and in-die quenching process proved to be sufficient in terms of deformation, quenching and the overall transportation of a sample between furnace, tool and oil bath. Issues regarding time and temperature criterions when handling the samples should be solved initially to future applications of the method. In addition, alterations to the procedure are necessary to ensure homogeneous deformation in the sample.

When introducing deformation to the quenching from solution heat treatment, the results are ambiguous. However, the results suggest that there is not much difference in either strength or hardness after simultaneous deformation and quenching from solution heat treatment. The strength increase of the samples being directly artificially aged and not deformed is not shown after deformation and direct artificial aging.

The highest strength is achieved by quench interruption at 70°C before room temperature storage and 100°C before room temperature storage or direct artificial aging. As there are no obvious benefits of neither room temperature storage nor direct artificial aging, room temperature storage may be skipped without inflicting diminished mechanical properties on the final product. Thus, the optimal treatment in terms of strength, hardness and production efficiency combined, is quench interruption at 100°C and direct artificial aging.

Hence, due to small differences in strength and hardness for most treatments, there appears to be no disadvantages by either shortening the closed-die time, or by direct artificial aging. Relating this to the industrial press form hardening process; time, energy and costs may be spared by introducing quench interruption at 150°C and direct artificial aging to the production sequence.

7. Recommendations for further work

The results obtained in this project from the hot deformation in-die quenching experiments gives an indication of the effect of deformation, tool quenching, direct artificial aging and quench interruption. However, some deviations in the results provide uncertainties to the method. There are certain factors that may be altered to ensure improved reliability to the experiments and the in-die quenching and deformation procedure. Additional tests could also be conducted to confirm the results obtained in this project and the previous specialization project regarding the behaviour of the 6082.25 alloy.

A new solution for the sample dimensions should be found to expand the possibilities for subsequent mechanical testing of resulting properties. The micro tensile specimens tested in this project was favourable regarding the avoidance of the recrystallized layers in the profile, in addition to ensuring the inclusion of the through cross section area of the samples. However, the specimen volume and test area are very small, and hence introduce uncertainties in the tensile test results and in the specimen dimension measurements. By altering the sample dimensions of the samples tested in the tool, tensile specimens of larger volume can be obtained providing more reliability and probably less deviations in the tensile test results.

To further investigate the differences and more clearly observe the effect of direct artificial aging, the experiments should be repeated under expanded conditions such as an elongated storage period. This may lead to more separation in the results showing a clearer benefit of either direct artificial aging or room temperature storage.

If the production process in the industry is to be altered by shortening the closed-die time or transferring the formed components directly to artificial aging after deformation and quenching from solution heat treatment, the tests should be magnified to industrial scale. Tests should be done on components treated as they would in the industry to study the effect and the efficiency when press forming larger material parts with slower cooling rates, inhomogeneous cooling and transportation time limits. The tests conducted in this project may not be directly comparable to industrial conditions, and the results from these experiments should be confirmed before implementing new procedures.

References

1. *CO2 emissions from transport (% of total fuel combustion)*. 2016 22.05.2017]; Available from: http://data.worldbank.org/indicator/EN.CO2.TRAN.ZS?end=2014&start=1985.
2. Hydro. *Transport*. 2016 22.03.2017]; Available from: http://www.hydro.com/no/hydro-i-norge/Om-aluminium/Hverdagsliv/Aluminium-i-transport/.
3. Myrold, B., *Press Form Hardening of Aluminium - The influence of quench delay time and pressure cooling on the hardening potential of AA6082.* 2017.
4. Norge, S., *NS-EN 573-3. Aluminium og aluminiumlegeringer. Kjemisk sammensetning og form på plastisk bearbeidede produkter.*, in *Del 3: Kjemisk sammensetning og produktenes form*. 2014.
5. Solberg, J.K., m. Norges teknisk-naturvitenskapelige universitet Institutt for, and e. Norges teknisk-naturvitenskapelige universitet Institutt for materialteknologi og, *Teknologiske metaller og legeringer*. 2008, Trondheim: Institutt for materialteknologi, Norges teknisk-naturvitenskapelige universitet.
6. Totten, G.E. and D.S. MacKenzie, *Handbook of Aluminum: Vol. 1: Physical Metallurgy and Processes*. 2003: : CRC Press.
7. King, F., *Aluminium and its alloys*. Ellis Horwood series in metals and associated materials. 1987, Chichester: Ellis Horwood.
8. Li, Y.J. and L. Arnberg, *Quantitative study on the precipitation behavior of dispersoids in DC-cast AA3003 alloy during heating and homogenization.* Acta Materialia, 2003. **51**(12): p. 3415-3428.
9. Cartmell, L.J., F. King, and G. Salt, *Hot rolling of sheet and strip: aluminium and aluminium alloys.* Metals Technology, 1975. **2**(1): p. 313-317.
10. Howard, R., N. Bogh, and D. Scott Mackenzie, *Heat Treating Processes and Equipment*, in *Handbook of Aluminum*. 2003, CRC Press.
11. Howard, R., *Aluminum Heat Treatment Processes, Applications and Equipment.* Industrial Heating, 2007. **74**(2): p. 61-65.
12. Torsæter, M., et al., *The influence of composition and natural aging on clustering during preaging in Al–Mg–Si alloys.* Journal of Applied Physics, 2010. **108**(7).
13. Yamada, K., T. Sato, and A. Kamio, *Effects of quenching conditions on two-step aging behavior of Al-Mg-Si alloys.* Aluminium Alloys: Their Physical And Mechanical Properties, Pts 1-3, 2000. **331-3**: p. 669-674.
14. Ozawa, E. and H. Kimura, *Behavior of excess vacancies during the nucleation of precipitates in aluminum-silicon alloys.* Materials Science and Engineering, 1971. **8**(6): p. 327-335.
15. Zhen, L. and S.B. Kang, *DSC analyses of the precipitation behavior of two Al–Mg–Si alloys naturally aged for different times.* Materials Letters, 1998. **37**(6): p. 349-353.
16. Kavalco, P.M., L.C.F. Canale, and G.E. Totten, *Quenching of aluminum alloys: cooling rate, strength, and intergranular corrosion.* Heat Treating Progress, 2009. **9**(7): p. 25.
17. Li, N., et al., *Investigation on fast and energy-efficient heat treatments of AA6082 in HFQ processes for automotive applications*. 2015. p. <xocs:firstpage xmlns:xocs=""/>.
18. Marioara, C., et al., *The influence of alloy composition on precipitates of the Al-Mg-Si system.* Metallurgical and Materials Transactions A, 2005. **36**(3): p. 691-702.
19. Kovaćs, I., J. Lendvai, and E. Nagy, *The mechanism of clustering in supersaturated solid solutions of A1-Mg2Si alloys.* Acta Metallurgica, 1972. **20**(7): p. 975-983.
20. Dieter, G.E. and D. Bacon, *Mechanical metallurgy*. SI metric ed. ed. McGraw-Hill series in materials science and engineering. 1988, London: McGraw-Hill.
21. Callister, W.D.R., D. G., *Materials Science and Engineering, SI Version*. 8th edition ed. 2011: Wiley.

22. Smallman, R.E. and R.J. Bishop, *Modern Physical Metallurgy and Materials Engineering*. 6th ed. ed. Modern Physical Metallurgy and Materials Engineering - Science, Process, Applications. 1999, Burlington: Elsevier Science.
23. Noseda Grau, V., et al., *Solute clustering behavior between 293K and 373K in a 6082 Aluminum alloy.* Journal of Alloys and Compounds, 2016. **684**: p. 481-487.
24. Ninive, P., O. Løvvik, and A. Strandlie, *Density Functional Study of the β " Phase in Al-Mg-Si Alloys.* Metallurgical and Materials Transactions A, 2014. **45**(6): p. 2916-2924.
25. Polmear, I.J., *Light Alloys: From Traditional Alloys to Nanocrystals*. 4th ed. ed. 2005: United Kingdom: Butterworth Heinemann.
26. McQueen, H.J., et al., *Hot Deformation and Processing of Aluminum Alloys*. 2016: CRC Press.
27. Lodgaard, L. and N. Ryum, *Precipitation of dispersoids containing Mn and/or Cr in Al–Mg–Si alloys.* Materials Science and Engineering: A, 2000. **283**(1–2): p. 144-152.
28. Strobel, K., et al., *Relating Quench Sensitivity to Microstructure in 6000 Series Aluminium Alloys.* MATERIALS TRANSACTIONS, 2011. **52**(5): p. 914-919.
29. Milkereit, B., et al., *Continuous cooling precipitation diagrams of Al–Mg–Si alloys.* Materials Science & Engineering A, 2012. **550**: p. 87-96.
30. Sarmiento, G.S., et al., *Water and polymer quenching of aluminum alloys: A review of the effect of surface condition, water temperature, and polymer quenchant concentration on the yield strength of 7075-T6 aluminum plate.* Journal of ASTM International, 2009. **6**(1).
31. Milkereit, B., et al., *Isothermal Time-Temperature-Precipitation Diagram for an Aluminum Alloy 6005A by In Situ DSC Experiments.* Materials, 2014. **7**(4): p. 2631-2649.
32. Gao, M., et al., *TTP Curves and Microstructural Evolution Mechanism After Quenching in Aluminum Alloy 6082.* Application and Innovation for Metals, Alloys, and Engineered Materials, 2012. **1**(3): p. 165-169.
33. Shang, B.C., et al., *Investigation of quench sensitivity and transformation kinetics during isothermal treatment in 6082 aluminum alloy.* Materials and Design, 2011. **32**(7): p. 3818-3822.
34. Nie, J.F., *Physical Metallurgy of Light Alloys*. Vol. 1. 2014. 2009-2156.
35. Verhoeven, J.D., *Fundamentals of physical metallurgy*. 1975, New York: Wiley.
36. MacKenzie, D.S., *Design of quench systems for aluminum heat treating Part I--quenchant selection.* Industrial Heating, 2006. **73**(6): p. 53.
37. Ji, K., et al., *Determination of the Interfacial Heat Transfer Coefficient in the Hot Stamping of AA7075.* Manufacturing Review, 2016. **3**: p. 16.
38. Mendiguren, J., et al., *Experimental characterization of the heat transfer coefficient under different close loop controlled pressures and die temperatures.* Applied Thermal Engineering, 2016. **99**: p. 813-824.
39. Jensrud, O., K.E. Snilsberg, and A. Kolbu, *Conceptual testing of Press Form Hardening of High-Strength Aluminium Alloys.* Aluminium Extrusions and Finishing - The international magazine of the aluminium extrusion and finishing industry, 2016.
40. Marioara, C.D., et al., *The influence of temperature and storage time at RT on nucleation of the β" phase in a 6082 Al–Mg–Si alloy.* Acta Materialia, 2003. **51**(3): p. 789-796.
41. Tan, E. and B. Ögel, *Influence of heat treatment on the mechanical properties of AA6066 alloy.* Turkish Journal of Engineering and Environmental Sciences, 2007. **31**(1): p. 53-60.
42. Humphreys, F.J. and M. Hatherly, *Recrystallization and Related Annealing Phenomena*. Vol. 2nd ed. 2004, Amsterdam: Pergamon.
43. Guo-Zheng, Q., *Characterization for Dynamic Recrystallization Kinetics Based on Stress-Strain Curves*, in *Recent Developments in the Study of Recrystallization*, P. Wilson, Editor. 2013, InTech: Rijeka. p. Ch. 02.
44. Humphreys, F.J., G.S. Rohrer, and A.D. Rollett, *Recrystallization and related annealing phenomena*. 3rd ed. ed. 2017: Elsevier.
45. Holmedal, B., *Lecture notes from the course TMT4266 at NTNU. Published on ItsLearning during the course*. 2016.
46. Ghosh, M., A. Miroux, and L.A.I. Kestens, *Correlating r-value and through thickness texture in Al–Mg–Si alloy sheets.* Journal of Alloys and Compounds, 2015. **619**: p. 585-591.

47. Dieter, G.E. and D. Bacon, *Mechanical Metallurgy*. McGraw Hill series in materials science and engineering. 1988, London: McGraw Hill.
48. Altenpohl, D., *Aluminum : technology, applications, and environment : a profile of a modern metal*. 6th ed. ed. Aluminium von innen. 1998, Washington, D.C: Aluminum Association.
49. Neugebauer, R., et al., *Press hardening — An innovative and challenging technology.* Archives of Civil and Mechanical Engineering, 2012. **12**(2): p. 113-118.
50. 6892-1, I., *Metallic materials, Tensile testing. Part 1: Method of test at room temperature*. 2009.
51. Pedersen, K., *Dispersoid density AA6082 alloy chorus*. 2002: SINTEF internal report.
52. Jensrud, O., *Personal Communication*. 2018.

Appendix A: Test matrix for hot deformation and in-die quenching experiments

Table A1: Parameters remained constant for all experiments.

Number of parallels	3	
Material	6082.25	Extruded sheet
Solution heat treatment temperature	540	°C
Heating time to solution heat treatment temperature	10	min.
Total solution heat treatment time	30	min.
Deformation start temperature	505-508	°C
Lubricant	Molykote G-Rapid Plus	
Artificial aging temperature	190	°C
Artificial aging time	3	h.

Table A2: Test matrix showing the various parameters for the different experiments

Treatment	**Quenched to temperature**	**Degree of deformation**	**Cooling medium**	**Cooling of tool before or during experiments**	**Room temperature storage**
	[°C]	[%]	(Water/Tool)	(Before/During)	(Yes/No)
Tool quenching vs. water quenching	25	0	Water	-	Yes
	25	0	Water	-	No
	25	0	Tool	Before	Yes
	25	0	Tool	Before	No
Cooling of tool before vs. during experiments	25	15	Tool	Before	Yes
	25	15	Tool	Before	No
	25	15	Tool	During	Yes
	25	15	Tool	During	No
Deformation vs. no deformation	25	15	Tool	Before	Yes
	25	15	Tool	Before	No
	25	0	Tool	Before	Yes
	25	0	Tool	Before	No
Quench interruption experiments and effect of direct artificial aging	200	15	Tool	Before	Yes
	150	15	Tool	Before	Yes
	100	15	Tool	Before	Yes
	70	15	Tool	Before	Yes
	25	15	Tool	Before	Yes
	200	15	Tool	Before	No
	150	15	Tool	Before	No
	100	15	Tool	Before	No
	70	15	Tool	Before	No
	25	15	Tool	Before	No

Appendix B: Recrystallization before and after treatment

B1: Images from light optical microscopy – as-extruded

Images of randomly selected samples obtained from along the as-extruded profile are shown in this Figure B1. These images were obtained additional to those presented in Chapter 4.1.1.

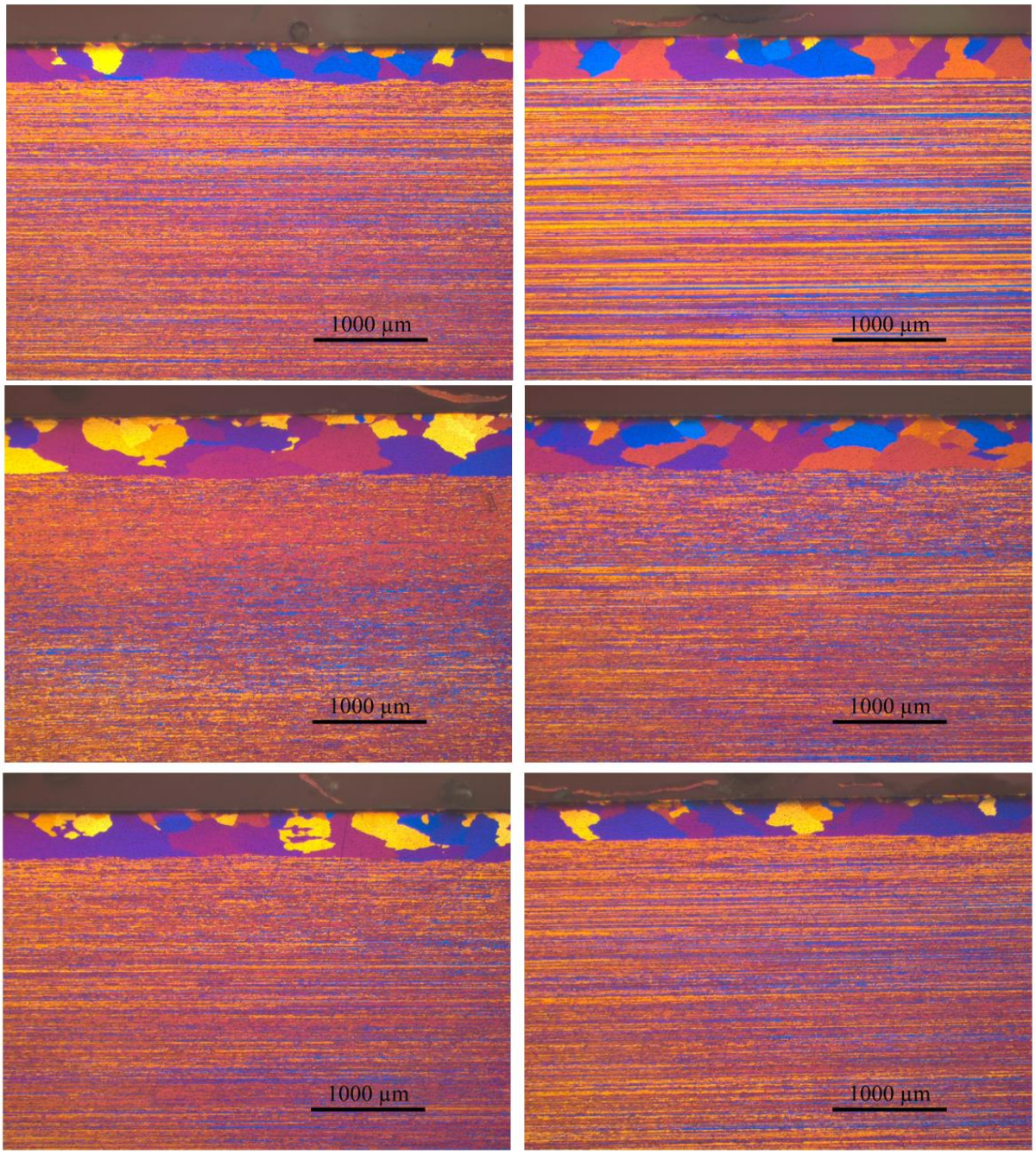

Figure B.1: Images obtained in light optical microscopy of the recrystallized surface layer. The images are obtained from the longitudinal plane in randomly selected samples along the as-extruded profile.

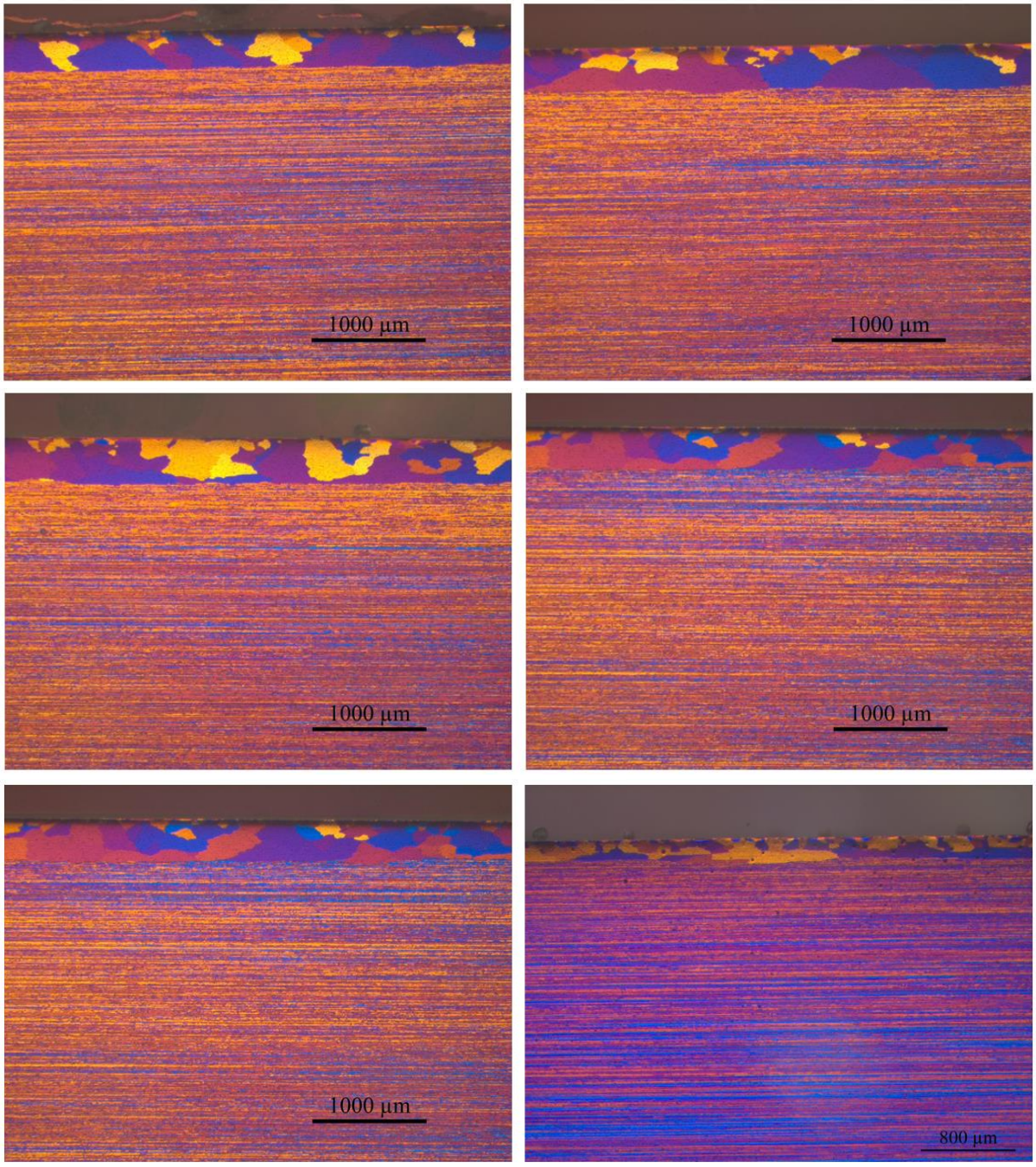

Figure B.1: Images obtained in light optical microscopy of the recrystallized surface layer. The images are obtained from the longitudinal plane in randomly selected samples along the as-extruded profile.

B2: Images from light optical microscopy of samples after solution heat treatment and/or deformation

Images of selected samples after solution heat treatment and/or deformation are shown in Figures in this Section.

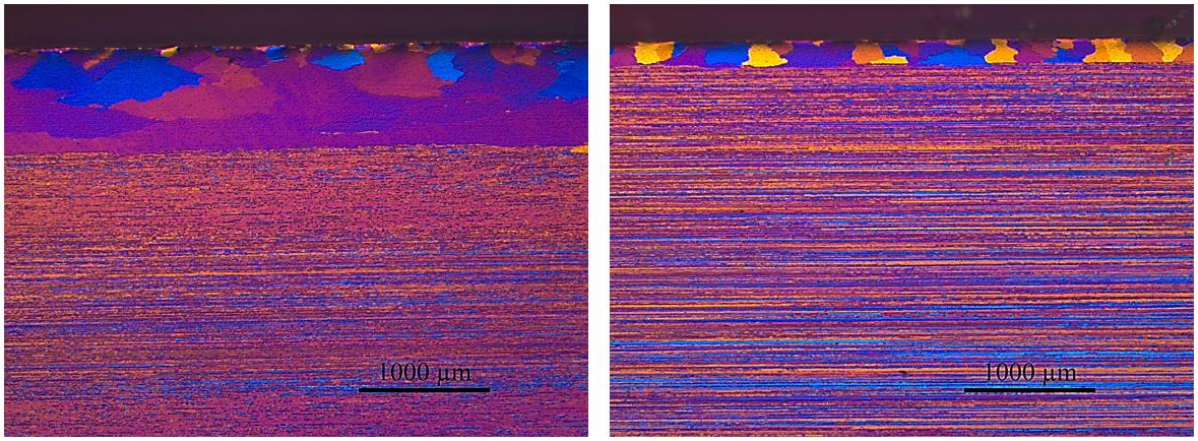

Figure B.2.1: The recrystallized surface layer in the longitudinal plane after solution heat treatment and tool quenching to room temperature. The samples have not been deformed during quenching.

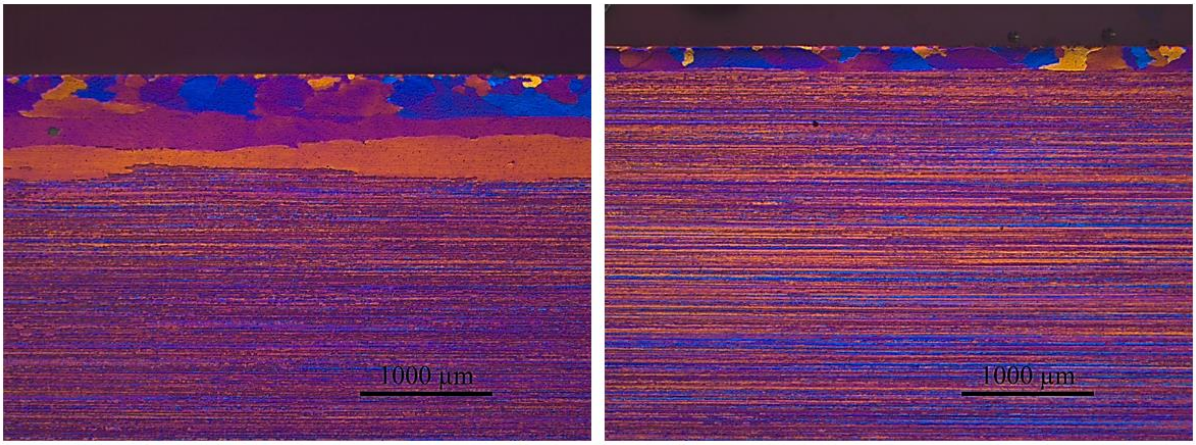

Figure B.2.2: The recrystallized surface layer in the longitudinal plane deformation and quenching to room temperature from solution heat treatment.

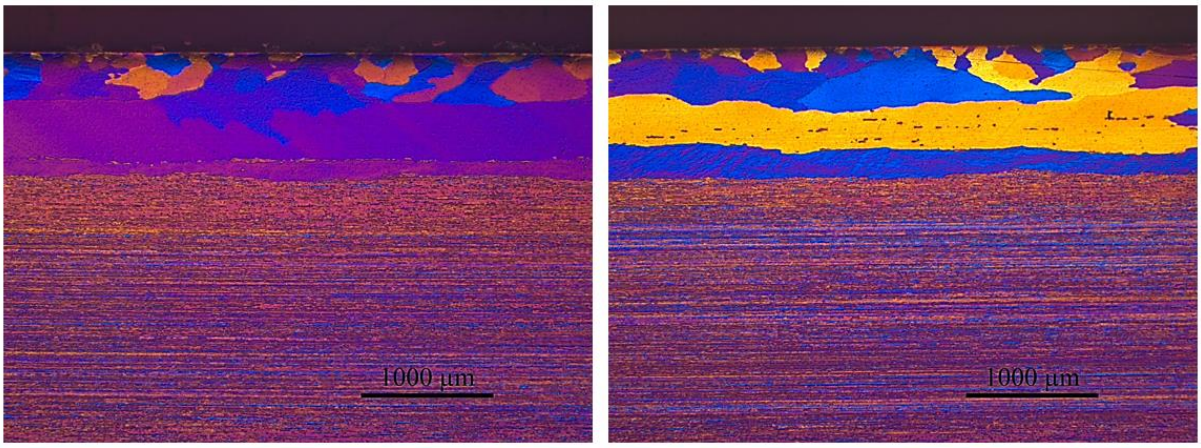

Figure B.2.3: The recrystallized surface layer in the longitudinal plane after deformation and quench interruption at 150°C.

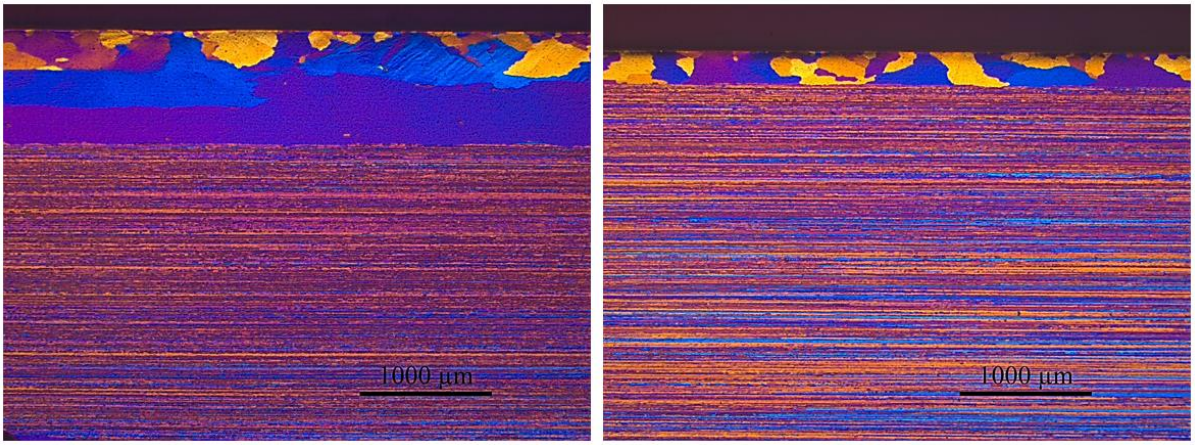

Figure B.2.4: The recrystallized surface layer in the longitudinal plane after deformation and quench interruption at 100°C.

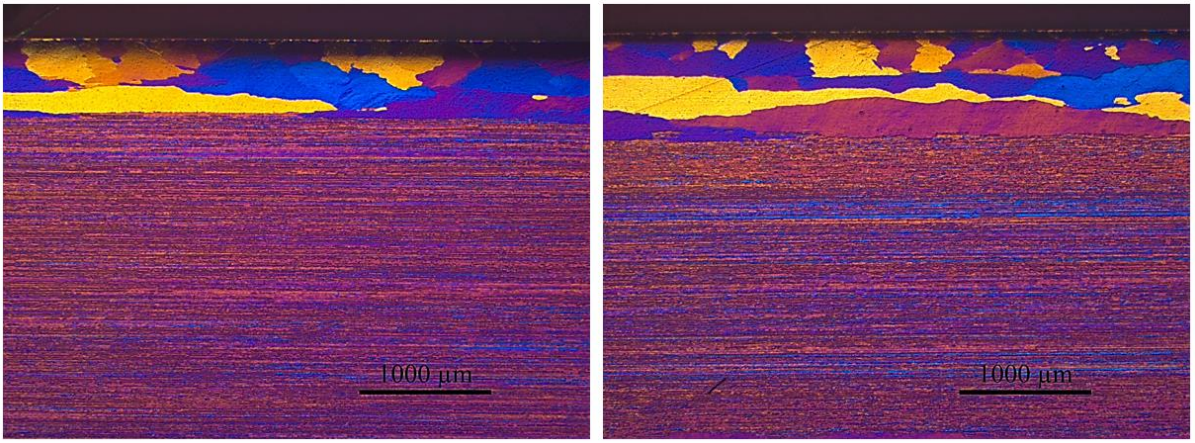

Figure B.2.5: The recrystallized surface layer in the longitudinal plane after deformation and quench interruption at 70°C

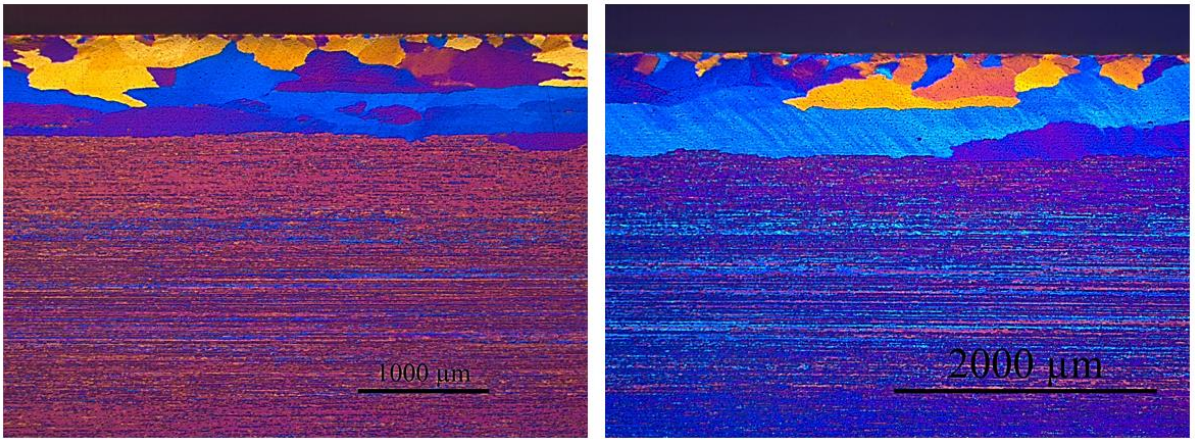

Figure B.2.6: The recrystallized surface layer in the longitudinal plane after deformation and quenching to room temperature.

Appendix C: Tensile test results

Table C.1: Results from the tensile tests for the samples being tool quenched without deformation, and for the samples being water quenched.

Quenching	Storage	Parallel number	Yield stress	Tensile strength	Elongation	Fracture elongation
		sample.specimen	Rp0,2 [Mpa]	Rm [Mpa]	Agt [%]	At [%]
Tool quenched	RTS	1.1	305,1	329,4	7,1	17,9
		1.2	307,0	333,6	6,8	18,4
		1.3	303,1	326,5	6,2	17,0
		2.1	299,1	325,2	6,4	18,1
		2.2	299,0	328,3	6,6	17,9
		2.3	299,1	327,0	6,7	17,8
		3.1	333,8	356,6	6,5	19,5
		3.2	333,9	356,3	6,7	17,8
		3.3	334,0	355,4	6,0	14,1
	DAA	1.1	319,1	337,0	6,3	17,8
		1.2	319,1	335,0	6,4	19,4
		1.3	317,3	340,1	6,7	18,7
		2.1	325,7	346,5	5,8	18,5
		2.2	325,4	346,4	5,8	18,8
		2.3	322,9	344,7	6,6	19,2
		3.1	317,7	338,7	6,0	19,4
		3.2	317,0	338,4	5,9	17,6
		3.3	316,9	338,8	6,2	17,5
Water quenched	RTS	1.1	323,8	351,2	6,3	16,5
		1.2	330,2	352,3	6,7	17,4
		1.3	330,7	350,3	6,7	17,9
		2.1	316,0	339,6	5,3	17,3
		2.2	320,9	340,3	5,7	18,7
		2.3	317,2	338,6	5,7	19,0
		3.1	324,5	343,2	6,1	17,7
		3.2	319,1	341,8	5,2	13,5
		3.3	320,2	342,2	6,3	19,0
	DAA	1.1	315,5	336,3	6,1	19,7
		1.2	319,2	336,2	5,3	19,0
		1.3	335,5	354,1	6,0	17,2
		2.1	344,7	368,7	5,8	16,0
		2.2	345,1	369,7	6,1	18,7
		2.3	335,7	359,7	6,1	16,1
		3.1	330,5	349,7	6,0	16,7
		3.2	337,5	357,4	6,1	15,8
		3.3	327,4	349,9	6,4	17,4

Table C.2: Results from the tensile tests for the samples being deformed in a pre-cooled tool and for the samples being deformed in the constantly quenched tool.

Cooling of tool	Storage	Parallel number	Yield stress	Tensile strength	Elongation	Fracture elongation
		sample.specimen	Rp0,2 [Mpa]	Rm [Mpa]	Agt [%]	At [%]
Pre-cooling	RTS	1.1	314,2	335,0	5,2	14,0
		1.2	313,9	335,1	5,9	17,7
		1.3	322,3	340,2	5,0	17,4
		2.1	308,7	328,8	5,3	15,6
		2.2	319,6	338,6	5,4	19,5
		2.3	311,2	331,1	5,1	17,6
		3.1	301,1	329,0	5,6	19,9
		3.2	316,3	333,8	5,7	18,5
		3.3	316,0	335,8	5,6	15,7
	DAA	1.1	313,0	335,3	6,1	17,0
		1.2	312,2	333,7	5,7	17,1
		1.3	317,6	337,3	5,7	17,2
		2.1	314,3	334,3	5,3	18,3
		2.2	316,7	334,1	5,8	15,5
		2.3	316,0	333,7	5,9	19,6
		3.1	302,4	323,2	5,3	17,7
		3.2	310,1	331,1	5,7	19,2
		3.3	304,5	323,5	5,2	18,0
Constant cooling	RTS	1.1	321,8	341,9	5,5	21,9
		1.2	314,3	337,6	5,7	21,8
		1.3	322,4	342,7	5,1	17,0
		2.1	327,1	349,2	5,4	20,7
		2.2	331,7	351,6	5,6	19,3
		2.3	330,6	350,6	6,0	19,6
		3.1	330,3	351,8	6,3	17,9
		3.2	333,8	353,1	5,6	19,5
		3.3	331,1	355,1	5,8	19,0
	DAA	1.1	320,2	342,9	6,0	23,7
		1.2	315,7	333,4	5,6	20,0
		1.3	311,2	331,2	5,3	16,5
		2.1	333,8	355,3	5,9	20,2
		2.2	328,9	351,9	6,3	20,8
		2.3	330,8	349,0	5,4	19,8
		3.1	334,8	356,2	5,8	17,3
		3.2	327,2	351,1	5,7	15,8
		3.3	326,3	349,9	5,6	18,6

Table C.3: Results from the tensile tests for samples with and without deformation.

Quenching	Storage	Parallel number	Yield stress	Tensile strength	Elongation	Fracture strain
		sample.specimen	Rp0.2 [Mpa]	Rm [Mpa]	Agt [%]	At [%]
Deformation	RTS	1.1	314,2	335,0	5,2	14,0
		1.2	313,9	335,1	5,9	17,7
		1.3	322,3	340,2	5,0	17,4
		2.1	308,7	328,8	5,3	15,6
		2.2	319,6	338,6	5,4	19,5
		2.3	311,2	331,1	5,1	17,6
		3.1	301,1	329,0	5,6	19,9
		3.2	316,3	333,8	5,7	18,5
		3.3	316,0	335,8	5,6	15,7
	DAA	1.1	313,0	335,3	6,1	17,0
		1.2	312,2	333,7	5,7	17,1
		1.3	317,6	337,3	5,7	17,2
		2.1	314,3	334,3	5,3	18,3
		2.2	316,7	334,1	5,8	15,5
		2.3	316,0	333,7	5,9	19,6
		3.1	302,4	323,2	5,3	17,7
		3.2	310,1	331,1	5,7	19,2
		3.3	304,5	323,5	5,2	18,0
No deformation	RTS	1.1	305,1	329,4	7,1	17,9
		1.2	307,0	333,6	6,8	18,4
		1.3	303,1	326,5	6,2	17,0
		2.1	299,1	325,2	6,4	18,1
		2.2	299,0	328,3	6,6	17,9
		2.3	299,1	327,0	6,7	17,8
		3.1	333,8	356,6	6,5	19,5
		3.2	333,9	356,3	6,7	17,8
		3.3	334,0	355,4	6,0	14,1
	DAA	1.1	319,1	337,0	6,3	17,8
		1.2	319,1	335,0	6,4	19,4
		1.3	317,3	340,1	6,7	18,7
		2.1	325,7	346,5	5,8	18,5
		2.2	325,4	346,4	5,8	18,8
		2.3	322,9	344,7	6,6	19,2
		3.1	317,7	338,7	6,0	19,4
		3.2	317,0	338,4	5,9	17,6
		3.3	316,9	338,8	6,2	17,5

Table C.4: Results from the tensile tests for the samples being quenched interrupted at different temperatures.

Quench interruption temperature	Storage	Parallel number sample.specimen	Yield stress Rp0,2 [Mpa]	Tensile strength Rm [Mpa]	Elongation Agt [%]	Fracture strain At [%]
200°C	RTS	1.1	308,5	332,7	5,7	20,8
		1.2	315,1	335,4	6,0	20,3
		1.3	311,3	331,2	4,8	13,9
		2.1	318,2	339,5	6,0	18,5
		2.2	317,4	339,8	5,5	18,7
		2.3	311,2	333,6	5,2	19,2
		3.1	317,0	338,6	6,3	23,5
		3.2	316,5	335,2	6,3	21,1
		3.3	319,0	337,9	5,4	19,9
	DAA	1.1	288,6	306,6	5,8	20,4
		1.2	293,5	311,8	5,4	17,4
		1.3	284,1	302,2	4,7	15,4
		2.1	284,0	303,8	5,7	19,8
		2.2	288,1	305,4	4,5	8,1
		2.3	285,8	307,3	5,7	20,1
		3.1	279,2	298,6	4,4	17,0
		3.2	306,2	326,1	5,4	20,3
		3.3	307,8	330,2	5,7	19,1
150°C	RTS	1.1	317,6	338,9	5,8	20,4
		1.2	318,7	338,3	5,6	19,4
		1.3	317,5	337,1	6,1	22,3
		2.1	309,9	331,9	5,6	20,6
		2.2	313,3	332,8	5,2	20,6
		2.3	310,7	332,5	5,9	18,5
		3.1	311,4	331,7	5,7	24,3
		3.2	309,8	329,9	5,3	19,6
		3.3	310,7	333,4	5,9	22,1
	DAA	1.1	310,4	329,2	5,7	20,7
		1.2	313,8	332,5	5,4	21,0
		1.3	310,3	329,1	5,4	17,4
		2.1	319,4	338,9	5,9	19,4
		2.2	323,3	343,3	5,6	18,3
		2.3	320,4	340,4	5,7	20,8
		3.1	316,5	335,7	5,9	19,5
		3.2	314,8	338,5	5,8	20,5
		3.3	312,0	331,2	5,8	18,0
100°C	RTS	1.1	315,0	332,7	5,5	18,9
		1.2	312,3	333,2	5,6	20,6
		1.3	317,7	337,4	5,6	20,2
		2.1	324,1	343,4	5,1	18,1
		2.2	313,1	334,7	5,2	19,8
		2.3	323,6	346,9	5,5	18,8
		3.1	327,0	348,4	6,0	19,9
		3.2	328,3	350,1	6,1	20,5
		3.3	326,4	347,5	5,5	19,7
	DAA	1.1	325,9	345,6	6,3	21,6
		1.2	329,0	349,7	5,3	20,4
		1.3	322,0	345,6	5,6	20,4
		2.1	306,0	326,2	5,9	20,7
		2.2	317,2	337,5	5,6	20,7
		2.3	309,6	326,2	5,4	14,1
		3.1	328,2	347,2	5,4	16,3
		3.2	325,7	346,9	5,8	17,3
		3.3	318,4	339,9	5,6	16,3

Table C5: Results from the tensile tests for the samples being quenched interrupted at different temperatures.

70°C	**RTS**	1.1	329,8	355,4	5,7	18,3
		1.2	338,4	358,6	6,3	20,6
		1.3	334,4	353,7	5,1	10,8
		2.1	330,0	349,4	6,2	19,2
		2.2	326,8	347,3	5,6	21,4
		2.3	332,2	352,0	5,2	14,8
		3.1	341,4	364,5	6,3	17,5
		3.2	341,8	363,7	5,9	20,4
		3.3	341,6	363,9	5,8	19,4
	DAA	1.1	329,8	355,4	5,2	19,3
		1.2	338,4	358,6	5,3	19,2
		1.3	334,4	353,7	5,4	22,0
		2.1	330,0	349,4	5,5	17,5
		2.2	326,8	347,3	5,2	21,0
		2.3	332,2	352,0	5,6	20,4
		3.1	334,5	357,1	5,7	21,8
		3.2	332,5	353,8	5,0	20,0
		3.3	335,1	356,9	5,7	20,0
25°C	**RTS**	1.1	314,2	335,0	5,2	14,0
		1.2	313,9	335,1	5,9	17,7
		1.3	322,3	340,2	5,0	17,4
		2.1	308,7	328,8	5,3	15,6
		2.2	319,6	338,6	5,4	19,5
		2.3	311,2	331,1	5,1	17,6
		3.1	301,1	329,0	5,6	19,9
		3.2	316,3	333,8	5,7	18,5
		3.3	316,0	335,8	5,6	15,7
	DAA	1.1	316,2	338,8	6,1	17,0
		1.2	315,6	337,3	5,7	17,1
		1.3	317,6	337,3	5,7	17,2
		2.1	304,8	324,2	5,3	18,3
		2.2	314,4	331,6	5,8	15,5
		2.3	314,3	332,0	5,9	19,6
		3.1	299,2	319,8	5,3	17,7
		3.2	303,8	324,3	5,7	19,2
		3.3	301,5	320,3	5,2	18,0